WEAK-INTERACTION AND NUCLEAR-STRUCTURE ASPECTS OF NUCLEAR DOUBLE BETA DECAY

Jouni SUHONEN[a], **Osvaldo CIVITARESE**[b]

[a] *Department of Physics, University of Jyväskylä, P.O. Box 35, FIN-40351, Jyväskylä, Finland*
[b] *Department of Physics, University of La Plata, C.C. 67, 1900-La Plata, Argentina*

ELSEVIER

AMSTERDAM – LAUSANNE – NEW YORK – OXFORD – SHANNON – TOKYO

ELSEVIER

Physics Reports 300 (1998) 123–214

PHYSICS REPORTS

Weak-interaction and nuclear-structure aspects of nuclear double beta decay

Jouni Suhonen[a,*], Osvaldo Civitarese[b]

[a] *Department of Physics, University of Jyväskylä, P.O. Box 35, FIN-40351, Jyväskylä, Finland*
[b] *Department of Physics, University of La Plata, C.C. 67, 1900-La Plata, Argentina*

Received September 1997; editor: G.E. Brown

Contents

Abstract

Weak-interaction and nuclear-structure aspects of double beta decay are reviewed. Starting from effective electroweak lagrangians, decay rates for the two-neutrino and neutrinoless modes of the nuclear double beta decay transitions are defined and second-order perturbative expressions for the nuclear decay amplitudes are given. Nuclear matrix elements

* Corresponding author.

PII S0370-1573(97)00087-2

of the relevant operators are presented, as extracted from data and from shell-model and QRPA calculations as well as from other theoretical approximations. The analysis is performed both for the two-neutrino and neutrinoless modes of the decay. The expressions for ground-state-to-ground-state and ground-state-to-excited-state transitions are presented. Updated experimental and theoretical information on $\beta^-\beta^-$ decays in ^{48}Ca, ^{76}Ge, ^{82}Se, ^{96}Zr, ^{100}Mo, ^{116}Cd, ^{124}Sn, ^{128}Te, ^{130}Te, ^{136}Xe, ^{150}Nd, and on $\beta^+\beta^+$, β^+ EC and double EC decays in ^{78}Kr, ^{92}Mo, ^{96}Ru, ^{106}Cd, ^{124}Xe, ^{130}Ba, ^{136}Ce is analyzed and compared with theoretical results. The relevance of single-beta-decay transitions feeding some of the nuclei where double-beta-decay transitions occur is pointed out. The systematics of various phase-space factors and extracted matrix elements is presented.

PACS: 23.40.Bw; 23.90. + w; 23.40.Hc; 21.60. − n

Keywords: Weak interactions; Double beta decay; Nuclear matrix elements

1. Introduction

The nuclear double beta decay is a very rare nuclear decay mode which, for a long period of time was considered just out of reach, both experimentally and theoretically. However, the direct measurements of nuclear-double-beta-decay half-lives in the decay of ^{82}Se by Elliot et al. [94] and ^{76}Ge by Miley et al. [173] and by Vasenko et al. [266], the subsequent results obtained by other experimental groups [7,9,91,96,98,162] for other nuclei and the very recent measurement of the decay of ^{48}Ca by Balysh et al. [18], constitute important advances in the field since the pioneering work of Wu et al. [278].

From the theoretical side, the consequences upon fundamental concepts of nuclear and particle physics, potentially signaled by this rare decay, have been explored by Georgi and Glashow [115] and Fritzsch and Minkowski [111] and by many others in the last three or four decades (for a review of the grand-unification theories see [165]). The link of nuclear and particle physics, as revealed in the understanding of nuclear electroweak decays, was reviewed years ago by Leader and Predazzi [166], Vergados [269] and by Boehm and Vogel [46] while more specific aspects of the problem have been reviewed by [51,85,106,125,200] and more recently by [259,122,152,153,155]. However, the sensitivity of the theoretical predictions based on nuclear models, particularly when dealing with the range of physically acceptable values of nuclear double-beta-decay observables, and the variety of nuclear models proposed since the above reports were published largely justifies the need of an up-dated review, like the one which we are trying to convey herewith.

In reviewing the available theoretical information on nuclear double-beta-decay processes we have avoided the discussion of already well known ingredients and we have summarized, instead, the main aspects of each model. Since the list of contributions (as listed in the references) is considerably large, a detailed presentation of each of them would be impossible and unwanted omissions in the citations may also occur for which we apologize in advance.

In presenting these results we have kept in mind that theoretical results in this field are of no use unless they are given in a way which allows an unambiguous comparison with data. To answer the question about the agreement between data and models we have chosen to review the available results on a case-by-case basis, rather than trying to draw general conclusions which perhaps would not be valid for the complete set of data [262].

Since the calculation of double-beta-decay observables relies on both the models of electroweak decays and nuclear-structure models the essentials of them will be presented in Sections 2 and 3, basically to clarify the significance of the expressions given in Sections 4 and 5 where the application of the resulting formalism to the two-neutrino and neutrinoless double-beta-decay modes is pursued. Section 6 is devoted to the case-by-case discussion of the known double-beta-decay systems.

The rest of the report has been organized as shown in the table of contents.

2. Weak-interaction Lagrangian

The standard model of the electroweak interactions, due to Weinberg, Salam and Glashow, is perhaps the most illustrative example about a theory based on the use of concepts belonging to gauges theories and symmetry-breaking mechanisms with a solid bearing with nature. In spite of its

success the theory, however, relies upon a number of premises which may (or may not) remain valid if new scenarios about neutrino-mass hierarchies, right-handed interactions and lepton-flavour mixing are introduced. If the standard model, which allows for quark-flavour mixing but not lepton-flavour mixing, which allows for left-handed doublets of leptons, but not right-handed ones, is viewed as a sort of low-energy limit of a more general theory then the question about the nature and quality of the experimental probes of this more general theory would immediately be raised. Nuclear double-beta-decay transitions are one of these experimental probes. However, the difficulties inherent in the detection of these decays are amplified by the difficulties related to the model-dependent theoretical analysis of the data. A review of the possibilities offered by the current versions of the standard model and its extensions can be found in Refs. [46,179]. In order to facilitate the theoretical analysis of the data we have restricted in this report the discussion of the theoretical aspects of the physics of the standard model and its extensions to a brief presentation of the (grand-unification) models which are used to extract values of the neutrino-mass shift, the current–current coupling constants and the scale of the symmetry breaking responsible for the neutrino-mass sector of the electroweak lagrangian. Details can be found in Refs. [2,106,179,269].

2.1. *The standard model (SM) and its extensions*

In the standard model of electroweak interactions the neutrinos are described as massless fermions, members of a left-handed doublet. The absence of right-handed neutrinos reflects upon the exclusion of lepton-number violating electroweak transitions, like the neutrinoless double beta decay. In this fashion, only the two-neutrino double beta decay is allowed, since this decay mode is independent of the properties of the neutrinos. The expression for the electroweak lagrangian, in the SU(2)⊗U(1) representation, would thus acquire the familiar V–A structure [109,235] (see also [279]). The use of this lagrangian and the associated weak-interaction hamiltonian h_W in the context of the beta decay has been explored in detail starting from the sixties [34,221,279] and the consequences of the V–A structure of it, as determined by the observables of the nuclear single beta decay, have been discussed in text-books [46,47].

The action of h_W on a pair of nucleons, to produce the sequential decay of them, can be described, say, in the $\beta^-\beta^-$ scenario where from an initial nuclear state (the initial nuclear ground state) one nucleon decays into another nucleon and a pair of leptons (an electron–electron-neutrino pair) is produced and the daughter nucleus is left in the ground state or an excited state (the states of the intermediate nucleus). This transition is a virtual one, since the ground state of the initial nucleus has a lower energy than the intermediate state consisting of the two leptons and the intermediate nucleus. The nuclear double beta decay takes place when a second virtual weak decay is considered between the intermediate and final nuclei. A second pair of leptons is produced and the final decay sequence can (two-neutrino mode) or cannot (neutrinoless mode) conserve lepton number. In the case of lepton-number conservation (two electrons and two electron-neutrinos in the final state) a second-order perturbative treatment of the standard-model hamiltonian, containing only left-handed couplings, suffices for the calculation of the decay rates, since the sequence of virtual decays is allowed by all the selection rules which are controlling the weak decay in the current version of the SM. A sizable hindrance of this decay mode is coming from the final-state four-lepton kinematics which reduces the associated phase space severely.

The case of the interference between the first and second virtual decays is more involved, since it would only be produced if neutrinos do have a mass (resulting from the shift between the Dirac and Majorana masses) or if left–right, right–left and right–right couplings are present in the effective hamiltonian. Even in the presence of right-handed weak currents one still needs a non-zero mass for the neutrino (see the discussion below Eq. (2.10) in this section). The SM does not have these couplings and a non-zero Majorana mass and thus the neutrinoless double beta decay is prohibited in it. The observation of this decay, which has a more favourable phase space than the two-neutrino decay (since only two leptons are found in the final state) and which violates lepton-number conservation, would mean that an extended version of the SM is needed. Moreover, if right-handed currents are observed, by the way of this decay, then new physics should be added to the familiar electroweak sector of the SM lagrangian.

The fact that the neutrino-mass sector of the weak lagrangian can contribute to the neutrino propagator and to the electroweak vertices also opens the way for an exciting possibility, namely that the neutrino-mass sector can be interpreted as the result of a spontaneous symmetry breaking of the local U(1) symmetry corresponding to the original global baryon-number–lepton-number symmetry of the lagrangian. The coupling between leptons and singlet scalar majorons can do the job if the scale of the symmetry breaking does not exceed the value of 100 keV [246] (see also Section 5.2.3). Thus the observation of a majoron-accompanied neutrinoless decay mode would necessarily signal the need of new physics beyond the SM [86,106,269].

The minimal extension of the standard model accommodates right-handed currents and the corresponding couplings between left-handed and right-handed terms [33,84]. These minimal extensions of the SM are quite naturally embedded in the framework of the grand-unification theories (GUT). The most trivial GUT, the SU(5) GUT [115], has been ruled out by experiments on proton decay but several more complicated GUT scenarios are alive and under enthusiastic study at the present [179]. These schemes contain majorana mass for the neutrinos generated by the so-called see-saw mechanism, a simple scheme to generate a left-handed electron neutrino which is mostly consisting of light Majorana-mass eigenstates and a right-handed one mostly consisting of heavy Majorana-mass eigenstates (see [85]). To achieve this the mass-term of the weak-interaction lagrangian is supposed to contain very light ($m_L \sim 0$) left-handed masses, very heavy right-handed ones $m_R \sim M_{GUT} \sim 10^{14}$ GeV and the Dirac masses should be of the order of typical fermion (charged lepton or quark) masses. In the GUT the electron-neutrino majorana mass is expected to be within the range 10^{-4}–10^{-9} eV.

Inspired by the GUT models we start from the most general effective weak-interaction hamiltonian density

$$h_W = (G_F \cos\theta_C/\sqrt{2})(j_{L\mu}J_L^{\mu\dagger} + \kappa j_{L\mu}J_R^{\mu\dagger} + \eta j_{R\mu}J_L^{\mu\dagger} + \lambda j_{R\mu}J_R^{\mu\dagger}) + \text{h.c.}\,, \tag{2.1}$$

where G_F is the Fermi coupling constant ($G_F = 1.16637 \times 10^{-5}$ GeV^{-2}) and θ_C is the mixing angle of Cabibbo–Kobayashi–Maskawa mechanism for mixing quark flavours. In the case of the $\beta^-\beta^-$ decay mode the left- and right-handed leptonic ($j_{L\mu}$, $j_{R\mu}$) currents are given by the well known expressions

$$j_{L\mu} = \bar{e}\gamma_\mu(1 - \gamma_5)\nu_{e,L}\,, \tag{2.2}$$

$$j_{R\mu} = \bar{e}\gamma_\mu(1 + \gamma_5)\nu'_{e,R}\,, \tag{2.3}$$

where the weak eigenstates of the neutrino, $\nu_{e,L}$ and $\nu'_{e,R}$, are given in terms of the mass eigenstates N_{jL} and N_{jR} as

$$\nu_{eL} = \sum_{j=1}^{2N_g} U_{ej} N_{jL} , \tag{2.4}$$

$$\nu'_{eR} = \sum_{j=1}^{2N_g} V_{ej} N_{jR} , \tag{2.5}$$

where N_g is the number of generations and the notation used is the standard one [46,85]. The matrices U and V are the mixing matrices of the weak eigenstates (left- and right-handed electron neutrinos, ν_{eL} and ν_{eR}) and the mass eigenstates (N_{jL} and N_{jR}) of the neutrino. For more discussion about the neutrino mass eigenstates and the mass matrices the reader is referred to [85,153,269]. At the quark level, the expressions for the hadronic currents are given in terms of the u and d quarks as

$$J_L^{\mu\dagger} = \bar{u}\gamma^\mu(1 - \gamma_5)d , \tag{2.6}$$

$$J_R^{\mu\dagger} = \bar{u}\gamma^\mu(1 + \gamma_5)d \tag{2.7}$$

and other quark-flavor terms are absorbed in the definitions of the parameters κ, λ, and η in Eq. (2.1). Further discussion about the hadronic currents is postponed till Section 2.3.

The current–current couplings are specified by the parameters κ, η and λ. The actual values of these coupings can only be determined once specific models for the neutrino mixing and masses of the gauge bosons are defined. Assuming left- and right-handed bosons in the minimal $SU(2)_L \otimes SU(2)_R$ sector of the theory, limits to the current–current couplings can be extracted from neutrinoless double beta decay by averaging the lepton contributions appearing in the electroweak vertices, namely

$$\langle\lambda\rangle = \lambda \frac{g'_V}{g_V} \sum_j{}' U_{ej} V_{ej} , \tag{2.8}$$

$$\langle\eta\rangle = \eta \sum_j{}' U_{ej} V_{ej} . \tag{2.9}$$

The summations are restricted to light-neutrino mass eigenstates (this is indicated by the primed sum) and the matrices U and V are given in Eqs. (2.4) and (2.5). The number of generations is restricted to N_g generations.

The neutrino-mass sector of the weak lagrangian, assuming the same expansion in terms of neutrino-mass eigenstates, can be written

$$\langle m_\nu\rangle = \sum_j{}' \lambda^{CP} m_j |U_{ej}|^2 , \tag{2.10}$$

where λ^{CP} are the CP phases.

From Eq. (2.10) one notices that the neutrinoless double beta decay cannot proceed via the mass mechanism if all neutrinos are massless, i.e. $mj = 0$ for all j. In this case also the right-handed-current mechanism is prohibited as in Eqs. (2.8) and (2.9) the primed sum then includes all the mass

eigenstates and the orthogonality condition [85] $\sum_{j=1}^{2N_\nu} U_{ej}V_{ej} = 0$ kills the contribution. The quantities $\langle\lambda\rangle$ and $\langle\eta\rangle$ are extremely small even when some or all of the neutrinos are massive but light, since then the leading-order contributions of Eqs. (2.8) and (2.9) vanish due to the orthogonality of U and V, and the next-order corrections in the mass-dependent neutrino propagator bring in effective quantities of the form (see [251]) $\lambda\langle m^2\rangle$ and $\eta\langle m^2\rangle$, where $\langle m^2\rangle \equiv \sum_j' m_j^2 U_{ej}V_{ej}$, which are suppressed by m_j^2.

The above-introduced average values of the coupling constants and neutrino-mass shift along with the physical mechanisms contributing to the nuclear double beta decay can be determined only after the matrix elements of the hadronic currents of the interaction h_W are calculated, i.e. when the currents act on nuclear wave functions. Concerning the leptonic sector of the weak hamiltonian the fact that the decay takes place inside a nucleus introduces several modifications, as compared with the free weak decay of a hadron with the production of a lepton pair.

In the present work we shall concentrate on the analysis of double-beta-decay transitions by imposing the following assumptions:

- Leptonic wave functions are restricted mostly to s and p waves, distortions due to the nuclear Coulomb field and atomic electrons are accounted for by Fermi factors and screening corrections (when needed). Unless stated otherwise all partial-wave expansions are limited to low-momentum transfer. The analysis of the decay rates, for the neutrinoless double beta decay, will be performed with and without introducing neutrino potentials which stem from the definition of the neutrino propagator. Averages over the energies of the denominators which appear in the definition of the decay rates will be performed as described in [85].
- The quark content of the decay vertices will be described by the Cabibbo–Kobayashi–Maskawa mixing angle and bare axial-vector (vector) couplings will be used. Recoil effects due to the weak decay of quarks inside a nucleon will be accounted for by effective operators [250]. The form factors of effective beta-decay operators are constructed from a model where the quark-confinement is represented by a scalar harmonic potential [112,149].
- The decoupling of the electron and neutrino variables, at each virtual decay vertex, will be used [85] to calculate lepton form factors separately.

2.2. Leptonic currents

Relativistic electron wave functions are obtained from the s- and p-wave solutions of the Dirac equation including Coulomb effects

$$\psi_s(\varepsilon, \boldsymbol{r}) = \psi_s^{(s1/2)}(\varepsilon, \boldsymbol{r}) + \psi_s^{(p1/2)}(\varepsilon, \boldsymbol{r}) + \psi_s^{(p3/2)}(\varepsilon, \boldsymbol{r}) + \cdots , \tag{2.11}$$

where the index s indicates the spin and

$$\psi_s^{(s1/2)}(\varepsilon, \boldsymbol{r}) = \sqrt{F_0(Z_f, \varepsilon)}\sqrt{\varepsilon + m_e}\begin{pmatrix} \chi_s \\ \dfrac{\sigma\cdot\boldsymbol{p}}{\varepsilon + m_e}\chi_s \end{pmatrix}, \tag{2.12}$$

$$\psi_s^{(p1/2)}(\varepsilon, \boldsymbol{r}) = \sqrt{F_0(Z_f, \varepsilon)}\sqrt{\varepsilon + m_e}\, i(\sigma\cdot\boldsymbol{r})\begin{pmatrix} g_1\dfrac{\sigma\cdot\boldsymbol{p}}{\varepsilon + m_e}\chi_s \\ f_{-1}\chi_s \end{pmatrix}, \tag{2.13}$$

$$\psi_s^{(p3/2)}(\varepsilon, \boldsymbol{r}) = \frac{i}{3}\sqrt{F_1(Z_f, \varepsilon)}\begin{pmatrix} \sqrt{\varepsilon + m_e}[3(\sigma\cdot\boldsymbol{p}) - (\sigma\cdot\boldsymbol{r})(\sigma\cdot\boldsymbol{p})]\chi_s \\ \dfrac{1}{\sqrt{\varepsilon + m_e}}[3(\boldsymbol{r}\cdot\boldsymbol{p})(\sigma\cdot\boldsymbol{p}) - (\sigma\cdot\boldsymbol{r})p^2]\chi_s \end{pmatrix}, \tag{2.14}$$

with

$$g_1 = \frac{\alpha Z_f}{2R} + \frac{\varepsilon + m_e}{3}, \qquad f_{-1} = \frac{\alpha Z_f}{2R} + \frac{\varepsilon - m_e}{3}. \tag{2.15}$$

In the above formulae Z_f is the charge of the decay daughter, m_e is the electron rest mass, ε is the electron energy, χ_s is the usual non-relativistic Pauli spinor and $F_0(Z_f, \varepsilon)$ and $F_1(Z_f, \varepsilon)$ are relativistic Fermi factors which account for the Coulomb interaction between the electron and the daughter nucleus [34] (for more information about $F_0(Z_f, \varepsilon)$ see Section A.1).

It is to be noted that in the lowest order the decay rates of the neutrinoless mode to the final nuclear ground state are calculated using the electron $s_{\frac{1}{2}}$ and $p_{\frac{1}{2}}$ waves in the combinations $s_{\frac{1}{2}} - s_{\frac{1}{2}}$ and $s_{\frac{1}{2}} - p_{\frac{1}{2}}$, and the decay rates to the 2^+ final states by using the $s_{\frac{1}{2}}$ and $p_{\frac{3}{2}}$ waves in the combination $s_{\frac{1}{2}} - p_{\frac{3}{2}}$. In the two-neutrino case, in the lowest order, all the leptons (including the two neutrinos) are in an s-wave state both for the transition to the 0^+ and 2^+ final nuclear states. In the derivation of the decay rate for the two-neutrino mode one can use free Dirac plane waves for the final-state neutrinos.

2.3. Hadronic currents

Assuming the validity of the impulse approximation the leading-order terms of the effective hadronic weak current (β^- decay) can be written as

$$J^{\mu\dagger}_{L/R} = \bar{\Psi}(x)\tau^-(g_V\gamma^\mu - ig_W\sigma^{\mu\nu}q_\nu \mp g_A\gamma^\mu\gamma_5 \pm g_P\gamma_5 q^\mu)\Psi(x), \tag{2.16}$$

where we have denoted by g_V the vector form factor, by g_A the axial-vector form factor, by g_W the weak-magnetism form factor and by g_P the induced pseudoscalar form factor. The quantity $\Psi(x)$ is the nucleon field at the space-time point x. For the β^+ decay τ^- is replaced by τ^+.

The non-relativistic reduction of the above current leads to the replacement of the vector term by $(0, 1)$ and of the axial-vector term by $(\sigma, 0)$, etc. The result of this reduction has been given in Eq. (5.1) in Section 5.

An alternative way of dealing with the renormalized weak nucleon current is to start from a quark model for a nucleon and to try to calculate the nucleon form factors of Eq. (2.16) by folding the quark currents of Eqs. (2.6) and (2.7) with the wave functions of the quarks inside the nucleon. This approach has been chosen in Ref. [250] where the relativistic quark-confinement model of [149] with quark-recoil corrections [112] has been used. In this model one starts from the relativistic harmonic-oscillator 0s wave functions for the up and down quarks (see e.g. [250]). The parameters of this model are fitted such that the model reproduces the ratio of the axial-vector and vector coupling constants $|g_A/g_V|^2 = 1.575$ and the averaged masses of the nucleons and delta isobars. The quark currents can now be folded with these wave functions to yield effective operators, denoted by $\hat{\beta}_\mu(\boldsymbol{R})$ ($\boldsymbol{R}$ is the coordinate of the center-of-mass of a nucleon) on the nucleon

level. These operators can now be Fourier-transformed into the momentum space. These are the operators we are interested in and they have the following structure [250]

$$\hat{\beta}_{\mathrm{F}} = \sum_j \tau_j^- \left(n_\eta \sum_{n=0}^{3} B_{1n} p^{2n} \right), \tag{2.17}$$

$$\hat{\beta}_{\mathrm{VF}} = \sum_j \tau_j^- \sigma_j \times \hat{\boldsymbol{q}} \left(n_\eta \frac{\varepsilon}{\sqrt{3}} \sum_{n=0}^{2} B_{2n} p^{2n+1} \right), \tag{2.18}$$

$$\hat{\beta}_{\mathrm{GT}} = \sum_j \tau_j^- \sigma_j \left(n_\eta \sum_{n=0}^{3} B_{3n} p^{2n} \right), \tag{2.19}$$

$$\hat{\beta}_{\mathrm{T}} = \sum_j \tau_j^- \left[(\sigma_j \cdot \hat{\boldsymbol{q}}) \hat{\boldsymbol{q}} - \frac{\sigma_j}{3} \right] \left((-\tfrac{2}{3}\varepsilon^2 n_\eta) \sum_{n=1}^{3} B_{4n} p^{2n} \right). \tag{2.20}$$

Here we have used the following notation: $p = q/\sqrt{3v}$, where $q = |\boldsymbol{q}|$ is the momentum of the virtual Majorana neutrino emitted in the first decay vertex ($\mathrm{d} \to \mathrm{u} + \bar{\nu} + \mathrm{e}^-$) and absorbed in the second decay vertex ($\mathrm{d} + \bar{\nu} \to \mathrm{u} + \mathrm{e}^-$), and $\hat{\boldsymbol{q}}$ is the correponding unit vector. The normalization factor reads $n_\eta = (1 + 3\varepsilon^2 + \frac{7}{2}\varepsilon^4 + \frac{15}{18}\varepsilon^6)\mathrm{e}^{-p^2/2}$. The values $\varepsilon^2 = 0.154$ and $\sqrt{v} = 247$ MeV are taken from [112]. The recoil coefficients B_k are listed in Ref. [250]. Thus, for each of the beta-decay operators we have a detailed momentum-dependence which arises from the momentum-dependence of the quark-neutrino vertex. Leading-order terms in the momentum yield to the usual definition of the $0\nu\beta\beta$ decay operators. The operators $\hat{\beta}$ include also a tensor part ($\hat{\beta}_{\mathrm{T}}$) and the operator $\hat{\beta}_{\mathrm{VF}}$ which contains both the pseudoscalar and weak-magnetism contributions (this is the recoil contribution of the decaying nucleon to the double-beta-decay rate, as given also by the standard formulation [85] starting from Eq. (2.16)).

One can now take the wavefunction $\psi_i^{(\mathrm{s.p.})}(\boldsymbol{R})$ to represent the motion of the nucleon in a single-particle orbital of the nuclear mean field and obtain the single-particle one-body form factors in the momentum space by folding with the single-particle wave function:

$$F_\mu^{(1,2)}(\boldsymbol{q}) = \int \psi_2^{(\mathrm{s.p.})}(\boldsymbol{R})^* [\hat{\beta}_\mu(\boldsymbol{q}) f^{(\mathrm{s\ or\ p})}(\boldsymbol{R})] \psi_1^{(\mathrm{s.p.})}(\boldsymbol{R}) \mathrm{e}^{i\boldsymbol{q}\cdot\boldsymbol{R}} \mathrm{d}^3 R\,, \tag{2.21}$$

where $f^{(\mathrm{s})}(\boldsymbol{R})$ is unity (s-wave contribution) and $f^{(\mathrm{p})}(\boldsymbol{R})$ is proportional to $\boldsymbol{R}$ (the p-wave contribution).

2.4. Lepton phase-space factors

The lepton phase-space factors are calculated with the wave functions given in Section 2.2. The leptonic currents of Section 2.1 are integrated with these relativistic wave functions and the procedure yields the energy-dependent phase-space factors of [85]. The integrals which are relevant for the present analysis are listed in Appendix A. Since the decoupling of the electron and neutrino contributions to the currents can be rather involved we would like to only sketch the steps which we have followed in obtaining the leptonic phase-space factors. Once the relativistic wave functions are obtained one can perform explicitly the contraction of spin and isospin indices, as it is

usually done in dealing with single-beta-decay transitions [34]. The remaining radial dependence can then be written in terms of multipole moments, as is done with the hadronic currents [47]. The leptonic contribution to the weak decay vertex can then be written as a sum over products of multipole operators and momentum-dependent coefficients (see Appendix B). Integration over the momentum variables yields the final expression for the phase-space factors, as given in Appendix A.

2.5. Second-order perturbative matrix elements for double beta decay

The decay rates for the various double-beta-decay modes (two-neutrino mode, neutrinoless mode, neutrinoless mode with the emission of a majoron, etc.) are calculated as second-order processes in the weak interaction hamiltonian h_{W}. The procedure is rather straightforward, although the algebra can be rather tedious. The reader is kindly referred to the articles of [85,125,259] and the books of [46,122] for details.

In the case of the two-neutrino double beta decay, neglecting isospin mixing, only the axial-vector component will contribute to the weak decay and the associated half-life for a decay to $J_f = 0^+, 2^+$ final states can be written as [84,85]

$$[t_{1/2}^{(2\nu)}(J_f)]^{-1} = \frac{g_{\mathrm{A}}^4(G_{\mathrm{F}}\cos\theta_{\mathrm{C}})^4}{96\ln 2\pi^7 m_{\mathrm{e}}^2} \times |\textstyle\sum_m (J_f^+ \| \sum_i \sigma(i)\tau^{\pm}(i) \| 1_m^+)(1_m^+ \| \sum_i \sigma(i)\tau^{\pm}(i) \| 0_{\mathrm{g.s.}}^+)|^2 \int F_0(Z_f, \varepsilon_1)$$

$$\times F_0(Z_f, \varepsilon_2) D(\bar{K}, \bar{L}) \omega_1^2 \omega_2^2 p_1 p_2 \varepsilon_1 \varepsilon_2 \, \delta(\varepsilon_1 + \varepsilon_2 + \omega_1 + \omega_1 + E_f - M_i) \, \mathrm{d}\omega_1 \, \mathrm{d}\omega_2 \, \mathrm{d}\varepsilon_1 \, \mathrm{d}\varepsilon_2 \,, \quad (2.22)$$

where $F_0(Z_f, \varepsilon)$ is the relativistic Fermi factor (see Section A.1), Z_f the atomic number of the final nucleus of double beta decay,

$$D(\bar{K}, \bar{L}) = \begin{cases} \bar{K}^2 + \bar{L}^2 + \bar{K}\bar{L} & \text{if } J_f = 0 \,, \\ (\bar{K} - \bar{L})^2 & \text{if } J_f = 2 \end{cases} \quad (2.23)$$

and the average quantities $\bar{K}$ and $\bar{L}$ have been defined as

$$\bar{K} = (\varepsilon_1 + \omega_1 + \overline{\Delta E})^{-1} + (\varepsilon_2 + \omega_2 + \overline{\Delta E})^{-1} \,, \quad (2.24)$$

$$\bar{L} = (\varepsilon_1 + \omega_2 + \overline{\Delta E})^{-1} + (\varepsilon_2 + \omega_1 + \overline{\Delta E})^{-1} \,, \quad (2.25)$$

where ω_1, ω_2 are the energies (equal to momenta) of the emitted neutrinos 1 and 2, respectively, and $\varepsilon_1, \varepsilon_2$ (p_1, p_2) are the energies (momenta) of the emitted electrons 1 and 2, respectively. The constants G_{F} and θ_{C} have been defined in connection with Eq. (2.1), and E_f is the energy ($E_f = M_f + E_{\mathrm{exc.}}$, where M_f is the mass of the final nucleus and $E_{\mathrm{exc.}}$ its excitation energy) of the final nucleus. The Gamow–Teller operator $\sum_i \sigma(i)\tau^-(i)$ corresponds to β^- decay and $\sum_i \sigma(i)\tau^+(i)$ to β^+ decay. The averaged intermediate–initial energy difference has been defined as $\overline{\Delta E} \equiv \langle E_m \rangle - M_i$, where M_i is the mass of the initial nucleus and $\langle E_m \rangle$ some average value of the (absolute) energy of the intermediate nucleus. The approximations leading to this expression are the following: (a) lepton energies are smaller than the excitation energies of the nuclear virtual states $|1_m^+\rangle$; (b) Only s-wave leptons are taken into account.

The amplitude for the neutrinoless decay mode is given by

$$R^{(0\nu)}(p_1, p_2) = \sum_{AB=\mathrm{LL,LR,RL}} \frac{G_{\mathrm{W}}^2}{\sqrt{2}} \int \frac{\mathrm{d}^3 q}{2\pi^3} \int \mathrm{d}^3 x\, \mathrm{d}^3 y \frac{\mathrm{e}^{\mathrm{i}q\cdot(x-y)}}{2\omega}$$

$$\times \sum_a \frac{1}{\mu_a(2,1)} \sum_{\rho\sigma} \langle \mathrm{e}^-(\boldsymbol{p}_2)\mathrm{e}^-(\boldsymbol{p}_1)|J^{AB}_{\rho\sigma}(\boldsymbol{x},\boldsymbol{y})|0\rangle \times \langle f|J^{\rho\dagger}_A(\boldsymbol{x})|a\rangle\langle a|J^{\sigma\dagger}_B(\boldsymbol{y})|i\rangle - (1\leftrightarrow 2)\,, \tag{2.26}$$

where $G_{\mathrm{W}} \equiv \frac{1}{\sqrt{2}} G_{\mathrm{F}} \cos\theta_{\mathrm{C}}$ (see Section 2.1) and

$$\mu_a(2,1) = \tfrac{1}{2}(M_f + M_i) + \tfrac{1}{2}\varepsilon_{21} - \omega - E_a\,, \qquad \omega = |q|\,, \qquad \varepsilon_{21} = \varepsilon_2 - \varepsilon_1\,,$$

and

$$J^{\mathrm{LL}}_{\rho\sigma}(\boldsymbol{x},\boldsymbol{y}) = \langle m_\nu\rangle \bar{\psi}_1(\boldsymbol{x})\gamma_\rho(1-\gamma_5)\gamma_\sigma\psi^{\mathrm{C}}_2(\boldsymbol{y}) + 2\langle\eta\rangle q^\mu \bar{\psi}_1(\boldsymbol{x})\gamma_\rho\gamma_\mu\gamma_\sigma\psi^{\mathrm{C}}_2(\boldsymbol{y})\,, \tag{2.27}$$

$$J^{\mathrm{LR}}_{\rho\sigma}(\boldsymbol{x},\boldsymbol{y}) = \langle\lambda\rangle q^\mu \bar{\psi}_1(\boldsymbol{x})(1-\gamma_5)\gamma_\rho\gamma_\mu\gamma_\sigma\psi^{\mathrm{C}}_2(\boldsymbol{y})\,, \tag{2.28}$$

$$J^{\mathrm{RL}}_{\rho\sigma}(\boldsymbol{x},\boldsymbol{y}) = \langle\lambda\rangle q^\mu \bar{\psi}_1(\boldsymbol{x})(1+\gamma_5)\gamma_\rho\gamma_\mu\gamma_\sigma\psi^{\mathrm{C}}_2(\boldsymbol{y})\,. \tag{2.29}$$

As said before, $\langle m_\nu\rangle$, $\langle\lambda\rangle$ and $\langle\eta\rangle$ are averages over neutrino generations, Eqs. (2.8), (2.9) and (2.10), q^μ is the four-momentum of the virtual neutrino, and $\psi_i(\boldsymbol{x})$ are relativistic Coulomb-distorted electron wave functions of Section 2.2. The symbols f, a, and i, stand for the final (f), intermediate (a) and initial (i) nuclear states, M_f, E_a, and M_i being their energies. The quantities ε_i ($i = 1, 2$) are the energies of the emitted electrons. The sum over the index a includes all possible excited states of the intermediate nucleus. The hadronic currents $J^{\mu\dagger}_{\mathrm{L(R)}}$ of Section 2.3 are used to express the many-body form factors $\langle f|J^{\mu\dagger}_A(\boldsymbol{x})|a\rangle$ and $\langle a|J^{\mu\dagger}_B(\boldsymbol{y})|i\rangle$ in terms of nucleon form factors multiplied by the one-body transition densities.

Once the expressions for the hadronic many-body form factors are obtained, the amplitude $R^{(0\nu)}(p_1, p_2)$ can be computed. The form factors are listed in Ref. [250] and they are of the form (see Eq. (2.21))

$$F_{\mathrm{F}}(\hat{\beta}_{\mathrm{F}})\,, \qquad \boldsymbol{F}_{\mathrm{GT}}(\hat{\beta}_{\mathrm{GT}})\,, \qquad \boldsymbol{F}_{\mathrm{VF}}(\hat{\beta}_{\mathrm{VF}})\,,$$

$$\boldsymbol{F}^{(\mathrm{p})}_{\mathrm{F}}(\boldsymbol{R}\hat{\beta}_{\mathrm{F}})\,, \qquad \boldsymbol{F}^{(\mathrm{p})}_{\mathrm{GT}}(\boldsymbol{R}\cdot\hat{\beta}_{\mathrm{GT}})\,, \qquad \boldsymbol{F}^{(\mathrm{p})}_{\mathrm{VF}}(\boldsymbol{R}\cdot\hat{\beta}_{\mathrm{VF}})\,, \qquad \boldsymbol{F}^{(\mathrm{p})}_{\mathrm{GT}}(\boldsymbol{R}\times\hat{\beta}_{\mathrm{GT}})\,, \qquad \boldsymbol{F}^{(\mathrm{p})}_{\mathrm{VF}}(\boldsymbol{R}\times\hat{\beta}_{\mathrm{VF}})\,. \tag{2.30}$$

Here the expression inside parenthesis corresponds to the expression confined within the square brackets in Eq. (2.21). The nuclear matrix elements are then defined by the integral over the neutrino momentum $\boldsymbol{q}$ as

$$M = \int \mathrm{d}^3 q \sum_a \Gamma(\omega, \mu_a) S(F_{ai}, F_{fa})\,, \tag{2.31}$$

where S is a scalar function of the form factors (2.28) for the initial-to-intermediate (ai) and intermediate-to-final (fa) virtual transitions. For more detailed account of the S and Γ factors above see [250].

It has to be noted that since in the formulation of [250] all the leading terms are kept for the various half-life contributions, a great number of different matrix elements and lepton phase-space integrals are generated, more than in the traditional formulation [85] presented in Section 5.2.1, Eqs. (5.2), (5.3), (5.4), (5.5), (5.6), (5.7) and (5.8). In Section 6.1 the results of this method [252] are compared with the results of the traditional approaches obtained from the above-mentioned equations.

3. Nuclear models for double beta decay

General nuclear-structure concepts have been applied to the description of nuclear double-beta-decay (NDBD) transitions, as in the earliest studies by [120,121,125,154,228]. The first calculations of the relevant transition amplitudes were performed by using very limited shell model basis [125,228]. Assuming that the weak-interaction sector of the problem was known to a desired accuracy the emphasis of the early studies was centered upon the way in which nuclear wave functions can be handled to compute nuclear matrix elements of the participant weak-current operators. However, the extracted values of these matrix elements did not compare well with the experimental information which was available at that time (^{48}Ca [31], ^{82}Se [175], ^{128,130}Te [151]) and the same situation prevailed practically until a decade ago [85].

As compared with theoretical studies of the electromagnetic nuclear transitions, like the electric multipole transitions and the magnetic dipole transitions, NDBD transitions were largely unexplored, partly, due to the experimental difficulties inherent in their measurement.

The main drawback of the relatively modest theoretical development was (and still is) the lack of a clear identification of the relevant degrees of freedom which may dominate the physics of NDBD. Recently, with the availability of new experimental results, the situation is changing and the limitations of the theoretical approaches become more evident.

With the exception of very few cases (see, e.g. [58,59,193,282,285]) full-scale shell-model results (i.e. without truncations in the number of configurations emerging from a chosen set of single-particle orbitals) are still missing. Thus one has to rely upon other techniques, like the random phase approximation (RPA) [60,68,124,187,253,275] and its various extensions [203,256]. Because it can be applied to the description of NDBD transitions in heavy nuclei (and most of the NDBD candidates are heavy-mass nuclei) where full shell-model calculations are unfeasible, we shall concentrate mainly on the discussion of the ability and failures of the RPA method to compute NDBD matrix elements. We shall also report on the other methods which can be applied to compute NDBD matrix elements and discuss the features which can be extracted from data.

3.1. Transition operators for double beta decay

The transition operators for double beta decay are obtained from the non-relativistic form of the (effective) hadronic weak β current (see Section 2), with leading-order (independent of the nucleon size) terms of the form

$$\rho_{\mathrm{V}} = g_{\mathrm{V}}\tau^{\pm}\delta(\boldsymbol{r}), \tag{3.1}$$

$$\boldsymbol{j}_{\mathrm{A}} = g_{\mathrm{A}}\tau^{\pm}\sigma\delta(\boldsymbol{r}), \tag{3.2}$$

and velocity-dependent operators of the form

$$\rho_{\rm A} = g_{\rm A}\tau^{\pm}\frac{1}{2c}\left[\delta(\boldsymbol{r})\sigma\cdot\boldsymbol{v} + \sigma\cdot\boldsymbol{v}\delta(\boldsymbol{r})\right], \tag{3.3}$$

$$\boldsymbol{j}_{\rm V} = g_{\rm V}\tau^{\pm}\left\{\frac{1}{2c}\left[\delta(\boldsymbol{r})\boldsymbol{v} + \boldsymbol{v}\delta(\boldsymbol{r})\right] + \frac{\hbar}{2Mc}\mu_{\beta}\nabla\times\sigma\delta(\boldsymbol{r})\right\}. \tag{3.4}$$

Since the momentum transfer involved in the decay is low one can perfom the expansion of the weak current in the impulse approximation and get the dominant terms for the allowed (parity-conserving) and the forbidden (parity-changing or -conserving) multipole moments

$$M^{\pm}_{\lambda\mu}(\rho V) = g_{\rm V}\tau^{\pm}f(r)Y_{\lambda,\mu}, \tag{3.5}$$

$$M^{\pm}_{\lambda\mu}(\rho_{\rm A}, \kappa = 0) = \frac{g_{\rm A}}{c}\tau^{\pm}f(r)(\sigma\cdot\boldsymbol{v}Y_{\lambda,\mu}), \tag{3.6}$$

$$M^{\pm}_{\lambda\mu}(j_{\rm A}, \kappa) = g_{\rm A}\tau^{\pm}f(r)(Y_{\kappa}\sigma)_{\lambda\mu}, \tag{3.7}$$

and similarly for the multipole moment associated to the vector part of the current $j_{\rm V}$ (see Ref. [47] for more details).

These operators, which are of the axial (A) or vector (V) type, describe Fermi and Gamow–Teller transitions, at lowest order, and more general vector or axial-vector type of multipole transitions. A list of relevant operators is given in Sections 4 and 5 where they are introduced to describe two-neutrino and neutrinoless double beta decays.

As an example of an allowed single beta decay mediated by the Gamow–Teller operator the transitions between members of a spin–isospin single-particle doublet can be written

$$M(\beta) \equiv (n_2 l_2 j_2\|\sigma\|n_1 l_1 j_1) = -\sqrt{6}\delta_{n_1 n_2}\delta_{l_1 l_2}\hat{j}_1\hat{j}_2(-1)^{j_2+l_1+1/2}W(\tfrac{1}{2}\tfrac{1}{2}j_1 j_2; 1 l_1), \tag{3.8}$$

where $\hat{j} = \sqrt{2j+1}$, and we always stick to the convention of [90] in the definition of the reduced matrix element[1] $(n_f l_f j_f\|O_J\|n_i l_i j_i)$. Here W is the usual Racah coefficient and related to the 6-j symbol as defined in [90]. Evaluating the Racah coefficient yields for a spin-flip transition

$$|M(\beta)_{\text{spin-flip}}| = \sqrt{8 l_1(l_1+1)(2l_1+1)}. \tag{3.9}$$

For the two-neutrino double-beta-decay transitions connecting an initial configuration of two neutrons (both on the same initial single-particle orbital $n_1 l_1 j_1$) with a final one of two protons (both on the same final single-particle orbital n_2, l_2, j_2) belonging to the same spin-isospin

[1] Some authors, e.g. [203,204] etc., use the convention of [212] in definition of the reduced matrix element and the associated Wigner–Eckart theorem.

single-particle doublet yields

$$M_{\mathrm{DGT}} = \frac{M(\beta\beta)}{T/2},$$

$$M(\beta\beta) = (n_2 l_2 j_2 \| \sigma \| n_1 l_1 j_1)(n_2 l_2 j_2 \| \sigma \| n_1 l_1 j_1) \begin{Bmatrix} j_2 & 1 & j_1 \\ 1 & j_2 & 0 \end{Bmatrix}$$

$$= -\sqrt{3}(n_2 l_2 j_2 \| \sigma \| n_1 l_1 j_1)^2 \hat{j}_1^{-1} \hat{j}_2^{-1}. \tag{3.10}$$

Above we have approximated the energy denominator of the double Gamow–Teller matrix element (M_{DGT}) of the two-neutrino NDBD by $\frac{1}{2}T$, where T is the decay energy (Q value) for the β^- decay of the intermediate nucleus in units of the electron rest mass. The above single-particle configurations represent the extreme single-particle limit in the double and single beta decays (for further details of the various degrees of approximation see Section 4). From this very simple example it can be seen that most of the reduction in the magnitude of the allowed NDBD matrix elements is produced by angular-momentum recoupling.

The corresponding phase-space factors for the two-neutrino NDBD and for the single beta decay can be roughly approximated by the term of highest power in T in their approximate analytical expressions obtained by using the Primakoff–Rosen approximation [198] for the Coulomb distortion of the electron wave function at the nuclear surface. Using expressions (A.8) and (A.11) of Section A.1, one obtains

$$G(\beta\beta) \simeq \tfrac{1}{7} g_0 T^{11}/1980, \tag{3.11}$$

$$G(\beta) \simeq g_{\mathrm{GT}} T^5/30, \tag{3.12}$$

where we have just taken the leading term in order to get a simple order-of-magnitude estimate for the decay rates, and we have approximated $Q_{\beta\beta} \simeq Q_\beta$ which is roughly true if the decay energy of the NDBD is at least few MeV (a better approximation would consist of $Q_{\beta\beta} \simeq Q_\beta - m_e c^2$).

Using the explicit value of Eq. (3.9) the ratio of the involved double-beta and single-beta matrix elements can be approximated as

$$M(\beta\beta)/M(\beta) = \sqrt{3}\hat{j}_1^{-1}\hat{j}_2^{-1}(n_2 l_2 j_2 \| \sigma \| n_1 l_1 j_1)$$

$$\simeq \sqrt{\frac{24 l_1(l_1+1)}{(2l_1+1)(2j_1+1)(2j_2+1)}} = \sqrt{\frac{6}{2l_1+1}} \leq 1. \tag{3.13}$$

If the phase-space factors of Eqs. (3.11) and (3.12) are included, the ratio between the transition half-lives of the NDBD and the single beta decay would be given by

$$t_{1/2}(\beta\beta)/t_{1/2}(\beta) = \frac{G(\beta)}{G(\beta\beta)} \left| \frac{M(\beta)}{M_{\mathrm{DGT}}} \right|^2 = \frac{G(\beta)}{G(\beta\beta)} \frac{T^2}{4} \left| \frac{M(\beta)}{M(\beta\beta)} \right|^2$$

$$\simeq \frac{T^2}{4} \times 462 \frac{g_{\mathrm{GT}}}{g_0} \frac{1}{T^6} = \frac{231}{2} \frac{1}{T^4} \frac{g_{\mathrm{GT}}}{g_0}. \tag{3.14}$$

Taking a typical case, say two-neutrino NDBD of ^{116}Cd for which $Q_\beta \simeq 3$ MeV, we obtain a rough estimate ($g_A = 1.0$)

$$t_{1/2}(\beta\beta)/t_{1/2}(\beta) \simeq 0.097\, g_{GT}/g_0 \simeq 1.3 \times 10^{26}. \tag{3.15}$$

This is to be compared with the corresponding experimental result [42,167]

$$M(\beta\beta)/M(\beta) = 0.83\,,$$
$$t_{1/2}(\beta\beta)/t_{1/2}(\beta) \simeq 3.75 \times 10^{19}\ \text{yr}/14.1\ \text{s} = 8.4 \times 10^{25}\,. \tag{3.16}$$

Above it was seen that in the case of ^{116}Cd the extreme single-particle limit produces an acceptable value for the ratio between the single and double Gamow–Teller matrix elements. However, as seen in the examples of Section 4, summarized in Table 2, the extreme single-particle limit produces far too large values of the absolute NDBD matrix elements and one may conclude that the interactions among nucleons in the nucleus are largely responsible for the observed suppression on the NDBD matrix elements. The main question, of course, will be related to the kind of correlations which one should include in the nuclear hamiltonian in order to reproduce the data. Moreover, as seen from the literature, the way in which these correlations are treated will depend from model to model thus adding more complexity to the problem. We shall address these questions as we proceed with the present section.

3.2. Nuclear matrix elements in the shell-model approach

Shell-model descriptions of the NDBD matrix elements have been obtained by exact diagonalizations performed in limited model spaces (with and without truncations in the configuration space emerging from the single-particle valence space, see e.g. [283]) and approximately, like the ones obtained with the Monte–Carlo shell-model method of [207]. Recent results for the NDBD transitions in the shell-model approach can be found in [59,156,188,248] whereas previous attempts at the shell-model calculation of NDBD observables have been made by Skouras and co-workers [228], Zhao et al. [282,283] and by the Strassbourg–Madrid collaboration [58,209]. The recent observation of the decay of ^{48}Ca and the associated extracted value of the double-beta matrix element [18] allows for a direct comparison between different shell-model results, including those of the Monte–Carlo shell-model approach. This comparison has been done in Section 6.1.

Both the conventional shell-model approach and the Monte–Carlo shell-model method (SMMC) have been tested against each other for the case of ^{48}Ca [207] and also for the case of the deacy of ^{76}Ge [156]. In both cases the agreement is rather good and thus it is concluded that the SMMC could be a good alternative to conventional shell-model treatments. However, the results of the SMMC method are still very sensitive to the extrapolation procedure which has to be used to extract the matrix elements [156] and the uncertainties can be very large, particularly, for the case of heavy systems, like ^{128,130}Te, due to the very small values of the relevant matrix elements for the two-neutrino mode [38,172].

3.3. Nuclear matrix elements in the RPA method

The set of virtual excitations appearing in the matrix elements of the weak-interaction hamiltonian (Section 2.6) can be expressed in terms of particle–hole or two-quasiparticle proton–neutron

configurations [124]. For most cases the experimental information about the spectrum and other properties of the intermediate odd–odd nucleus involved in the double beta decay is limited to few low-lying states. As it has been already discussed, the two-neutrino mode is highly selective and as a consequence of the dominance of allowed virtual Gamow–Teller excitations only states with $J^\pi = 1^+$ will appear in the sum over intermediate states. For the neutrinoless double beta decay, due to the propagator of the virtual neutrino, states with positive or negative parity and with unrestricted values of the angular momentum are allowed in the sum over virtual intermediate states. The microscopic description of these states is a difficult problem and one is naturally forced to make approximations in order to determine the main features of the structure of these states.

The RPA approximation has been widely used to describe the microscopic structure of nuclear excitations, particularly in those cases where the direct application of shell-model techniques is unfeasible. The particle–hole (RPA) and two-quasiparticle (QRPA) versions of it have been systematically applied to nuclear-structure problems since the pioneering works of Brown and Bolsterli [50] and Baranger [29]. The RPA method is by now a matter of books. The essentials of the method can be found in [29,211,215]. For the sake of completeness we shall discuss hereafter the basic elements of the RPA (or QRPA) theory which are needed to describe double-beta-decay observables.

Following the notation of [29,253] the *pn*-excitations of a nucleus with open shells are described by the two-quasiparticle creation (annihilation) operators

$$A^\dagger(pn, JM) = [\alpha_p^\dagger \alpha_n^\dagger]_{JM}; \quad \tilde{A}(pn, JM) = (-1)^{J+M}(A^\dagger(pn, J, -M))^\dagger . \tag{3.17}$$

The linear combination of them defines the one-phonon creation (annihilation) operator

$$Q_{JM}^\dagger(m) = \sum_{pn} [X_{pn}(J^\pi, m)A^\dagger(pn, JM) - Y_{pn}(J^\pi, m)\tilde{A}(pn, JM)] , \tag{3.18}$$

which is acting on the correlated QRPA vacuum. The treatment of pn-excitations in the QRPA basis was introduced by Hableib and Sorensen [124] and since then applied by several authors [60,68,99,100,126,139,187,249,253,275].

The proton–neutron RPA (QRPA) equations have the general form

$$\begin{pmatrix} A & B \\ B & A \end{pmatrix}\begin{pmatrix} X \\ Y \end{pmatrix} = \Omega\begin{pmatrix} 1 & 0 \\ 0 & -1 \end{pmatrix}\begin{pmatrix} X \\ Y \end{pmatrix}, \tag{3.19}$$

where the metric matrix on the right-hand side has a simple diagonal form [211]. In this model the states representing the excited states of a double-odd-mass nucleus are given by a diagonalization procedure where the corresponding amplitudes are determined from the non-hermitian eigenvalue problem associated to the matrix given by the above equation. In the basic form of the proton–neutron QRPA the sub-matrices A and B are given by the equation [253,275]

$$\begin{aligned} A_{pn,p'n'} = {} & \delta_{pp'}\delta_{nn'}(E_p + E_n) - 2g_{\rm pp}G(pnp'n', J)(u_p u_n u_{p'} u_{n'} + v_p v_n v_{p'} v_{n'}) \\ & - 2g_{\rm ph}F(pnp'n', J)(u_p v_n u_{p'} v_n' + v_p u_n v_{p'} u_{n'}) , \end{aligned} \tag{3.20}$$

$$\begin{aligned} B_{pn,p'n'} = {} & 2g_{\rm pp}G(pnp'n', J)(u_p u_n v_{p'} v_{n'} + v_p v_n u_{p'} u_{n'}) \\ & - 2g_{\rm ph}F(pnp'n', J)(u_p v_n v_{p'} u_{n'} + v_p u_n u_{p'} v_{n'}) , \end{aligned} \tag{3.21}$$

where E_p and E_n are the proton and neutron quasiparticle energies and $G(pnp'n', J)$ and $F(pnp'n', J)$ are the particle–particle and particle–hole two-body matrix elements defined by Baranger in [29]. The u and v factors appearing in (3.20) and (3.21) are the usual BCS occupation factors. The coefficients $g_{\rm ph}$ and $g_{\rm pp}$ are overall scaling factors of the two-body matrix elements in the particle–hole and particle–particle channels, respectively. Usually $g_{\rm ph}$ is determined by requiring the QRPA to reproduce the empirical excitation energy [141,142] of the Gamow–Teller giant resonance and $g_{\rm pp}$ is left as a free parameter of the theory or to be fixed by some other means, like by beta-decay or double-beta-decay data.

Several methods have been proposed to evaluate the elements of the forward (A) and backward (B) blocks of the QRPA matrix and we shall extend the discussion of these methods later on. Irrespective of the method used to determine A and B and the eigenvalues of Eq. (3.19) one has to transform the operators appearing in the hadronic sector of the electro-weak current into the quasiparticle basis (this will be done to facilitate the description of the open-shell systems without any loss of generality since one can always take the corresponding limits of the BCS amplitudes associated to vanishing pairing gaps to describe the case of closed-shell systems) and from this basis to the QRPA one.

By adopting the standard BCS transformations between the single-particle and -quasiparticle states, one has for the one-body beta-decay operators (3.5)–(3.7) the structure [253]

$$M^{-}_{\lambda\mu} = \sqrt{\tfrac{1}{3}}\sum_{pn}(p\|M_\lambda\|n)[u_p v_n A^\dagger(pn,\lambda\mu) + v_p u_n \tilde{A}(pn,\lambda\mu) + u_p u_n D(pn,\lambda\mu) - v_p v_n \tilde{D}^\dagger(pn,\lambda\mu)\,, \tag{3.22}$$

$$M^{+}_{\lambda\mu} = -\sqrt{\tfrac{1}{3}}\sum_{pn}(p\|M_\lambda\|n)[v_p u_n A^\dagger(pn,\lambda\mu) + u_p v_n \tilde{A}(pn,\lambda\mu) - v_p v_n D(pn,\lambda\mu) + u_p u_n \tilde{D}(pn,\lambda\mu)]\,, \tag{3.23}$$

where M_λ is the $M^{\pm}_{\lambda}$ operator without the isospin ladder operators $\tau^{\pm}$ and the quasiparticle-pair operators A and $\tilde{A}$ have been defined in Eq. (3.17). Furthermore,

$$D(pn,\lambda\mu) = [\alpha^\dagger_p \tilde{\alpha}_n]_{\lambda\mu}\,; \quad \tilde{D}(pn,\lambda\mu) = (-1)^{\lambda+\mu} D(pn,\lambda,-\mu)\,. \tag{3.24}$$

The pair-creation and -annihilation terms of Eqs. (3.22) and (3.23) can be transformed into the QRPA basis by inverting Eq. (3.18) and its hermitian conjugate for each proton–neutron pair of quasiparticles. The final result of this transformation is given by

$$M^{-}_{\lambda\mu} = \sum_m [\Lambda(m) Q^\dagger_{JM}(m) - \Gamma(m)\tilde{Q}_{JM}(m)]\,, \tag{3.25}$$

with

$$\Lambda(m) = \sqrt{\tfrac{1}{3}}\sum_{pn}(p\|M_\lambda\|n)[u_p v_n X_{pn}(J^\pi,m) - u_n v_p Y_{pn}(J^\pi,m)]\,, \tag{3.26}$$

and

$$\Gamma(m) = \sqrt{\tfrac{1}{3}}\sum_{pn} (p\|M_\lambda\|n)[u_n v_p X_{pn}(J^\pi, m) - u_p v_n Y_{pn}(J^\pi, m)] \,. \tag{3.27}$$

Similar expressions hold for the beta-decay multipole moments $M^+_{\lambda\mu}$. The scattering terms (i.e. terms where the operators $D(pn, \lambda\mu)$ and $D(pn, \lambda, -\mu)$ appear) are neglected since only quasiparticle pairs are included in the QRPA basis. Furthermore, in the QRPA one assumes the so-called quasiboson commutation relations

$$[A(pn, JM), A^\dagger(p'n', J'M')] \equiv \langle \mathrm{BCS}|[A(pn, JM), A^\dagger(p'n', J'M')]|\mathrm{BCS}\rangle$$
$$= \delta_{pp'}\delta_{nn'}\delta_{JJ'}\delta_{MM'} \tag{3.28}$$

for the quasiparticle-pair operators leading to boson commutation relations for the QRPA phonons (see Eq. (3.36)). Above we have denoted by $|\mathrm{BCS}\rangle$ the BCS ground state. This, in turn, yields through Eqs. (3.22) and (3.23) for the β^-- and β^+-decay amplitudes the QRPA expressions

$$(J^\pi, m\|M^-_\lambda\|\mathrm{QRPA}) = \delta_{J\lambda}\sum_{pn} (p\|M_\lambda\|n)[u_p v_n X_{pn}(J^\pi, m) + v_p u_n Y_{pn}(J^\pi, m)] \,, \tag{3.29}$$

$$(J^\pi, m\|M^+_\lambda\|\mathrm{QRPA}) = -\delta_{J\lambda}\sum_{pn} (p\|M_\lambda\|n)[u_n v_p X_{pn}(J^\pi, m) + u_p v_n Y_{pn}(J^\pi, m)] \,, \tag{3.30}$$

where $|\mathrm{QRPA}\rangle$ is the correlated ground state of the QRPA.

QRPA description of the two-neutrino NDBD transitions to excited states has been formulated in [75,119,243]. The general structure of the involved nuclear matrix elements can be found in [13,119,240,259] and the model of [75,243], the multiple-commutator model, will be reviewed in Section 3.4.9 of this report.

Some general features, listed below, can be extracted from the results already obtained by using this (or some other equivalent) approach.

The order of magnitude of the experimentally extracted matrix elements is typically varying from one tenth to one-hundredth the value of the single-particle estimate (for the case of the two-neutrino mode of the NDBD) and about one order of magnitude smaller for the matrix elements contributing to the mass sector of the transition amplitude for the neutrinoless decay. This overall suppression has triggered considerable theoretical efforts since it can be regarded as a signal of some collectivity yet to be identified, brought in by the physics of the NDBD.

Among the few lasting results about the microscopic description of the NDBD one can mention the inclusion of two-particle correlations of the proton–neutron type in the construction of the QRPA matrix equations. These correlations were in fact present in the original formulation of the RPA theory for open-shell nuclei, due to Baranger [29] and were reintroduced more recently by Vogel and collaborators [99,100,275] and by several other groups [68,184,185,187]. With the introduction of these attractive two-particle correlations, which are further renormalized in its quasiparticle form mainly for $J^\pi = 1^+$ proton–neutron channels, the values of the matrix elements are significantly reduced, almost to the point of complete agreement with the matrix elements

extracted from data. However, the relative uncertainties introduced in the results by the renormalization of the attractive isoscalar particle–particle configurations has been pointed out as a major drawback of the model. A decade-long controversy about the physical meaning of such a renormalization and the need to determine the physical value of the renormalization parameter followed the early attempts of Refs. [68,184,185,187].

To honour the truth it must be said that some of the proposed cures for the strong effects upon the NDBD matrix elements due to the above renormalization are, at least, exotic. The physical value of the renormalization parameter affecting the strength of particle-like proton–neutron configurations can be determined from the analysis of single-beta-decay transitions feeding the ground state and some of the excited states of the initial and/or final nuclei involved in the NDBD transitions, as done in Refs. [13,14]. Concerning the physical meaning of the renormalization, a fairly good amount of information has accumulated that indicates that a sort of dynamical symmetry breaking may occur as shown by the break-down of the QRPA approach [70]. Even in this instance the advantages introduced by the above-mentioned renormalization outnumber the shortcomings since the tendency of the attractive p-n correlations to suppress the matrix elements found in the QRPA approach, for realistic values of the just mentioned renormalization [71,184,249,253], has been confirmed by shell-model calculations [100,186], by the use of a generalized-seniority scheme [101] and by other methods, like the ones based on group theory [127–129]. By the other side, the sensitivity of the matrix elements for the neutrinoless NDBD mode, upon the renormalization of 1^+ channels of the proton–neutron interaction, is less manifest.

As said above, several cures for the strong suppression of the two-neutrino nuclear matrix elements have been proposed [160,230,256,280] but none of them is free from ambiguities. We shall discuss these approximations in the next section, as well as other methods to compute NBDB matrix elements.

3.4. Other approximations for the nuclear matrix elements

In this section we shall briefly review some of the approximations found in the literature on the calculation of nuclear matrix elements for the two-neutrino (and for the neutrinoless) double-beta-decay mode. Details about the different approximations can be found in the corresponding references. The calculated results produced by each of them will be presented and discussed in Sections 4 and 6. For the sake of brevity only the essentials of each approximation are presented in this section.

3.4.1. Closure and averages of energy denominators

Though the treatment of nuclear double-beta-decay transitions implies the use of the second-order perturbation theory, which in turn involves the inclusion of a complete set of intermediate nuclear states, as it has been described in Section 2.6, the possibility of defining an effective two-body transition from the initial to the final nucleus implies the replacement of the energy denominators appearing in the expressions of the matrix elements (see Section 4) by an average value. The use of this approximation would then allow for the sum over intermediate states to be carried out exactly using the closure property of a complete set of intermediate states. The physics of this approximation has to do with the possible existence of an excited state which can carry most

of the total strength associated to the transition. The energy of this state could then be determined from the average energy denominator needed to fulfill the equality of the NDBD matrix elements with and without closure.

The results of the use of this approximation, for the case of both the neutrinoless and the two-neutrino modes of nuclear double beta decay, can be found in [125]. This approximation has been shown to work badly for the case of the two-neutrino mode [121,228,264] due to the high sensitivity of the relevant matrix elements upon the chosen set of intermediate virtual states. The available shell-model results [59,188] show that the dependence of the matrix elements upon the low-lying intermediate states is indeed very strong, for the few cases where they have been calculated. Contrary to this, the closure approximation seems to work well for the neutrinoless NDBD. This has been shown by Suhonen et al. [250] by explicitly including the intermediate states into the perturbative expression (see Section 2.6) of the corresponding nuclear matrix elements. The finding of Ref. [250] was later on confirmed by the calculations of [107,196] by using the momentum-space representation [272] of the neutrinoless NBDB matrix elements.

3.4.2. Summation methods for intermediate states

An alternative way of avoiding the summation over intermediate states was proposed in [65]. This method was based on the inversion of the energy denominators appearing in the NDBD-matrix elements and its replacement in terms of a series expansion of commutators. This method, known as the operator expansion method [134,280,281] neglects, however, kinetic energy terms of the commutators. In consequence, the different terms of the expansion do not correspond to an algebra and they cannot be summed up exactly.

The problem of the summation over intermediate virtual excitations, unavoidable in the second-order perturbative expansion from where the nuclear matrix elements stem, was addressed in Refs. [74,102], mostly as the answer to the OEM expansion. By using Lanczos algorithms, at the level of the Greens function introduced to represent the summation over intermediate virtual excitations in the form of a propagator, the inadequacy of the OEM expansion was shown in [102]. A similar result was reported in [74], by using Borel's transformations. It was shown that the sum over intermediate virtual excitations has to be carried out explicitly and that, in agreement with the findings of [102], the OEM fails in yielding physically acceptable values for the matrix elements. A possible cure to the problem of how to include kinetic energy terms in the OEM expansion was reported in [74]. Subsequent applications of this improved version of the intermediate-summation method can be found in [56,129].

3.4.3. Double Gamow–Teller states and the SU(4) Wigner symmetry

In this approach, the strong suppression of the nuclear matrix elements for the NDBD is expected to be produced by the SU(4) selection rules which prohibit the transitions between members of bands with different total spin S and isospin T values. In this scheme the ground state of the final nucleus in a double-beta-decay transition, mediated by allowed operators, belongs to a (S,T) band which differs from the ground state of the initial nucleus, thus making the transition totally suppressed. Thus, the transition strength for the NDBD transitions of the Gamow–Teller or Fermi type should be exhausted by a single state of the final nucleus which displays the structure of a double Fermi or double Gamow–Teller resonance, in a fashion similar to the ordinary beta-decay population of the Isobaric Analogue State or the Giant Gamow–Teller Resonance of the

intermediate nucleus appearing in the decay chain. Sum rules associated with these transitions to "double" states pertaining to a complete SU(4) symmetry have been deduced in Refs. [11,182,274,284,285] and the consequences of this symmetry upon the resulting transitions to Double Analoge or Double Gamow–Teller states have been discussed in [105,274].

However, the presence of spin–orbit and Coulomb interactions in finite nuclei results in breaking of the full SU(4) symmetry, practically over all the periodic mass table. Therefore, the amount of quenching due to a remanent of the symmetry is hard to compute since in addition to this mean-field symmetry breaking one has residual interactions. An interesting but still very preliminarly approach to the treatment and restoration of symmetries, both spontaneous and dynamical, can be found in [265]. The application of the concepts advanced in [265] to the NDBD calculations is in progress [67].

The notion of the SU(4) symmetry breaking has been applied for the calculation of two-neutrino double-beta-decay rates of open-shell nuclei to the final ground state, as proposed in [37,216]. In [216] this scheme of calculation is based on the perturbative breaking of the Wigner supermultiplet SU(4) symmetry by the spin–orbit part of the nuclear mean field. However, the effects of the residual interactions have not been accounted for in the treatment of [216] and the results are somehow demonstrative about the use of concepts related to symmetry-breaking mechanisms. In [37] part of the residual interactions are accounted for but not the spin–orbit splitting of the mean field, and thus no reliable quantitative estimates for the values of the two-neutrino double-beta-decay matrix elements can be given within this scheme. An other point of view has been adopted in [139,157], where the use of the SU(4) symmetry was invoked as a means to account for the suppression of the double-beta-decay rates to the ground state. As said before, the existence of spin–orbit couplings rules out this conception (see also [104] for further discussion of the breaking of the SU(4) symmetry).

3.4.4. Renormalized QRPA

The renormalized version of the QRPA (RQRPA) was first applied to NDBD studies by Toivanen and Suhonen [256]. The method is based on the work of Rowe [214] and the expectation values of the number operator in the QRPA correlated ground state are introduced in the quasi-boson commutators of the QRPA method along the lines of [57,143,146]. In dealing with the QRPA matrices, this amounts to a renormalization of the forward- and backward-going blocks A and B in Eq. (3.19). This renormalization causes a shift of the point where the QRPA becomes unstable against the increase of particle–particle proton–neutron correlations. However, the method introduces an undesirable violation of the QRPA sum-rules. This sum-rule violation has been studied within a solvable model in [131,132] and in realistic shell-model spaces by using either schematic [158] or realistic [257] two-body interactions. To overcome this failure it seems likely that the complete program of the renormalized QRPA approach would have to be refined [4,89].

It is to be mentioned that since [256] several other authors have used the RQRPA method to compute double-beta-decay observables in realistic model spaces using realistic two-body interactions [224,225] and similar formulations have been presented, like the one of [183]. In all these approaches, however, the sum-rule violation is present, more or less pronounced. Like other RPA (QRPA) inspired approaches, the self-consistent treatment of [89,223] aims at the restoration of the Pauli principle by redefining the ground-state occupancies of particle-hole (quasiparticle) states to

take into account the distortion coming from correlations induced by the RPA (or QRPA) phonons. So far, the self-consistent RPA (SCRPA) has concentrated on treating like-particle excitations but a similar method might be feasible to develop also for the proton–neutron-type excitations needed in the NDBD calculations.

3.4.5. Group-theoretical approaches

Although limited to somehow restricted model spaces, the attempts to compute exactly the matrix elements governing NDBD transitions by exploiting group-theoretical methods have been very useful. Starting from the work of Vogel and collaborators [275] and continued in the work of [56,128–133], the study of the role played by fundamental symmetries in the structure of the nuclear matrix elements has attracted considerable attention. These studies have become the source of very interesting considerations about the nature of different approximations and they also shed light on the validity of them. Due to the complexity of the problem, which implies simultaneous use of operators belonging to different groups, like monopole-pair operators, charge-dependent dipole-pair operators, spin-dependent operators, etc., one cannot work with a single group to accommodate all of these operators. Moreover the structure of the single-particle model space would also set limits on the available group representations.

The predictions of exactly solvable models, for the case of Double Fermi and Double Gamow–Teller transitions, show that some of the features found in realistic calculations do have an interpretation in terms of group symmetries. Present group theoretical estimates of NDBD matrix elements are limited to SU(2) [131], SO(5) [132,133] and O(8) representation [104] and results obtained from the application of the pseudo SU(3) scheme for deformed nuclei [127–129] have also been reported.

3.4.6. Proton–neutron pairing interactions

The role of the proton–neutron pairing was investigated for the two-neutrino NDBD of ^{48}Ca by [61] and in the case of description of fp-shell nuclei by [63] using a special Hartree–Fock–Bogoliubov (HFB) method and the associated determination of the proton–neutron pairing strength. The calculation of the nuclear excitations was done by extending the QRPA equations to take into account explicitly the proton–neutron pairing correlations.

The inclusion of proton–neutron pairing interactions, as an additional type of correlations to be considered in the search of a smooth behavior for the model dependence of the nuclear matrix elements for the two-neutrino mode has since then continued [62]. The same sort of approximations have been applied to nuclear-structure calculations of the neutrinoless mode [195]. It has been known for decades that proton–neutron pairing correlations are restricted to a very narrow region of the mass table, where $N \approx Z$ [103,118]. Unless the isospin symmetry of the model hamiltonian is badly broken, proton–neutron pairing correlations are not expected to become dominant in the cases of interest for double-beta-decay transitions. In treating these correlations self-consistently [72,73] most of the effects which have been reported in [195] would most likely be less dramatic.

3.4.7. The multiple-commutator model

The multiple-commutator model (MCM) was introduced in [237] to evaluate beta-decay-transition matrix elements between states of a double-odd nucleus and excited states of the neighboring double-even isobar (nucleus of the same mass number A). In this model the states of

the double-odd nucleus are treated by the proton–neutron QRPA method discussed in Section 3.3 of this report, and the structure of these states is given in Eq. (3.18). At the same time the excited states of the double-even nucleus are obtained from a charge-conserving like-particle (pp-nn) QRPA [29,211] with the following phonon structure

$$|I^\pi M;k\rangle = Q^\dagger_{IM}(k)|\mathrm{QRPA}\rangle$$

$$= \sum_{a,a'} [Z_{aa'}(I^\pi,k)A^\dagger(aa',IM) - W_{aa'}(I^\pi,k)\tilde{A}(aa',IM)]|\mathrm{QRPA}\rangle\,, \tag{3.31}$$

$$A^\dagger(aa',IM) = \frac{1}{\sqrt{1+\delta_{aa'}}}[\alpha^\dagger_a\alpha^\dagger_{a'}]_{IM}\,, \qquad \tilde{A}(aa',IM) = (-1)^{I+M}A(aa',I,-M)\,, \tag{3.32}$$

where a, a' denote all quantum numbers needed to specify a single-quasiparticle harmonic-oscillator state for protons ($a = p$) or neutrons ($a = n$), and k numbers the states with the same angular momentum I and parity π. In the MCM one assumes that the correlated vacua of the two involved QRPA calculations coincide. This is true to a very good approximation since the vacua of both calculations base on the same BCS vacuum and thus both QRPA formalisms have the same leading term in their ground-state wave function as seen from the Thouless-theorem form of the QRPA vacuum in [253].

The transition matrix elements of the charge-changing operators of Eqs. (3.5), (3.6) and (3.7) are given by

$$\begin{aligned}\beta^-_{I\lambda J}(u,v) \equiv (I^\pi_k\|M^-_\lambda\|J^\pi_m) &= 2\sqrt{(2I+1)(2J+1)}(-1)^{I+\lambda+J}\textstyle\sum_{pn}(p\|M_\lambda\|n)\\ &\times\{\textstyle\sum_{p'}W(JIj_nj_p;\lambda j_{p'})[u_nu_pX_{p'n}(J^\pi,m)Z_{pp'}(I^{\pi'},k) - v_nv_pY_{p'n}(J^\pi,m)W_{pp'}(I^{\pi'},k)]\\ &+\textstyle\sum_{n'}(-1)^{n+n'+I}W(JIj_pj_n;\lambda j_{n'})[v_nv_pX_{pn'}(J^\pi,m)Z_{nn'}(I^{\pi'},k)\\ &- u_nu_pY_{pn'}(J^\pi,m)W_{nn'}(I^{\pi'},k)]\}\,,\end{aligned} \tag{3.33}$$

for the decay from the initial state of angular momentum J and parity π of the doubly odd nucleus to the final excited state of angular momentum I and parity π' of the doubly even nucleus. Quantities k and m number the state with the same multipolarity and the factors u and v are the usual BCS occupation factors obtained from the BCS calculation of the even–even daughter nucleus. The symbol W above denotes the ordinary Racah symbol defined e.g. in [90]. For a similar decay to a final state belonging to a two-phonon multiplet $(1/\sqrt{2})[2^+_1\otimes 2^+_1]_I$ (with positive parity $\pi' = +$), made of two lowest quadrupole phonons, the decay amplitude reads

$$\begin{aligned}\beta^-_{I\lambda J}(u,v) \equiv (I^+\|M^-_\lambda\|J^\pi_m) &= \frac{40}{\sqrt{2}}\sqrt{(2I+1)(2J+1)}(-1)^{J+\lambda+1}\\ &\times\sum_{pnp'n'}(p\|M_\lambda\|n)[u_pv_nZ_{pp'}(2^+,1)Z_{nn'}(2^+,1)X_{p'n'}(J^\pi,m)\\ &+ v_pu_nW_{pp'}(2^+,1)W_{nn'}(2^+,1)Y_{p'n'}(J^\pi,m)]\begin{Bmatrix} j_p & j_{p'} & 2\\ j_n & j_{n'} & 2\\ \lambda & J & I\end{Bmatrix}.\end{aligned} \tag{3.34}$$

The corresponding one- and two-phonon expressions for the β^+/EC decay can be obtained from the relation

$$(I_k^{\pi'} \| M_\lambda^+ \| J_m^\pi) = (-1)^{I+r} \beta_{I\lambda J}^-(v, u), \tag{3.35}$$

where $r = 0$ for the vector operators (V) and $r = 1$ for the axial-vector operators (A). Special cases of the above formulae (3.33) and (3.34) are the allowed transitions, $\lambda = 0$(Fermi), 1(Gamow–Teller), $\pi' = \pi$, and the first-forbidden ones, $\lambda = 0, 1, 2$, $\pi' = -\pi$. For further details about the involved operators see [237].

In [206] it is shown that the MCM result of Eq. (3.33) corresponds exactly to the result emerging from a consistent use of boson-expansion theory when implementing both the proton–neutron and the proton–proton and neutron–neutron quasiparticle pairs into a unified framework. A slightly different conclusion is reached for the two-phonon result of Eq. (3.34): the methods of Griffiths and Vogel [119] and the MCM provide similar results although they are conceptually different from each other. This difference concerns the fact that in [119] no use of explicit commutation relations of the involved two-quasiparticle operators are exploited and thus no link with a boson-expansion formalism can be drawn. Moreover, although in the MCM one uses the commutators of the two-quasiparticle operators, the commutation order differs from the one used in the boson-expansion approach and the final results are different in these two approaches.

The MCM was for the first time applied to two-neutrino double beta decay to excited one-phonon states in [243] and one- and two-phonon states in [75]. Later systematical applications were made in the works of [13,257]. In the tables of Section 6 the QRPA results concerning excited final states stem from the MCM calculations even though only the word QRPA is indicated in the tables.

3.4.8. Higher-QRPA approaches

A higher-QRPA (HQRPA for short) approach, based on boson-expansion formalism, was first introduced in the context of two-neutrino double beta decay by Raduta et al. [203,204]. In this model one introduces ordinary proton–neutron QRPA phonons, Eq. (3.18), of multipolarity $L^\pi = 1^+$ (dipole) and like-particle QRPA phonons, Eq. (3.31), of multipolarity $L^\pi = 2^+$ (quadrupole) and treats them as genuine bosons invoking the quasiboson commutation relations (3.28) for the two-quasiparticle operators of Eqs. (3.17) and (3.32). Then

$$[Q_{LM}(k), Q_{L'M'}^\dagger(k')] = \delta_{LL'}\delta_{MM'}\delta_{kk'}, \tag{3.36}$$

where $L,L' = 1,2$ and the phonons are either proton–neutron or like-particle phonons according to their multipolarity (as described above). Here k and k' enumerate phonons of the same multipolarity.

In the HQRPA approach the initial and final ground states of double beta decay base on different BCS vacua, as is the case also with the proton–neutron QRPA approach of Section 3.3. However, in the HQRPA approach the initial and final ground states contain, in addition to the correlated vacuum state, also components corresponding to the like-particle quadrupole phonons ($L^\pi = 2^+$). In the intermediate nucleus, in turn, the state consists of both the proton–neutron dipole phonons as also of the $L^\pi = 2^+$ phonons. In both cases up to two $L^\pi = 2^+$ phonons have been taken into account in these expansions of the initial, intermediate and final states.

In order to evaluate the transition matrix elements of the charge-changing operators of Eqs. (3.5), (3.6) and (3.7) between the initial (final) state and the intermediate states one has to

expand the quasiparticle representation of these operators (see Eqs. (3.22) and (3.23)) in terms of the dipole and quadrupole phonons defined earlier in this section (see Eq. (3.36)). In [203,204] this boson expansion has been taken up to first order, i.e. including one dipole boson and up to two quadrupole bosons into the expansion. The boson-expansion coefficients of the operators are determined by requiring the proton–neutron quasiparticle-pair operators to have the same commutation properties in the quasiparticle and boson representations. Recently this form of the HQRPA has been applied under the name of second-QRPA (SRPA in the tables of Section 6.1) to description of two-neutrino double-beta-decay transitions to the final ground state and excited states in [231–234].

A slightly different type of HQRPA description can be achieved by the boson-mapping method [219]. In this approach one maps the fermion-pair operators of Eqs. (3.18) and (3.31) into boson operators obeying exact boson commutation relations. At the same time one establishes a one-to-one correspondence between the fermion and boson spaces (spanned by one, two, ... ,N bosons or two, four, ... ,$2N$ fermions). The boson image of the fermion hamiltonian can be determined by requiring that the matrix elements of the fermion hamiltonian in the fermion space be equal to the matrix elements of the boson image in the boson space. This mapping can be done exactly to order N requiring equal matrix elements in a fermion space including up to $2N$ fermions and in a boson space including up to N bosons. The same kind of mapping can be performed for the charge-changing operators of Eqs. (3.5), (3.6) and (3.7). After construction of the boson images of the operators it is an easy task to evaluate the hamiltonian and the transition matrix elements since exact boson commutation relations can be exploited. In [219] this mapping method has been used within a schematic model [131] to explore limits of applicability of the HQRPA-type of methods in connection with energy spectra of doubly-odd nuclei, quality of the correlated HQRPA ground state and matrix elements of the charge-changing operators. In addition, conclusions about the HQRPA description of the two-neutrino double beta decay has been drawn.

3.4.9. Other approaches

In this section we list various approaches for description of double-beta-decay observables which are not included in the previous sub-sections of Section 3. We start our discussion from the study of the suppression mechanism of the double Gamow–Teller (DGT) matrix element in terms of its division into spin-flip ($j_p = j_n \pm 1$) and non-spin-flip ($j_p = j_n$) contributions [14,78] (for the DGT matric element the orbital angular momentum l does not change in the single-particle transitions). The interference of these contributions was studied in schematic [78] and realistic [14] models as a function of the strength of the proton–neutron particle–particle interaction, g_{pp} (called κ in the schematic model). It was found in both models that with increasing g_{pp} destructive interference of these contributions increases resulting finally into complete cancellation of the DGT matrix element. Concerning the role of the Gamow–Teller giant resonance state and its components $\mu = 0$ and $\mu = \pm 1$ in this cancellation process the results of [14,78] disagree with the findings of [202] where a very schematic model of Moszkowski [181] was used to study the cancellation mechanisms of the DGT matrix element.

The effect of nuclear deformation on two-neutrino double-beta-decay rates was investigated in [201,205]. In this work a schematic model was used including pairing, spin–isospin and

quadrupole–quadrupole interactions in the model hamiltonian. This hamiltonian was treated by the higher-QRPA formalism [203,204] of Section 3.4.9 in a single-particle basis obtained by angular-momentum projection from an orthogonal set of deformed intrinsic wave functions. In this way the nuclear deformation is brought into the game and behaviour of the double Gamow–Teller (DGT) matrix element can be observed as functions of the deformation and the strength of the proton– neutron particle–particle interaction parameter g_{pp}.

Application of this model to the two-neutrino decay of ^{82}Se to the ground state of ^{82}Kr indicated that the deformation and the magnitude of g_{pp} both contribute to the fragmentation of the β^- strength (left branch of the $\beta^-\beta^-$ decay) but that the deformation also increases the β^+ strength (right branch of the $\beta^-\beta^-$ decay) and shifts it towards lower energies. However, for the adopted common deformation for the mother (^{82}Se) and daughter (^{82}Kr) nuclei the magnitude of the DGT matrix element, as a function of g_{pp}, does not deviate significantly from the spherical case. Especially on the "physical region" of g_{pp} the difference between the deformed and spherical solutions is insignificant. It remains to be seen if larger differences occur for other $\beta^-\beta^-$ decaying nuclei.

A shortcoming of calculations based on quasiparticles is the lack of particle-number conservation. This drawback has been tried to circumvent by using particle-number-projection procedures in Refs. [69–71,159,238,241]. Generally the effects of the particle-number projection seem to be minor for the medium–heavy and heavy nuclei.

4. Two-neutrino double beta decay

This chapter will be devoted to the definition of the half-life expressions, with the associated nuclear matrix elements, for the two-neutrino NDBD, and to the comparison of an extremely simplified nuclear model with available experimental data in a hope for better seeing the overall trends exhibited by the nuclear matrix elements and to make more transparent the results of more realistic theoretical approaches. It has to be noted that no quantitative predictions are expected to evolve by the simple theoretical scheme of this Section, but rather to study if some qualitative features of the NDBD can be understood at the level of a simple-minded model. The results of this simplified model are also discussed in the light of results from more realistic approaches used in the current literature of the NDBD. Both the matrix elements for the ground-state-to-ground-state transitions and ground-state-to-excited-state transitions of the two-neutrino NDBD are discussed.

4.1. Ground-state-to-ground-state transitions

The decay rates for the two-neutrino NDBD ($2\nu\beta\beta$) mode can be easily deduced from Eq. (2.22) assuming that (i) the leptons are in an s-wave state; (ii) lepton energies and nuclear mass differences are replaced by the electron rest-mass energy ($m_e c^2$) and the double-beta Q-value ($Q_{\beta\beta}$) by assuming that the leptons share the phase space equally [85], and (iii) a complete set of virtual excitations of the intermediate double-odd-mass nucleus is included in the second-order perturbative matrix element and the use of closure (see Section 3.4.1) or any other approximation about average energy denominators is avoided.

After integrating over lepton coordinates and summing over nuclear states one obtains for the double-beta-decay half-life

$$[t_{1/2}^{(2\nu)}]^{-1} = G^{(2\nu)}|M_{\mathrm{DGT}}^{(2\nu)}|^2 , \tag{4.1}$$

where the double Gamow–Teller matrix element (DGT) between the initial ($0_{\mathrm{g.s.}}^{(i)}$) and final ($0_{\mathrm{g.s.}}^{(f)}$) ground states is given by

$$M_{\mathrm{DGT}}^{(2\nu)} = \sum_m \frac{(0_{\mathrm{g.s.}}^{(f)} \| \sum_i \sigma(i)\tau^{\pm}(i) \| 1_m^+)(1_m^+ \| \sum_i \sigma(i)\tau^{\pm}(i) \| 0_{\mathrm{g.s.}}^{(i)})}{[\frac{1}{2}Q_{\beta\beta}(0_{\mathrm{g.s.}}^{(f)}) + E(1_m^+) - M_i]/m_{\mathrm{e}} + 1} , \tag{4.2}$$

where $E(1_m^+) - M_i$ is the energy difference between the mth intermediate 1^+ state and the initial ground state and τ^- (τ^+) corresponds to the β^- (β^+/EC) decay the sum $\sum_i$ then running over all the neutrons (protons) of the decaying nucleus. In the above equation all the masses are expressed in energy units and the Q value has been specified for the final ground state (for excited final states its value will be different, naturally). The phase-space integrals $G^{(2\nu)}$, associated with $\beta^-\beta^-$, $\beta^+\beta^-$, β^+EC and ECEC modes, are given in Appendix A. In the above equation we stick to the Gamow–Teller-type virtual transitions since the contribution coming from the Fermi-type virtual transitions has been shown to be small [125] (see also [259]). The above form of the Gamow–Teller operator one obtains from the definition of the beta-decay multipole operators in Eq. (3.7) by taking $f(r) \equiv 1$, $\lambda = 1$, $\kappa = 0$ and including g_{A} and the factors $1/\sqrt{4\pi}$, coming from the spherical harmonics Y_{00}, into the phase-space factor $G^{(2\nu)}$.

In principle, in addition to the allowed DGT contribution, there could be non-negligible contributions coming from the forbidden virtual beta-decay transitions to intermediate states. The lowest-order contributions of this type would be the first-forbidden virtual transitions populating intermediate states of multipolarity 0^-, 1^- and 2^-. Indeed, rather sizable first-forbidden contributions to the double-beta-decay matrix element (4.2) have been found in the calculations of Refs. [30,79]. In [30] population of 0^- and 1^- states in the double beta decay of several nuclei was considered and in [79] unique first-forbidden (UFF) virtual transitions to 2^- intermediate states in the ^{76}Ge decay were analyzed. However, in [79] it was shown that the contribution coming from the UFF channel to the double-beta-decay half-lives can be safely neglected since the accompanied phase-space integrals are suppressed by the factor $(p_{\mathrm{e}}R)^2(p_\nu R)^2$, where R is the nuclear radius and p_{e} (p_ν) is the momentum of the emitted electron (neutrino). In realistic cases the order of magnitude of this factor amounts to less than 10^{-6} suppressing totally the first-forbidden contributions in the decay rates. The suppression is naturally even stronger for virtual transitions of higher forbiddenness.

A compilation of experimental results has been published recently [262] and additional and/or more recent information is also available [7,10,17,18,22–24,26,27,80,81,92]. The overall trend exhibited by data shows that the half-lives for the positive results of the $2\nu\beta\beta$ processes vary between 10^{19} and 10^{21} yr [7,9,91,94–96,98,162,173,266]. That this variation cannot be understood only in terms of phase-space factors has been known already from the earlier studies [85,125,259]. The authors of [125] have used leptonic phase-space factors and simplified shell-model matrix elements (the weak-coupling limit) to evaluate Eq. (4.1) and found far too short half-lives.

We list the relevant phase-space factors in Table 1, both for double β^- (upper part) and β^+/EC transitions to the ground state (lower part).

Table 1
Upper part: Phase-space factors G in units of yr^{-1} (and for $g_A = 1.254$) for the ground-state transitions in the $2\nu\beta^-\beta^-$ case. The quantities T are the Q-values given in units of the electron rest mass. Lower part: The same for the 2vECEC, $2\nu\beta^+EC$ and $2\nu\beta^+\beta^+$ cases. The ε_b are the experimental binding energies for the K atomic shell in units of the electron rest mass

Nucleus	^{48}Ca	^{76}Ge	^{82}Se	^{96}Zr	^{100}Mo	^{116}Cd		
$T(\beta^-\beta^-)$	8.36	3.99	5.86	6.56	5.94	5.48		
$G(\beta^-\beta^-)$	4.0(− 17)	1.3(− 19)	4.3(− 18)	1.8(− 17)	8.9(− 18)	7.4(− 18)		
Nucleus	^{124}Sn	^{128}Te	^{130}Te	^{136}Xe	^{150}Nd			
$T(\beta^-\beta^-)$	4.48	1.70	4.96	4.85	6.59			
$G(\beta^-\beta^-)$	1.5(− 18)	8.5(− 22)	4.8(− 18)	4.9(− 18)	1.2(− 16)			
Nucleus	^{58}Ni	^{78}Kr	^{92}Mo	^{96}Ru	^{106}Cd	^{124}Xe	^{130}Ba	^{136}Ce
T(ECEC)	3.69	5.57	3.14	5.23	5.34	5.48	4.90	4.56
$T(\beta^+EC)$	1.71	3.60	1.18	3.28	3.39	3.54	2.98	2.64
$T(\beta^+\beta^+)$	≤ 0	1.63	≤ 0	1.32	1.44	1.61	1.05	0.72
G(ECEC)	4.3(− 23)	2.0(− 21)	4.1(− 22)	6.9(− 21)	1.6(− 20)	5.1(− 20)	4.1(− 20)	4.0(− 20)
$G(\beta^+EC)$	2.9(− 24)	1.2(− 21)	4.9(− 25)	1.1(− 21)	2.0(− 21)	4.4(− 21)	1.4(− 21)	6.4(− 22)
$G(\beta^+\beta^+)$	—	3.4(− 25)	—	2.7(− 26)	5.0(− 26)	1.2(− 25)	1.2(− 27)	1.4(− 29)
ε_b(exp.)	0.016	0.028	0.039	0.043	0.052	0.066	0.073	0.080

4.1.1. Double β^- transitions

The $\beta^-\beta^-$ decaying systems have nuclear mass differences of the order of 2–5 MeV. By taking the calculated leptonic phase-space factors (see Table 1 and notice that in these tables the energies are given in units of the electron rest mass) one can extract the experimental values of the nuclear matrix elements, $M^{(2\nu)}_{exp}$, which are shown in Table 2. The results of this table show that for ^{116}Cd the single-particle estimate $M^{(2\nu)}_{s.p.}$ (see the discussion accompanying Eqs. (4.3) and (4.4) below) is roughly correct ($d_{3/2} \rightarrow d_{5/2}$ is the dominant single-particle transition) and for ^{100}Mo this estimate yields a far too suppressed matrix element as given by the quantity $R_{s.p.}$ of this table. On the other hand, for the nuclei ^{48}Ca, ^{76}Ge, ^{82}Se and ^{96}Zr the single-particle estimate yields zero value for the matrix elements. These and the ^{100}Mo case are examples of the so-called Pauli-blocking effect, i.e. in nuclei with neutron excess the transitions from the neutron to the proton orbitals are strongly hindered because neutrons and protons occupy different major shells. Furthermore, it is interesting to note that the extracted matrix elements are in many cases (^{128}Te, ^{130}Te, ^{136}Xe, ^{150}Nd) of the order of one tenth of the single-particle estimate. This fact immediately raises the question about the mechanism responsible for this suppression. Possible explanations are configuration mixing, collective effects and Q-value effects (the decay of the isotopes ^{128,130}Te). However, a systematic study shows that, qualitatively, there is not a single explanation for it and that each of the cases has its own particular features. Similar effects have been found in the study of positron emission in neutron-deficient nuclei [249,253] and in β^- decay of neutron-rich systems [242].

Table 2
Single-particle estimates for the DGT matrix elements (column 3) for the $\beta^-\beta^-$ transitions to the g.s. The corresponding s.p. transition is indicated in column 2. Also the experimental half-life and the ratio R between theoretical and extracted matrix elements, $M^{(2\nu)}$(exp.), are shown

Nucleus	s.p. transition	$M^{(2\nu)}_{\text{s.p.}}$	$t^{(2\nu)}_{1/2}$ (exp.)	$M^{(2\nu)}$ (exp.)	$R_{\text{s.p.}}$
^{48}Ca	Not allowed	0	4.3(19)	0.024	...
^{76}Ge	Not allowed	0	1.4(21)	0.074	...
^{82}Se	Not allowed	0	1.1(20)	0.046	...
^{96}Zr	Not allowed	0	3.9(19)	0.038	...
^{100}Mo	$g_{7/2} \to g_{9/2}$	0.011	0.95(19)	0.106	0.10
^{116}Cd	$g_{7/2} \to g_{9/2}$	0.010	3.75(19)	0.059	0.17
	$d_{3/2} \to d_{5/2}$	0.056			0.95
^{124}Sn	$d_{3/2} \to d_{5/2}$	0.355	$> 1.8(17)$	< 1.92	> 0.18
^{128}Te	$d_{3/2} \to d_{5/2}$	0.146	$> 2(24)$	< 0.024	> 6.08
^{130}Te	$d_{3/2} \to d_{5/2}$	0.146	$> 0.8(21)$	< 0.016	> 9.05
^{136}Xe	$d_{3/2} \to d_{5/2}$	0.478	$> 2.3(20)$	< 0.030	> 16.0
^{150}Nd	$d_{3/2} \to d_{5/2}$	0.141	1.7(19)	0.022	6.42

In the following we shall discuss the nuclear matrix elements of Eq. (4.2) by comparing the values extracted from data with the ones obtained by using a very simplified nuclear model. This crudest approximation we shall call the *single-particle estimate* which is solely based on a mass-dependent phenomenological single-particle central potential of the Woods-Saxon type given in Ref. [47], p. 239. In this naive single-particle (s.p.) shell model we use the experimental double-beta-decay Q value and experimental mass-difference between the intermediate and initial nucleus in Eq. (4.2). Only protons and neutrons in one active shell at the respective Fermi surfaces, with occupation (unoccupation) factors given by $v_j = n_{\text{active}}/(2j+1)$ ($u_j = (2j+1-n_{\text{active}})/(2j+1)$), are considered. Due to Coulomb repulsion for protons the proton single-particle potential is shifted upwards in energy with respect to the neutron one and thus the only possible transitions in this scheme are the ones between the neutron and proton spin-flip partners $j_n = l - \frac{1}{2} \to j_p = l + \frac{1}{2}$. Thus, the extreme allowed neutron-to-proton β^- s.p. transition ($\Delta l = 0$, $\Delta j = 0, \pm 1$) from a neutron orbit (l_n, j_n) to a proton one (l_p, j_p) is given by

$$M^{(i)}_{\text{s.p.}} = u_{j_p} v_{j_n} ((j_p j_n) 1^+ \| \sigma \| (j_n j_n) 0^+)_{\text{s.p.}} = u_{j_p} v_{j_n} (-1)^{j_p + j_n} \hat{j}_n^{-1} (j_p \| \sigma \| j_n) , \tag{4.3}$$

where the associated single-particle matrix element of the Pauli operator is given in Eq. (3.8) and otherwise the notation is that of Eq. (4.2). The second branch of the $2\nu\beta^-\beta^-$ matrix element of Eq. (4.2), in turn, is given by

$$M^{(f)}_{\text{s.p.}} = u_{j_p} v_{j_n} ((j_p j_p) J^+ \| \sigma \| (j_p j_n) 1^+)_{\text{s.p.}} = -u_{j_p} v_{j_n} \sqrt{3(2J+1)} \begin{Bmatrix} j_p & 1 & j_n \\ 1 & j_p & J \end{Bmatrix} (j_p \| \sigma \| j_n) . \tag{4.4}$$

Combining now Eqs. (4.3) and (4.4) with the phenomenological energy denominator, and using $J = 0$ in Eq. (4.4) for the ground-state transition, one obtains the single-particle (s.p.) estimates of the double Gamow–Teller (DGT) matrix element of Eq. (4.2) listed in the third column of Table 2.

For ^{48}Ca, ^{76}Ge, ^{82}Se and ^{96}Zr the spin-flip transitions are Pauli-blocked and yield zero value for the corresponding DGT matrix elements. A non-zero value for these matrix elements can be obtained by replacing the sharp neutron and proton Fermi surfaces by a smeared one obtained by the use of e.g. the BCS or HFB (Hartree–Fock–Bogoliubov) approaches for open-shell nuclei. These approaches are the basis for the popular QRPA type of models presented in Section 3 and compared with the data in Section 6.

The extracted values of column five of Table 2 can be compared with the single-particle estimates by introducing polarization factors, like it is done in Ref. [47] for first-forbidden beta-decay transitions or for electromagnetic transitions. For the present case of $2\nu\beta\beta$ transitions a parametrization of the type

$$|M^{(2\nu)}_{\rm exp}| = |M^{(2\nu)}_{\rm theor}|(1 + \kappa) \tag{4.5}$$

does not lead to a universal value of κ. In view of this the observed reduction cannot be due to an overall polarization effect, like the one affecting electromagnetic transitions or single-beta-decay transitions [47]. Also the departure from the single-particle values varies drastically from case to case. This is an indication of a more subtle nuclear-structure mechanism going beyond the s.p. picture. In the study of [105] it has been shown that a single nuclear excitation cannot account for the observed values of the DGT matrix elements. As we shall discuss later, the available information shows that the contributions coming from one of the decay branches are not concentrated on a single state and that for some particular cases the sum of Eq. (4.2) includes several non-negligible contributions. Some experimental support is coming from the study of low-lying structures of the Gamow–Teller strength functions in the (p,n) reactions on ^{76}Ge, ^{82}Se, ^{128}Te and ^{130}Te [171]. Recently a cancellation mechanism consisting of the interference of the components of the Gamow–Teller giant resonance has been discussed in [3]. All of these findings are pointing towards a delicate interplay between nuclear-structure and phase-space limitations which should be analyzed case by case, for the double-beta-decay systems listed in Table 1 (upper and lower parts). Similar conclusions have been reached also by other authors [125].

It is interesting to compare the results of the extreme single-particle model of Table 2 with the results obtained by the use of more sophisticated models. As an example we have selected the case of the $2\nu\beta\beta$ transitions of ^{76}Ge: the g.s. to g.s. two-neutrino double beta decay transition is perhaps one of the most intensively studied transitions of the full set of data reported here. For this transition one knows the experimental half-life by direct measurements [173,266]. The extracted (experimental) matrix element is of the order of 0.14 MeV^{-1} (or 0.22 MeV^{-1} if $g_{\rm A} = 1.0$ is used), while the single-particle value is totally Pauli-suppressed. Note, that in the tables of this section and Section 6 the matrix elements are scaled by the electron rest mass to fit the tabulated (Tables 1 and 3) phase-space factors. As we shall see from the tables shown in Section 6, the standard QRPA method gives 0.18 MeV^{-1}, the corresponding shell model value is 0.68 MeV^{-1} [59] and the Monte–Carlo shell-model approach gives 0.12 ± 0.05 MeV^{-1} [207]. It means that the use of the very simple single-particle shell model alone would not account for the data (this is certainly the case also for most of the other nuclei as seen in Table 2). The RQRPA value is just fitted to yield the experimental value independently of the single-particle basis used to compute it (in [257] the corresponding g_{pp} was used to predict the decay rates to excited states) and the higher-order QRPA calculations give 0.16 MeV^{-1}, a value which is also similar to the standard QRPA result.

Table 3
Upper part: Phase-space factors G in units of yr^{-1} (and for $g_A = 1.254$) for the transitions to the excited 0^+ and 2^+ states in the $2\nu\beta^-\beta^-$ case. The experimental excitation energies are denoted by E and are given in units of MeV. Lower part: The same for the 0_1^+ excited states in the 2νECEC and $2\nu\beta^+$EC cases

Nucleus	^{48}Ca	^{76}Ge	^{82}Se	^{96}Zr	^{100}Mo	^{116}Cd
$E(2_1^+)$	0.983	0.559	0.777	0.778	0.540	1.293
$E(2_2^+)$	2.421	1.217	1.475	1.498	1.362	2.112
$E(0_1^+)$	2.997	1.112	1.488	1.148	1.125	1.757
$G(2_1^+)$	1.1(− 17)	1.2(− 21)	2.1(− 19)	2.1(− 18)	1.7(− 18)	5.8(− 21)
$G(2_2^+)$	6.6(− 21)	9.6(− 25)	1.8(− 21)	6.7(− 20)	1.2(− 20)	5.5(− 25)
$G(0_1^+)$	9.3(− 22)	1.9(− 22)	1.2(− 20)	4.7(− 19)	2.5(− 19)	2.2(− 21)

Nucleus	^{124}Sn	^{128}Te	^{130}Te	^{136}Xe	^{150}Nd
$E(2_1^+)$	0.603	0.441	0.538	0.818	0.334
$E(2_2^+)$	1.326	—	1.205	1.550	1.046
$E(0_1^+)$	1.157	—	1.792	1.580	0.740
$G(2_1^+)$	2.5(− 20)	3.2(− 27)	2.9(− 19)	3.6(− 20)	1.2(− 16)
$G(2_2^+)$	2.8(− 23)	0	1.8(− 21)	3.1(− 23)	3.5(− 18)
$G(0_1^+)$	4.6(− 21)	0	4.6(− 20)	1.2(− 21)	1.2(− 17)

Nucleus	^{58}Ni	^{78}Kr	^{92}Mo	^{96}Ru	^{106}Cd	^{124}Xe	^{130}Ba	^{136}Ce
$E(0_1^+)$	2.258	1.510	1.382	1.148	1.133	1.157	1.792	1.580
G(ECEC)	—	4.7(− 23)	1.9(− 26)	4.2(− 22)	1.1(− 21)	1.9(− 21)	2.5(− 21)	1.3(− 22)
$G(\beta^+\text{EC})$	—	4.4(− 27)	—	2.0(− 25)	6.3(− 25)	1.9(− 24)	1.2(− 25)	—

With such a rich variety of models, and since practically all of them are able to yield to roughly the correct magnitude for the needed matrix element (except for the shell-model results of [59]) one is tempted to conclude that, in spite of the diversity of the models, the strong suppression persists in all of them. Since other observables, when calculated with the same approximations, would show very different results (like electromagnetic quadrupole transitions, etc.) and the most undeniable technique, the shell model, is still overestimating the matrix element (as it should since the true interaction or an adequate valence space are not, of course, available) the only possible conclusion is that the relevant matrix element, for the description of the two-neutrino ground-state-to-ground-state double-beta-decay mode of ^{76}Ge, is ruled by small components of the wave functions which might be insensitive to the approximations, in the presence of the cancellation of the contributions due to the large components. The discussion of the strong suppression found in the QRPA and similar models will be further discussed in Section 6.

4.1.2. Double β^+, β^+EC and ECEC transitions

On the double β^+ side the single-particle transitions are strongly hindered due to the fact that protons cannot decay into neutron states belonging to the same major shell (the Pauli-blocking effect). In the case of double β^+/EC transitions (a generic notation for all the three modes) the first

reasonable approximation for the involved DGT matrix element is the single-quasiparticle one which is obtained by applying, say, the BCS method to smear out the proton and neutron Fermi surfaces.

The low Q-values of the double $\beta^+\beta^+$ (β^+EC) transitions have been a factor which has hindered experiments. However, these transitions are attractive from the experimental point of view due to the possibility to detect either the coincidence signals from four (two) annihilation γ-rays and two (one) positrons, or the annihilation γ-rays only. On the other hand, the Q-value for the 2νECEC process can be large enough (up to ≈ 2.8 MeV) but the detection of the g.s. transition is made difficult since only X-rays are emitted. Early attempts to measure these processes are the experiments of Norman et al. [191,192] and Bellotti et al. [36]. New methods to detect the two-neutrino double K capture to the first excited 0^+ state of the final nucleus was proposed by Barabash [21] and the feasibility of detection of this decay mode was discussed based on calculated nuclear matrix elements [239]. Later, further calculations on the double β^+/EC matrix elements, both for the two-neutrino and neutrinoless modes, were performed [140].

4.2. Transitions to excited states

The experimental efforts to detect 2$\nu\beta\beta$ transitions which, as said above, were concerned mostly with the measurements of g.s. to g.s. transitions have been extended to the measurements of transitions to excited states of the final nuclei [20,22–24,27,28,32,161,197,229,254]. The physics involved in these transitions is indeed very rich since for most of the double-beta-decay systems the low-lying states are collective quadrupole states and also monopole excitations of yet not well-determined structure. In fact, first excited quadrupole states and members of the two-quadrupole-phonon triplet have been for long a subject of experimental and theoretical discussion [6,8,49,163,208,247].

It means that in addition to the microscopic information involved in the description of virtual proton–neutron excitations of the participant intermediate nucleus, one has to supply the microscopic description of one- and two-quadrupole-phonon excitations built of proton–proton and neutron–neutron configurations. From this point of view the theoretical double-beta-decay studies offer new possibilities because in addition to the already described suppression of the g.s. to g.s. transitions one has to explain at the same time a large variety of single-beta-decay and electromagnetic observables.

The best known lower limits for the half-lives of double-beta-decay transitions (two-neutrino mode) to excited states are of the order of $10^{18} \rightarrow 10^{21}$ years for the double β^- transitions and 10^{16}–10^{22} years for double β^+, β^+/EC and ECEC transitions. Phase-space factors and half-lives for these transitions are presented in Tables 3–5 and references for the measurements are given in the tables of Section 6.

Most of these transitions can proceed by double beta decay to the first excited quadrupole state (2_1^+) of the final nucleus and from it by gamma decay to the g.s. In this case the coincidence between the emitted electrons and the gamma ray can be measured. In the case of transitions to higher excited states with $J^\pi = 0^+$ and 2^+ a gamma-ray cascade is measured, instead.

The first theoretical interpretations [75,119,243] which have been advanced about these transitions have shown that the nuclear matrix elements might not be suppressed and could be rather independent of details of the chosen two-body interaction. Thus, the prejudice that

these transitions might not occur (i.e. that the corresponding half-lives would be far beyond the reach of the experiments and thus having only some academic interest), on the basis of energy-denominator and phase-space considerations, seems to be outdated by the present theoretical [13,232,234,248,254,257] and experimental results [20,22,24,27,28,197,254]. These experiments indicate that the most favourable situation would be the one feeding the lowest excited 0^+ (0_1^+ in short) state. This finding is also supported by simple theoretical estimates (see Section 4.2.1) as well as results of more realistic theoretical approaches (see Section 6.1).

One interesting aspect of the transitions to excited final states is that different scenarios can be proposed to describe the structure of the involved final state. As said before, the 0^+ final (excited) state, can be analyzed as a member of a two-quadrupole-phonon triplet but it can also be an intruder (deformed) state, a one-phonon monopole state or even a more exotic state built upon the coexistence between deformed and spherical degrees of freedom. From the experimental side the information about the double beta decay to an excited state, like the 0_1^+ state mentioned above, can be supplemented with information about single-beta-decay feeding of the same state. Therefore one has the possibility of restricting the theoretical models, used to calculate double-beta-decay observables, to those which are also able to reproduce the lateral (single-beta-decay) feeding as well as the electromagnetic transitions between members of the triplet and to the one-phonon and ground state. For examples about this global study see [13] and the example of ^{116}Cd decay in Section 6.3.

In the case of transitions to excited states, the steps (i)–(iii) of Section 4.1 yield to separation of the leptonic phase space and nuclear matrix elements:

$$[t_{1/2}^{(2\nu)}(J_f)]^{-1} = G^{(2\nu)}(J_f)|M_{\mathrm{DGT}}^{(2\nu)}(J_f)|^2 , \tag{4.6}$$

where the nuclear matrix element is given by

$$M_{\mathrm{DGT}}^{(2\nu)}(J_f) = \frac{1}{\sqrt{s}}\sum_m \frac{\langle J_f^+ \| \sum_i \sigma(i)\tau^\pm(i) \| 1_m^+ \rangle \langle 1_m^+ \| \sum_i \sigma(i)\tau^\pm(i) \| 0_{\mathrm{g.s.}}^{(i)} \rangle}{([\frac{1}{2}Q_{\beta\beta}(J_f) + E(1_m^+) - M_i]/m_e + 1)^s} , \tag{4.7}$$

with $s = 1 + 2\delta_{J2}$. The expression for the half-life of the $J_f = 2$ transitions includes a cubic power in the denominator. This dependence is obtained if one assumes that the leptons are in an s-wave state. The notation used above is explained in detail below Eq. (4.2) in Section 4.1. The associated phase-space integrals are given in Appendix A. By using these integrals one obtains the phase-space estimates listed in Table 3, for the cases of interest in this report.

4.2.1. Double β^- transitions

In Tables 4 and 5 single-particle estimates for the $2\nu\beta\beta$ transitions to 2^+ and 0^+ excited final states are shown. These single-particle estimates are obtained from Eq. (4.7) by following the steps which have been introduced in describing the g.s. to g.s. transitions in Section 4.1.1 (in this case $J = 0$ or $J = 2$ in Eq. (4.4)). We also give the ratio R between these numbers and the corresponding numbers extracted from experimental data. Assuming no suppression of the nuclear matrix elements associated with transitions to excited states, and using the phase-space factors of Table 3 (upper part) one obtains the predicted half-lives, $t_{1/2}^{(2\nu)}$(th.), of Tables 4 and 5.

From Tables 4 and 5 one can see that the single-particle estimates for transitions to excited states contradict the data only in the case of decay of ^{150}Nd to $J^\pi = 0_1^+$ excited state in the ^{150}Sm nucleus

Table 4
Single-particle estimates for the DGT matrix elements (column 3) for the $\beta^-\beta^-$ transitions to the 2_1^+ state. The corresponding s.p. transition is indicated in column 2. Also the calculated and experimental half-lives and the ratio R between theoretical and extracted matrix elements, $M^{(2\nu)}$(exp.), are shown

Nucleus	s.p. transition	$M_{\text{s.p.}}^{(2\nu)}(2_1^+)$	$t_{1/2}^{(2\nu)}$(th.)	$t_{1/2}^{(2\nu)}$(exp.)	$R_{\text{s.p.}}$
^{48}Ca	Not allowed	0	∞	—	—
^{76}Ge	Not allowed	0	∞	$> 1.1(21)$	—
^{82}Se	Not allowed	0	∞	$> 1.4(21)$	—
^{96}Zr	Not allowed	0	∞	$> 7.9(19)$	—
^{100}Mo	$g_{7/2} \to g_{9/2}$	0.0016	2.3(23)	$> 1.6(21)$	> 0.08
^{116}Cd	$g_{7/2} \to g_{9/2}$	0.0025	2.8(25)	$> 2.3(21)$	> 0.01
	$d_{3/2} \to d_{5/2}$	0.018	5.3(23)		> 0.07
^{124}Sn	$d_{3/2} \to d_{5/2}$	0.062	1.0(22)	$> 4.1(19)$	> 0.06
^{128}Te	$d_{3/2} \to d_{5/2}$	0.023	5.7(29)	$> 4.7(21)$	$> 9.1(-5)$
^{130}Te	$d_{3/2} \to d_{5/2}$	0.025	5.3(21)	$> 4.5(21)$	> 0.92
^{136}Xe	$d_{3/2} \to d_{5/2}$	0.265	3.9(20)	—	—
^{150}Nd	$d_{3/2} \to d_{5/2}$	0.019	2.3(19)	$> 8.0(18)$	> 0.59

Table 5
As Table 4 for transitions to the 0_1^+ state

Nucleus	s.p. transition	$M_{\text{s.p.}}^{(2\nu)}(0_1^+)$	$t_{1/2}^{(2\nu)}$(th.)	$t_{1/2}^{(2\nu)}$(exp.)	$R_{\text{s.p.}}$
^{48}Ca	Not allowed	0	∞	—	—
^{76}Ge	Not allowed	0	∞	$> 1.7(21)$	—
^{82}Se	Not allowed	0	∞	$> 3(21)$	—
^{96}Zr	Not allowed	0	∞	$> 6.8(19)$	—
^{100}Mo	$g_{7/2} \to g_{9/2}$	0.016	1.6(22)	6.1(20)	0.20
^{116}Cd	$g_{7/2} \to g_{9/2}$	0.018	1.4(24)	$> 2.0(21)$	> 0.04
	$d_{3/2} \to d_{5/2}$	0.106	4.0(22)		> 0.22
^{124}Sn	$d_{3/2} \to d_{5/2}$	0.528	7.8(20)	$> 2.2(18)$	> 0.05
^{128}Te	$d_{3/2} \to d_{5/2}$	0.207	—	—	—
^{130}Te	$d_{3/2} \to d_{5/2}$	0.212	4.8(20)	—	—
^{136}Xe	$d_{3/2} \to d_{5/2}$	1.20	5.7(20)	—	—
^{150}Nd	$d_{3/2} \to d_{5/2}$	0.179	2.6(18)	$> 8.8(18)$	> 1.84

(see Table 5). It has to be noted that for ^{100}Mo one has a positive result for the measurement of the transition to the $J^\pi = 0_1^+$ state [22] for which the single-particle estimate gives a far too suppressed matrix element (Pauli-blocking).

In the case of the NDBD transitions to the 2_1^+ final state the simple single-particle shell model is clearly deficient since in Eq. (4.4) the 2_1^+ state is a simple two-particle state without any collectivity. In reality, in spherical even–even nuclei the 2_1^+ state is a very collective vibrational excitation with a wave function consisting of many two-quasiparticle excitations with amplitudes of the same order of magnitude. For ^{100}Mo, ^{116}Cd, ^{128}Te and ^{130}Te the results of the single-particle shell model are

in the region of estimates coming from more advanced theoretical treatments (see the tables of Section 6.1) whereas for ^{124}Sn, ^{136}Xe and ^{150}Nd the single-particle estimates are far too large, the reduction with respect to the single-particle value being a factor of ten or more. Especially in these cases the collectivity of the 2_1^+ final state seems to play a decisive role.

Also for the 0_1^+ final state one can extract some general properties by looking at the single-particle estimates in Table 5 and comparing them with the results of more realistic calculations of Section 6.1. Comparing the numbers in Tables 4 and 5 with each other reveals that the cubic energy denominator in Eq. (4.7) makes the 2_1^+ matrix elements almost one order of magnitude smaller than the 0_1^+ matrix elements. Comparing the values of Table 5 further with the more realistic results of Section 6.1 reveals that the simple estimate is giving the same order of magnitude of the DGT matrix element as the more realistic models for ^{116}Cd, ^{124}Sn, ^{130}Te and ^{136}Xe but is by two orders of magnitude too large for ^{150}Nd. For ^{100}Mo the simple estimate gives a far too suppressed value for the matrix element due to Pauli-blocking. For all the above nuclei, however, both the simple model and the more sophisticated models predict the 0_1^+ DGT matrix element to be much bigger in magnitude than the 2_1^+ matrix element. In real nuclei the degree of collectivity of the 0_1^+ states is not a trivial issue since the structure of this state can be of two-phonon type, of pairing-vibrational type or something more complicated, as already discussed in Section 4.2. Unfortunately, no experimental data besides the measured rate of decay of ^{100}Mo to the 0_1^+ state in ^{100}Ru exist thus preventing a systematic comparison of the single-particle rates with data.

As discussed earlier in this Section (see the last few paragraphs before the beginning of Section 4.1.2), the example of the g.s. to g.s. NDBD of ^{76}Ge would suggest that the decay amplitude is to certain extent insensitive to the differences in the ways by which the theoretical models approach the problem and most likely depend on small components of the involved wave functions, not very much affected by the different theoretical approaches. Thus, the question about other ways of testing the theoretical predictions rises naturally and has lead to suggestion that the decay to excited states might be less sensitive to small components of the wave functions, an observation first made in [75,243] and later confirmed by other authors [45]. The structure of the MCM matrix elements shown in Eqs. (3.33) and (3.34) seems to confirm this hypothesis, since the products of amplitudes of both the excited states of the intermediate nucleus and the quadrupole state of the final nucleus should be less dependent upon the cancellation of products of single-particle occupation numbers and large and small amplitudes observed in the decay to the ground state.

Relatively large values of the extracted matrix elements are found in the analysis of the decay to the first excited 0^+ state, a result which is particularly significant for the analysis of the decay of ^{100}Mo [119,245], ^{82}Se [254] and ^{116}Cd [197]. In these works the possibility that some of the final states reached by the NDBD transition could belong to a two-quadrupole-phonon triplet was considered and results concerning the decay to an excited monopole state belonging to the triplet have been obtained which show that the associated nuclear matrix element might not only be less sensitive to two-particle correlations but also that it can be larger than expected.

In this respect the possibility of identifying relevant correlations, as emerging from the features of the different decays, namely to the final ground state and to final excited states, together with the simultaneous description of electromagnetic transitions from these excited states of the final nucleus, has raised considerable attention, both experimentally and theoretically [22,75,232,234,245,254]. Adding to the known uncertainties in the calculations, the failure of

a unified QRPA description of GT and electromagnetic transitions for the ^{100}Mo – ^{100}Tc – ^{100}Ru triplet of nuclei was reported in several publications [119,232,234,245].

The coupling of one-quasiparticle (q.p.) states with low-lying collective quadrupole excitations can affect the distribution and the sequence of one-quasiparticle type of levels of odd-mass nuclei [169]. Due to this the low-energy spectrum of an odd-mass nucleus becomes generally more compressed than the unperturbed q.p. one. However, in many cases (see e.g. [255]) the perturbed quasiparticle energies, extracted from data, are very close to the unperturbed ones and they can thus be used to study the underlying single-particle structure near the proton and neutron Fermi surfaces. This can be achieved through a BCS calculation by comparing its results with data on low-lying states of proton- and neutron-odd nuclei. In this way alterations of single-particle energies near the Fermi surface can be controlled and one finally ends up with a single-particle basis which (approximately) reproduces the above-mentioned data. The associated single-particle basis will be later called adjusted basis and used in calculations of the double-beta-decay rates (see Section 6). These new obtained quasiparticle energies can be taken into account on the QRPA level and might lead to more realistic values of the QRPA-phonon energies, both for the even–even and odd–odd nuclei. In particular, this scheme affects vibrational properties of the final nuclei involved in the double-beta decays.

The inclusion of quasiparticle–vibration couplings in the treatment of double beta decay transitions to excited states was suggested in [76,77] and the corresponding formalism has been applied to describe transitions in ^{76}Ge. The results show that the different perturbative corrections added to the leading-order DGT matrix element exhibit a tendency to cancel. Similar results have been obtained long ago, when discussing the influence of charge-conserving and charge-changing vibrational modes upon single beta decay observables [40,41,48].

The features which cannot be accounted for by using the spherical QRPA method are certainly related to deformations in the single-particle potential. This may be the case for the transitions in some Mo and Ru isotopes, where, as a function of increasing neutron number and approaching the double beta decay system at $A = 100$, deformation effects have been identified. In particular, this seems to be the case for ^{100}Ru [150,263]. The same is true for the well-deformed cases, like ^{150}Nd, discussed in Section 6.1.

Another interesting possibility, from the experimental side, is the determination of the single-state dominance [113] by combining measurements of single-beta-decay and EC transitions with double-beta-decay measurements. Examples of this can be found in Refs. [42,113]. The reader is also asked to have a glimpse on the ^{116}Cd-decay example in Section 6.3.

4.2.2. Double β^+, β^+EC and ECEC transitions

As it was already mentioned in Section 4.1.2. The measurements of the 2νECEC (double-electron capture) to the first excited 0^+ state (0_1^+) of the final nucleus seems feasible in the light of both the experimental methods [21] and the magnitude of the involves nuclear matrix elements [13,240]. A series of such measurements has already been launched [27,28] and their results are tabulated in Section 6.2 for the cases of ^{92}Mo and ^{106}Cd.

In Ref. [21] the following estimates were made for the decay half-lives to the 0_1^+ final state: ^{78}Kr (2.4×10^{23} yr), ^{106}Cd ($(2.2–3.9) \times 10^{21}$ yr), ^{124}Xe (3×10^{21} yr) and ^{130}Ba (1.5×10^{23} yr). In these estimates it was assumed that the nuclear matrix elements for transitions to the final ground state and 0_1^+ state have the same magnitude. As seen in the tables for ^{78}Kr, ^{106}Cd and ^{130}Ba, in

Section 6.2, these half-life estimates are in the region of theoretical predictions. The only exception is the case of ^{124}Xe where the theoretical half-life is three orders of magnitude longer than the estimated one. This result immediatly leads to a conclusion that as for the ground-state-to-ground-state transitions, also for transitions to excited final states the nuclear matrix elements do not have a smooth predictable trend but rather vary, sometimes drastically, from case to case.

The conclusion of [21] was that based on the above-mentioned half-life estimates, these processes would be detectable by existing low-background detectors. The measurement is based on the detection of two γ rays of fixed energy coming from the de-excitation of the 0_1^+ final state, according to the scheme

$$(A, Z) + 2e^- \rightarrow (A, Z-2)^* + 2\nu_e \rightarrow \gamma_1 + \gamma_2 \,. \tag{4.8}$$

By using low-background devices based on Ge semiconductor detectors of large volume and 1 kg of the isotope of interest, a sensitivity of about $(3\text{–}5) \times 10^{22}$ yr per 1 yr of measurement could be reached [21]. On these grounds one could expect positive identifications of 0_1^+ transitions in the near future.

Inspecting the tables of Section 6.2 indicates that the theoretically predicted magnitudes of the matrix elements for the transitions to the first quadrupole state, 2_1^+, of the final nucleus are, at least, one order of magnitude smaller than the 0_1^+ matrix elements. This yields the detection of these transitions quite difficult (the available phase-space can be roughly estimated to be one order of magnitude larger than for the 0_1^+ transitions, as seen on the $\beta^-\beta^-$ side from Table 3 (upper part)) and probably excludes their detection in the nearest future.

5. Neutrinoless double beta decay

In Section 2 of this report we have laid the conceptual background of the neutrinoless double beta ($0\nu\beta\beta$) decay: the structure of the most general weak-interaction lagrangian with its connections to different aspects of the Majorana neutrinos. In this section we review briefly different aspects of the neutrinoless double beta decay, mainly those aspects which are essential to understand the discussion of the results of Section 6. Thus, emphasis is put to presentation of the background of those formulae of this section which are used to obtain numerical results in the tables of Section 6.

5.1. General background

The neutrinoless $\beta^-\beta^-$ decay is a process where two electrons are emitted in the final state whereas two positrons are emitted in the neutrinoless $\beta^+\beta^+$ decay. In the mixed mode, β^+EC, only one positron is emitted, and finally, in the ECEC mode, no primary particles are emitted but, instead, various types of secondary particles are emitted (this is required by the energy and momentum conservation in the decay process). These secondary particles emerge from internal pair formation (e^+e^- in the final state), internal electron conversion (e^- in the final state) and emission of one or two photons [88].

The $\beta^-\beta^-$ mode of the neutrinoless double beta decay is by far the most studied one among the above decay modes, both experimentally and theoretically. For this reason we shall concentrate in

this report mostly on this particular mode of decay. As said above, in this decay mode one has the final nucleus and two electrons in the final state. Because the initial state is the 0^+ ground state of the parent nucleus, angular-momentum conservation requires that the spin of the daughter nucleus and the coupled total angular momentum of the two emitted electrons be the same (this way these two angular momenta can be coupled to angular momentum 0). Thus, in the case of the ground-state-to-ground-state decay the total angular momentum J of the emitted electrons has to be $J = 0$ and in the transition to the 2^+ final nuclear state the electrons have to be coupled to $J = 2$. The angular momenta j of the individual electrons can be coupled from their spin, $s = \frac{1}{2}$, and orbital angular momentum l ($l = 0$ is the S-state, $l = 1$ is the P-state, $l = 2$ is the D-state, etc.). In this report we adopt the spectroscopic notation l_j (e.g. $S_{1/2}$, $P_{1/2}$, $P_{3/2}$, etc.) for the angular-momentum content of an electron state.

The mechanism of the neutrinoless $\beta^-\beta^-$ mode is based on the emission of an electron antineutrino $\bar{\nu}_e$ on the first decay vertex ($n \to p + e^- + \bar{\nu}_e$) and its absorption in the second vertex. The absorption part is an inverse β^- decay, $n + \nu_e \to p + e^-$, where electron neutrino, instead of antineutrino is required. The emission and absorption processes yield to exchange of a virtual neutrino (like the virtual photon in the Coulomb interaction) and the associated propagator produces a "neutrino potential". The emission of a neutrino and its absorption as an antineutrino is not possible in the standard electro-weak SU(2) × U(1) model of Weinberg [277], Salam [218] and Glashow [117] where the neutrino and its antineutrino are distinct particles. In addition, the neutrinoless decay always requires the neutrino to have a non-zero mass (see the discussion in [85]). This is one more requirement which the standard model cannot accommodate since its neutrinos are always massless Dirac particles ($\nu \neq \bar{\nu}$). The above requirements can be met by the introduction of a massive Majorana ($\nu = \bar{\nu}$) neutrino, contained quite naturally in several types of theory going beyond the standard model, including different types of grand-unification theories, superstring models, supersymmetric models, etc. Some possible mechanisms are listed in Section 5.1 below.

The first attempt towards grand unification was the SU(5) model of Georgi and Glashow [115]. The unitary group SU(5) is the smallest possible group that contains the SU(2) × U(1) × SU(3) electro-weak-colour group as a sub-group. In this model the gauge bosons are the gluons, the photon, the massive intermediate vector bosons $W^{\pm}$, Z^0, and the superheavy X and Y bosons which can mediate lepton- and baryon-number violating processes. In this model the neutrino is a Dirac particle and only left-handed weak bosons are included. However, this simple scheme of unification is ruled out by its too short predicted life-time (10^{31} yr) for the proton decaying via the X boson. Larger unification groups predict longer life-times for the proton at the same time allowing for right-handed charged weak currents and a Majorana mass for the neutrino. The most popular groups include SO(10) [108,165] and E6 [52,108]. The superstring theories support still larger group structures, e.g. E8 × E8 and SO(32) [106].

In any case, these modern gauge theories, in particular the popular SO(10) GUT, contain massive Majorana neutrinos accompanied by right-handed intermediate bosons mediating right-handed charged weak interactions (the mass of these heavy right-handed bosons is expected to be of the order of 1 TeV and the left-right mixing angle $|\tan \xi| \leq 10^{-5}$–0.035 [244]). In this light it is natural to start with the most general effective weak hamiltonian of Eq. (2.1) with the leptonic currents defined in Eqs. (2.2) and (2.3). The associated hadronic current can be taken to be of the

general form of Eq. (2.16). One can transform this current into its non-relativistic form by the Foldy–Wouthuysen transformation to arrive to the form [110,213]

$$J^{\mu\dagger}_{L/R}(\boldsymbol{x}) = \sum_{n=1}^{A} \tau_n^- \delta(\boldsymbol{x} - \boldsymbol{r}_n) \sum_{k=0,1,\ldots} [g_V V^{(k)\mu} + g_W W^{(k)\mu} \mp g_A A^{(k)\mu} \mp g_P P^{(k)\mu}]_n \,, \tag{5.1}$$

where we have given the expression for the β^- decay, the expression for the β^+ decay being given by replacing τ^- by τ^+. The coefficients $V^{(k)\mu}$, $W^{(k)\mu}$, $A^{(k)\mu}$ and $P^{(k)\mu}$ are given in detail in Table 2 of Ref. [259]. The form factors are denoted by g_V (the vector form factor), by g_A (the axial vector form factor), by g_W (the weak-magnetism form factor) and by g_P (the induced pseudoscalar form factor).

The hamiltonian of Eq. (2.1) with the currents (2.2), (2.3) and (5.1) is the starting point for derivation of the half-life expression of Section 5.2. An alternative way of dealing with the form factors of the nucleonic current is to start directly from the weak charged current on the quark level as was done in Section 2 in Eqs. (2.6) and (2.7). One can then use some suitable quark model of the nucleons to generate the nucleonic form factors. This is the approach chosen in [250] where a relativistic quark confinement model [112] is used to derive the effective nucleonic current and the associated effective one-body β transition operators (see Section 2.3). In this model the strength of the confinement potential and quark masses are fitted to reproduce the experimental ratio of g_A and g_V and the difference in the mass of a nucleon and a delta isobar.

5.2. *Ground-state-to-ground-state transitions*

At its lowest order the neutrinoless $\beta^-\beta^-$ decay to the ground state can proceed through emission of two electrons both in the $S_{1/2}$ state. This is not the case for the excited-state $\beta^-\beta^-$-decay transitions where at least one of the emitted electrons has to have orbital angular momentum and thus this decay mode is suppressed by the angular-momentum barrier. Below we list different mechanisms through which the neutrinoless decays can proceed to the final ground state (and to excited states).

5.2.1. *The two-nucleon mechanism*

In the two-nucleon mechanism of the $\beta^-\beta^-$ decay two neutrons of the decaying nucleus directly convert into two protons. In this sense the decay resembles two ordinary beta decays, except that the emitted neutrino has to be absorbed again in the process. This leads to the "neutrino potential" associated with the virtual neutrino propagator.

Using the general hamiltonian of Eq. (2.1) one can derive the following expression for the decay half-life of a nucleus in a neutrinoless NDBD transition to the final ground state (the derivation has been outlined in [85,88])

$$[t_{1/2}^{(0\nu)}]^{-1} = C_{mm}^{(0)} \left(\frac{\langle m_\nu \rangle}{m_e} \right)^2 + C_{m\lambda}^{(0)} \langle \lambda \rangle \left(\frac{\langle m_\nu \rangle}{m_e} \right) + C_{m\eta}^{(0)} \langle \eta \rangle \left(\frac{\langle m_\nu \rangle}{m_e} \right)$$
$$+ C_{\lambda\lambda}^{(0)} \langle \lambda \rangle^2 + C_{\eta\eta}^{(0)} \langle \eta \rangle^2 + C_{\lambda\eta}^{(0)} \langle \lambda \rangle \langle \eta \rangle \,, \tag{5.2}$$

where we have assumed CP conservation (see [85]), and

$$C_{mm}^{(0)} = G_1^{(0\nu)}(M_{GT}^{(0\nu)})^2(1-\chi_F)^2\,, \tag{5.3}$$

$$C_{m\lambda}^{(0)} = -(M_{GT}^{(0\nu)})^2(1-\chi_F)(S_e\chi_{2-}G_3^{(0\nu)} - \chi_{1+}G_4^{(0\nu)})\,, \tag{5.4}$$

$$C_{m\eta}^{(0)} = (M_{GT}^{(0\nu)})^2\,[S_e\chi_{2+}G_3^{(0\nu)} - \chi_{1-}G_4^{(0\nu)} - S_\beta(\chi_P G_5^{(0\nu)} - S_e\chi_R G_6^{(0\nu)})](1-\chi_F)\,, \tag{5.5}$$

$$C_{\lambda\lambda}^{(0)} = (M_{GT}^{(0\nu)})^2[\chi_{2-}^2 G_2^{(0\nu)} - \tfrac{1}{9}f_e(2S_e\chi_{1+}\chi_{2-}G_3^{(0\nu)} - \chi_{1+}^2 G_4^{(0\nu)})]\,, \tag{5.6}$$

$$C_{\eta\eta}^{(0)} = (M_{GT}^{(0\nu)})^2[\chi_{2+}^2 G_2^{(0\nu)} - \tfrac{1}{9}f_e(2S_e\chi_{1-}\chi_{2+}G_3^{(0\nu)} - \chi_{1-}^2 G_4^{(0\nu)}) - S_e\chi_P\chi_R G_7^{(0\nu)} + \chi_P^2 G_8^{(0\nu)} + \chi_R^2 G_9^{(0\nu)}]\,, \tag{5.7}$$

$$C_{\lambda\eta}^{(0)} = -2(M_{GT}^{(0\nu)})^2\{\chi_{2+}\chi_{2-}G_2^{(0\nu)} - \tfrac{1}{9}f_e[S_e(\chi_{1+}\chi_{2+} + \chi_{1-}\chi_{2-})G_3^{(0\nu)} - \chi_{1-}\chi_{1+}G_4^{(0\nu)}]\}\,. \tag{5.8}$$

In the above formulae we have defined

$$\chi_{1\pm} = \chi_{GTq} \pm 3\chi_{Fq} - 6\chi_T\,, \tag{5.9}$$

$$\chi_{2\pm} = \chi_{GT\omega} \pm \chi_{F\omega} - \tfrac{1}{9}\chi_{\mp}\,. \tag{5.10}$$

Furthermore, the mode-dependent factors assume the form

$$S_e = \begin{cases} +1, & \text{for } \beta^-\beta^- \text{ and } \beta^+\beta^+ \\ -1, & \text{for } \beta^+/\mathrm{EC}\,, \end{cases} \tag{5.11}$$

$$f_e = \begin{cases} +1, & \text{for } \beta^-\beta^- \text{ and } \beta^+\beta^+ \\ 1 - \frac{3\alpha}{2m_e R}, & \text{for } \beta^+/\mathrm{EC}\,. \end{cases} \tag{5.12}$$

$$S_\beta = \begin{cases} +1, & \text{for } \beta^-\beta^-, \\ -1, & \text{for } \beta^+\beta^+ \text{ and } \beta^+/\mathrm{EC}\,. \end{cases} \tag{5.13}$$

In the above formulae $\langle m_\nu\rangle$, $\langle\lambda\rangle$ and $\langle\eta\rangle$ are the effective electron-neutrino mass and effective weak coupling constants for coupling of right-handed lepton current with right-handed and left-handed nucleonic current, respectively, as seen in Eq. (2.1). Their exact definition is given in Section 2, Eqs. (2.8), (2.9) and (2.10). The phase-space factors $G_k^{(0\nu)}$, $k = 1,\ldots,9$, are defined in Section A.3, in Eq. (A.27), and their numerical values are listed in Table 6 for all the $\beta^-\beta^-$ decaying nuclei of interest in this report.

We have defined the ratios χ as ratios of a given matrix element and the double Gamow–Teller (DGT) matrix element. For example $\chi_F \equiv M_F^{(0\nu)}/M_{GT}^{(0\nu)}$ where $M_F^{(0\nu)}$ is the double Fermi (DF) matrix element. These two matrix elements are defined as

$$M_F^{(0\nu)} = \sum_a (0_f^+\|h_+(r_{mn}, E_a)\|0_i^+)\,, \tag{5.14}$$

$$M_{GT}^{(0\nu)} = \sum_a (0_f^+\|h_+(r_{mn}, E_a)\sigma_m\cdot\sigma_n\|0_i^+)\,, \tag{5.15}$$

Table 6
Phase-space integrals $G_i^{(0\nu)}$ of Eqs. (5.3), (5.4), (5.5), (5.6), (5.7) and (5.8) and the majoron phase-space factor $G^{(0\nu M)}$ of Eq. (5.21) in units of yr^{-1} (and for $g_A = 1.254$) for the $0\nu\beta^-\beta^-$ decays discussed in this article. The definitions of [85] have been used (see Sections A.3 and A.4)

Nucleus	$G_1^{(0\nu)}$	$G_2^{(0\nu)}$	$G_3^{(0\nu)}$	$G_4^{(0\nu)}$	$G_5^{(0\nu)}$
^{48}Ca	6.43(− 14)	4.20(− 13)	4.95(− 14)	1.36(− 14)	9.55(− 13)
^{76}Ge	6.31(− 15)	1.04(− 14)	3.58(− 15)	1.22(− 15)	1.91(− 13)
^{82}Se	2.73(− 14)	9.43(− 14)	1.91(− 14)	5.61(− 15)	6.82(− 13)
^{96}Zr	5.70(− 14)	2.46(− 13)	4.27(− 14)	1.18(− 14)	1.46(− 12)
^{100}Mo	1.13(− 13)	4.15(− 13)	8.40(− 14)	2.31(− 14)	4.00(− 12)
^{116}Cd	4.68(− 14)	1.47(− 13)	3.31(− 14)	9.53(− 15)	1.50(− 12)
^{124}Sn	2.58(− 14)	5.50(− 14)	1.64(− 14)	5.09(− 15)	9.45(− 13)
^{128}Te	1.66(− 15)	4.74(− 16)	4.75(− 16)	2.53(− 16)	9.84(− 14)
^{130}Te	4.14(− 14)	1.08(− 13)	2.81(− 14)	8.30(− 15)	1.46(− 12)
^{136}Xe	4.37(− 14)	1.10(− 13)	2.95(− 14)	8.75(− 15)	1.60(− 12)
^{150}Nd	1.94(− 13)	8.80(− 13)	1.54(− 13)	4.02(− 14)	6.25(− 12)

Nucleus	$G_6^{(0\nu)}$	$G_7^{(0\nu)}$	$G_8^{(0\nu)}$	$G_9^{(0\nu)}$	$G^{(0\nu M)}$
^{48}Ca	1.05(− 11)	8.24(− 10)	4.05(− 11)	4.20(− 9)	1.98(− 15)
^{76}Ge	1.46(− 12)	8.81(− 11)	5.92(− 12)	3.28(− 10)	5.86(− 17)
^{82}Se	4.84(− 12)	3.78(− 10)	2.77(− 11)	1.29(− 9)	4.84(− 16)
^{96}Zr	8.89(− 12)	8.19(− 10)	7.01(− 11)	2.39(− 9)	1.24(− 15)
^{100}Mo	1.86(− 11)	2.05(− 9)	2.26(− 10)	4.64(− 9)	8.23(− 16)
^{116}Cd	7.76(− 12)	7.00(− 10)	6.95(− 11)	1.76(− 9)	7.87(− 16)
^{124}Sn	4.76(− 12)	3.87(− 10)	3.93(− 11)	9.52(− 10)	3.13(− 16)
^{128}Te	4.90(− 13)	2.86(− 11)	2.89(− 12)	7.08(− 11)	4.43(− 18)
^{130}Te	7.05(− 12)	6.19(− 10)	6.57(− 11)	1.46(− 9)	5.94(− 16)
^{136}Xe	7.45(− 12)	6.59(− 10)	7.23(− 11)	1.50(− 9)	6.02(− 16)
^{150}Nd	2.61(− 11)	2.98(− 9)	3.68(− 10)	6.02(− 9)	4.66(− 15)

where m and n label the coordinate points of the two weak decays and the neutrino potential $h_+(r, E_a)$ has been defined as

$$h_+(r, E_a) \simeq \frac{R_A}{r}\phi(\bar{A}r)\,, \tag{5.16}$$

and $\bar{A} = E_a - \frac{1}{2}(M_i + M_f)$. Here M_i (M_f) is the nuclear mass of the initial (final) nucleus, E_a the energy of the intermediate state $|a\rangle$ and the function $\phi(r)$ is defined in [259]. In the above definition the neutrino potential has been multiplied by R_A to yield it unitless as in [85]. In the closure approximation $E_a \to \langle E_a \rangle$ and the intermediate summation can be performed relatively easily by defining effective two-body transition operators to be combined with two-step transition densities going through the intermediate J^π states (see, e.g., [185,260]). In this case the matrix elements Eqs. (5.14) and (5.15) have the apparently simple form presented in these equations. Otherwise, one has to do the cumbersome work of expanding the neutrino potentials in multipoles and couple

them with the β transition operators to yield new effective one-body r-dependent transition operators acting at a decay vertex and leading to intermediate states of all multipolarities J^π.

Alternative methods of explicitly including the intermediate states J^π into the calculation are the expansion method of [250] presented briefly in Section 2 of this report, and the momentum-space representation method of [272]. In fact, these two methods are the only ones up to now to include the intermediate summations explicitly into the decay-rate calculations of the neutrinoless double beta decay.

The DGT and DF matrix elements are the ones needed in the mass mode of the neutrinoless double beta decay and they emerge from the leptonic S wave. For the definition of the rest of the S-wave matrix elements, connected with the right-handed current and thus associated with the four-momentum $q^\mu = (\omega, \boldsymbol{q})$ of the virtual neutrino, the reader is referred to [85]. There one also defines the matrix elements related to leptonic P waves. An alternative way of presenting these matrix elements is discussed in Section 2, in connection with the definition of the effective weak operators starting from a relativistic quark-confinement model. The various types of matrix element yield interesting contributions to the double-beta-decay rate. Among the most widely discussed are the recoil contribution and the P-wave contribution (see Refs. [185,250,260]).

5.2.2. Contribution from heavy neutrinos

In the case of propagation of heavy neutrions one has to make in the mass term of Eq. (5.2) the replacement

$$\langle m_\nu \rangle \to \langle m_\nu \rangle + m_e^2 \langle\langle M_\nu^{-1} \rangle\rangle (\chi_{Fh} - \chi_{GTh})/(\chi_F - 1)\,, \tag{5.17}$$

with

$$\langle\langle M_\nu^{-1} \rangle\rangle = \sum_i{}'' \; m_i^{-1} U_{ei}^2\,, \tag{5.18}$$

where the double-primed sum is taken over heavy neutrinos with $m_i \gg 1$ GeV. The ratios χ_{Fh} and χ_{GTh} are defined through division by the ordinary double Gamow–Teller matrix element (as in Section 5.2.1 above) and the matrix elements $M_{Fh}^{(0\nu)}$ and $M_{GTh}^{(0\nu)}$ are defined in [260].

One can estimate the upper limit of the quantity $\langle\langle M_\nu^{-1} \rangle\rangle$ by the use of the experimental lower limit of the decay half-life of the neutrinoless $\beta^-\beta^-$ decay. The obtained limits for $\langle\langle M_\nu^{-1} \rangle\rangle$ are of the order of 5×10^{-8}–5×10^{-7} GeV^{-1} [259].

5.2.3. The majoron-emission mechanism

Violation of the lepton-number symmetry in the context of weak interactions makes neutrino–majoron coupling possible. In general, a majoron is a light or massless boson which couples to Majorana neutrinos and can be emitted in neutrinoless double beta decay, say, in the $\beta^-\beta^-$ mode as

$$2n \to 2p + 2e^- + \phi \quad (\beta^-\beta^-\phi \text{ decay})\,, \tag{5.19}$$

$$2n \to 2p + 2e^- + 2\phi \quad (\beta^-\beta^-\phi\phi \text{ decay})\,. \tag{5.20}$$

In the above processes one or two [180] majorons (ϕ) can be emitted. The "classical" majoron models [64,179] include the triplet majoron [85,86,114,116], the douplet majoron [12,220] and the

singlet majoron [39]. The triplet and douplet majoron models have been ruled out by the recent LEP data [168] but, as shown in [39,246], the singlet-majoron model could contribute significantly to neutrinoless double beta decay. It was found that for the range of scale between 10 and 100 keV of the global $U(1)_{B-L}$ symmetry breaking the Majorana neutrinos can be massive and can couple to majorons and to a scalar partner of the majoron [39]. This mechanism does not bring in any new lepton flavours and is thus not ruled out a priori by the LEP data.

In addition to the above described "classical" majoron models, a host of new majoron models have been deviced [19,53,55]. In these new majoron models a majoron can carry units of leptonic charge [53], majoron does not need to be a Goldstone boson [53] and decays with emission of two majorons can exist [19,180]. Furthermore, a vector majoron model is possible [55].

In the classical and new majoron models the decay half-life can be well approximated by the expression

$$[t_{1/2}^{(0\nu M^0)}]^{-1} = |\langle g_{M^0}\rangle|^{2m}\,(M_{M^0})^2 G^{(0\nu M)}\,, \tag{5.21}$$

where $m = 1$ for the emission of a single majoron ($\beta\beta\phi$ decay) and $m = 2$ for the emission of two majorons ($\beta\beta\phi\phi$ decay), and $\langle g_{M^0}\rangle$ is the effective majoron–majorana–neutrino coupling constant averaged over light-neutrino generations. It is to be noted that in the above half-life formula the effective coupling constant $\langle g_{M^0}\rangle$, the nuclear matrix element M_{M^0} and the phase-space factor $G^{(0\nu M)}$ are different for different adopted majoron models.

The classical majoron models all stem from the following effective majoron–Majorana–neutrino interaction lagrangian [53]

$$L_{\nu\nu\phi} = -\tfrac{1}{4}\sum_{jk} \bar{N}_j[a_{jk}(1-\gamma_5) + b_{jk}(1+\gamma_5)]N_k\phi^* + \text{h.c.}\,, \tag{5.22}$$

where a_{jk} and b_{jk} are coupling strengths between the left- and right-handed components of the various majorana neutrinos N_j. To a good approximation [138] the effective majoron–Majorana–neutrino coupling constant now becomes

$$\langle g_{M^0}\rangle = \sum_{ij}{}' \; U_{ei}U_{ej}b_{ij}\,, \tag{5.23}$$

where the mixing matrix U is defined in Eq. (2.4) of Section 2. In this case the nuclear matrix element in the half-life expression (5.21) reads

$$M_{M^0} = M_{GT}^{(0\nu)}(1-\chi_F) \tag{5.24}$$

and is tabulated in Sections 6.1 and 6.2 for the nuclei under discussion in this report. In this case the phase-space factor $G^{(0\nu M)}$ for majoron emission has been defined in Section A.4 and their numerical values are listed in the last column of Table 6 for all the $\beta^-\beta^-$ decaying nuclei of this report.

For part of the new majoron models the above phase-space factor and nuclear matrix element can be used but most of the new models have a different associated nuclear matrix element and a different phase-space factor (see the discussion in [138]). In [138] a calculation of the new type of nuclear matrix elements and the new phase-space factors was performed. The nuclear model used was the proton–neutron QRPA model (see Section 3.3 of this report). It was found that the new

type of nuclear matrix elements are very much suppressed in comparison with the matrix element of Eq. (5.24). Thus the associated half-lives are much longer than the ones typical of the classical majoron models. In addition, the extracted limits for the coupling coefficients of the new majoron models are much weaker than for the classical ones even if the half-lives would be comparable. This can be seen directly from the differences in the phase-space factors [138]. This leads to the final conclusion that the sensitivity of the double-beta-decay experiments to the new majoron models is extremely weak and thus these models are beyond experimental verification in the near future.

5.2.4. The excited-nucleon mechanism

In the excited-nucleon mechanism, or N^* mechanism (or the delta mechanism), the neutrinoless decay proceeds via delta isobars (Δ^-, Δ^0, Δ^+ or Δ^{++}), the lowest excited states of a nucleon. In this case the weak decays take place within a nucleon or an isobar converting two quarks into two other quarks (adjacent in the isospin projection to the decaying quarks) thus changing the charge state by two units and creating an isobar or a nucleon, respectively. Also isobar-to-isobar decay is possible. The various possible Δ mechanisms include the nucleon-Δ modes

$$2n \xrightarrow{\pi^+,\rho^+} p\Delta^- \xrightarrow{\beta^-\beta^-} 2p + 2e^-, \tag{5.25}$$

$$2n \xrightarrow{\beta^-\beta^-} n\Delta^{++} + 2e^- \xrightarrow{\pi^-,\rho^+} 2p + 2e^-, \tag{5.26}$$

and the Δ–Δ modes

$$2n \xrightarrow{\pi^+,\rho^+} p\Delta^- \xrightarrow{\beta^-\beta^-} p\Delta^+ + 2e^- \xrightarrow{\pi^0,\rho^0} 2p + 2e^-, \tag{5.27}$$

$$2n \xrightarrow{\pi^0,\rho^0} n\Delta^0 \xrightarrow{\beta^-\beta^-} n\Delta^{++} + 2e^- \xrightarrow{\pi^+,\rho^+} 2p + 2e^-, \tag{5.28}$$

where the strong interaction part has been presented by the exchange of π^0, π^+ and ρ^0, ρ^+ mesons between the involved baryons. In the processes (5.25), (5.27) and (5.28) the strong interactions cause the initial nuclear wave function to have a (small) admixture of Δ^- or Δ^0 isobars in it, and in the processes (5.26)–(5.28) the strong interactions cause the existence of an admixture of Δ^+ or Δ^{++} isobars in the final-state wave function of the nucleus. Due to the small probability ($P_\Delta \sim 0.01$) of finding a Δ isobar in the tail of either the initial- or the final-state nuclear wave function, the nucleon-Δ mechanism is suppressed in the neutrinoless $\beta^-\beta^-$ decay proportional to $\sqrt{P_\Delta}$ and the Δ–Δ mechanism proportional to P_Δ [199] with respect to the two-nucleon mechanism. An additional suppression factor comes from the overlap of the (initial or final) nuclear states with and without a Δ admixture [199].

In principle, two properties of the decay compete in determining the decay rate of this mechanism: first, this mode of decay is suppressed by the very large mass difference of the isobar and the nucleon (in nuclear scale of 1 MeV) yielding to low probability of finding an isobar in the initial or final nuclear ground state. Second, the decay rate is enhanced by the shorter distance of propagation (within a *nucleon*) of the virtual neutrino yielding to larger values of the neutrino

potential (see Eq. (5.16)) since it behaves like $1/r$ when $r \to 0$. However, the decay rate associated to this mode is expected to be suppressed as compared with the s-wave two-nucleon mechanism since the two electrons have to be emitted in a $S_{1/2}$–$P_{1/2}$ combination [259]. Interestingly enough, this mode may compete with the two-nucleon mechanism in the case of decay to the 2^+ final state since now in both mechanisms the leading contribution is coming from the $S_{1/2}$–$P_{3/2}$ combination (see Section 5.3).

The contributions coming from the nucleon–Δ mechanisms of Eqs. (5.25) and (5.26) to the neutrinoless $\beta^-\beta^-$ transition $^{48}Ca \to {}^{48}Ti(0^+_{g.s.})$ was studied within an extremely simplified $f_{7/2}$ shell model with renormalized Kuo–Brown interaction matrix elements [164] in Ref. [273]. A constituent quark model with non-static contributions was used for the baryons. In this work it was concluded that such contributions are negligible in comparison with the two-nucleon contribution for any Δ-admixture probability P_Δ. If this is a general result should be further studied for heavier nuclei within more sophisticated theoretical frameworks.

Additional possible mechanisms involving a $\beta^-\beta^-$ decay within a hadron are the decay through pions

$$2n \to np + \pi^- \xrightarrow{\beta^-\beta^-} np + \pi^+ + 2e^- \to 2p + 2e^-, \tag{5.29}$$

which was estimated in [267] to compete in importance with the two-nucleon mechanism.

5.2.5. Double beta decay mediated by supersymmetric particles

One possible mechanism to achieve neutrinoless beta decay is to resort to supersymmetric (SUSY) models with R-parity ($R = (-1)^{3B+L+2S}$, where B is the baryonic charge, L the leptonic charge and S the spin) violation [178]. In Refs. [135–137,270] this SUSY mechanism has been investigated within the minimal supersymmetric standard model (MSSM) with explicit R-parity violation in the superpotential. In [135–137] new supersymmetric contributions to this process were found and the accompanied contributions to the neutrinoless $\beta^-\beta^-$ decay of ^{76}Ge were evaluated using new type of nuclear matrix elements calculated using the proton–neutron QRPA formalism. Using the presently known best experimental lower limit for the half-life of the neutrinoless $\beta^-\beta^-$ decay of ^{76}Ge the authors of [137] were able to obtain constraints for the parameters involved in the R-parity violating MSSM.

In the "traditional" SUSY models of the MSSM type [123,190] the neutrinoless double beta decay was mediated through R-parity conserving gluino and neutralino interactions with quarks, electrons and their superpartners (squarks and selectrons). The R-parity violating MSSM contribution to neutrinoless $\beta^-\beta^-$ decay has been studied in [178,270] and more recently in [135,136] where new supersymmetric mechanisms were added into the decay rate. In the R-parity violating processes the neutrinoless $\beta^-\beta^-$ decay is mediated by selectrons, neutralinos, squarks and gluinos. Additional mechanisms mediated by squarks and sleptons, helping to set more stringent limits to SUSY parameters, were discussed in [15] and analyzed more carefully (from the nuclear-structure point of view) in [137]. The conclusion of [137] was that the works of [15,135,136,178,270] complete the tree-level R-parity violating mechanisms of the MSSM and that stringent limits for the SUSY parameters can be extracted, based on these mechanisms and the experimental half-life limits of the neutrinoless double beta decay.

5.3. Ground-state-to-excited-state transitions

Experimentally, the detection of the $0^+_{g.s.} \to 2^+$ neutrinoless $\beta^-\beta^-$ transitions is made more difficult than the detection of the $0^+_{g.s.} \to 0^+_{g.s.}$ transitions by the less favourable phase space (Q-value and P-wave effects). However, the $0^+_{g.s.} \to 2^+$ transition allows the use of the coincidence method, through the de-excitation γ-ray from the 2^+ state, to clean the experimental spectrum from the background. Also the different sensitivities of these two decay transitions to the coupling strengths of the right-handed currents should encourage the experimentalists to further studies of the $0^+_{g.s.} \to 2^+$ neutrinoless $\beta^-\beta^-$ transitions.

In the two-nucleon mechanism the half-life of the neutrinoless $\beta^-\beta^-$ decay can be written as [259]

$$[t^{(0\nu)}_{1/2}(2^+_f)]^{-1} = G^{(0\nu)}_{1+}(2^+)\left(M_\lambda\langle\lambda\rangle - M_\eta\langle\eta\rangle + M_m\frac{\langle m_\nu\rangle}{m_e}\right)^2 + G^{(0\nu)}_{2+}(2^+)\left(M'_\eta\langle\eta\rangle + M_m\frac{\langle m_\nu\rangle}{m_e}\right)^2$$
$$+ G^{(0\nu)}_{1-}(2^+)\left(M_\lambda\langle\lambda\rangle - M_\eta\langle\eta\rangle - M_m\frac{\langle m_\nu\rangle}{m_e}\right)^2 + G^{(0\nu)}_{2-}(2^+)\left(M'_\eta\langle\eta\rangle - M_m\frac{\langle m_\nu\rangle}{m_e}\right)^2, \qquad (5.30)$$

where the phase-space factors $G^{(0\nu)}_{k\pm}(2^+)$, $k = 1,2$, have been defined in Section A.3 in Eq. (A.52).

The lowest contribution to the neutrinoless transition to the final 2^+ state comes from the $S_{1/2}$–$P_{3/2}$ combination of the emitted electrons. The neutrinoless decay to the final 2^+ state is relatively more sensitive to $\langle\lambda\rangle$ and less sensitive to the mass mode than the decay to the final ground state [125,258]. However, the decay rate of the 2^+ transition in the two-nucleon mode is suppressed by (a) the smaller Q value, (b) the emission of a $P_{3/2}$ electron (the amplitude of a $P_{3/2}$ electron is $\frac{1}{80}$ of the $S_{1/2}$ electron on the surface of a nucleus) and (c) the involved nuclear matrix elements are much smaller than the ones associated with the ground-state transition, as revealed by a nuclear-structure calculation of the ^{76}Ge $\beta^-\beta^-$ decay [258] using the projected mean-field method of [222].

The excited-nucleon mechanism of Section 5.2.4 can become important in the decay rate to 2^+ final states since there the combination $S_{1/2}$–$P_{3/2}$ of emitted electrons is also possible and the involved decay rate is enhanced by the shorter distance of propagation (within a nucleon!) of the virtual neutrino. The propagation effect can be seen from the neutrino potential of Eq. (5.16) which grows like $1/r$ when $r \to 0$ (i.e. when r approaches the length scale of quark separation distance of the order of 0.5 fm). The contribution to the 2^+ transition stemming from the delta isobars in the excited-nucleon mechanism was studied in [258,271]. In these studies the nucleon–Δ mechanisms of Eqs. (5.25) and (5.26) were used as a starting point. In (5.25) one has Δ^- admixtures in the initial nuclear state and in Eq. (5.26) one has Δ^{++} admixtures in the final nuclear state.

In [258] a mean-field method [222] was used to investigate the role of the two-nucleon and nucleon–Δ mechanisms in neutrinoless $\beta^-\beta^-$ transition from ^{76}Ge to the 2^+_1 final nuclear state in ^{76}Se. It was found that in the two-nucleon mechanism the matrix element M_λ of Eq. (5.30) was considerably suppressed due to cancellations among the various parts constituting this matrix element, enhancing the importance of the nucleon–Δ mechanism in determining $\langle\lambda\rangle$ from the half-life expression (5.30). However, it was found that the relative magnitude of the nucleon–Δ mode was much smaller than the rough estimate of [85]. In the case of the coupling proportional to $\langle\eta\rangle$, no cancellations in the two-nucleon-mode matrix element occurs and the contribution from the nucleon–Δ mechanism can be neglected with respect to the two-nucleon contribution.

Furthermore, it was noticed that the upper limits for $\langle\lambda\rangle$ and $\langle\eta\rangle$ emerging from the $0^+_{g.s.} \to 2^+$ decay are much less stringent than the ones coming from the $0^+_{g.s.} \to 0^+_{g.s.}$ transition.

In the work of [271] the nucleon–Δ contribution was studied in the $^{48}Ca \to {}^{48}Ti$ decay using a simple $f_{7/2}$ shell model with renormalized Kuo–Brown interaction matrix elements [164]. In this study it was found that the nucleon–Δ contribution is important, even larger than the two-nucleon contribution, in the rate of the neutrinoless $\beta^-\beta^-$ decay to 2^+ final states in ^{48}Ti. However, the nucleon–Δ contribution was not nearly as large as estimated in [85] due to the very small admixtures (total probability $P_\Delta \sim 10^{-4}$) of Δ isobars in the initial or final nuclear states. The same suppression effect was found in the ordinary β decay in the work of [236] using a realistic nucleon–Δ interaction [189] and an extended QRPA method. In any case, it seems that the nucleon–Δ mechanism should be included into decay-rate studies of $0^+_{g.s.} \to 2^+$ transitions in the neutrinoless double beta decay. Further studies of this assertion for heavier nuclei with more sophisticated nuclear models are called for.

An other important result of the work of [271] was that the contribution of the nucleon–Δ processes is negligible in the case of the $0^+_{g.s.} \to 2^+$ transition in the two-neutrino mode of $\beta^-\beta^-$ decay of ^{48}Ca. Generalization of this statement needs support from other calculations for heavier nuclei.

6. Discussion

In this section we shall comment on the theoretical results for double beta decay on a case-by-case basis. The aim of the section is to present the key results obtained by using different models, i.e. to illustrate the situation in the double-beta-decay matrix-element calculations from the perspective of the theory. In this review we concentrate on recent results and do not try to cover all the history of the double-beta-decay calculations. This is especially true for the transitions to the final ground state where in the two-neutrino mode the QRPA-type calculations lack predictive power and, instead, we concentrate on calculations where also the excited-state transitions are treated simultaneously.

It would be a rather difficult task to pick up all the details for each transition. Since most of the tables are self-explanatory we would like to illustrate, from the results shown in these tables, some of the features which may be considered to be well established by now. The experimental data is compared with the results of the shell model (when available) and the QRPA and its various extensions (see Section 3.4). As stated in the previous paragraph, for the two-neutrino double-beta-decay mode the information also includes the results of transitions to excited final states. The coefficients of the half-life expression (5.2) for the neutrinoless mode are listed, together with the calculated values of the matrix element for the singlet-majoron mode [39,246] of the decay. The half-lives, for neutrinoless modes, have been calculated by assuming (a) a mass term only and (b) a given set of values for the right–left and right–right couplings of the weak hamiltonian. In both cases the most stringent experimental half-life limit [17] has been used to define the upper bounds for the neutrino mass and the coupling parameters.

The questions which we would like to answer, from the collection of results which are presented below, can be summarized as follows:

- Model dependence of the matrix elements for the two-neutrino mode;
- Reliability of the extracted limits for the weak-interaction couplings and neutrino-mass shift.

In all the performed analysis the bare value $g_A = 1.254$ of the axial-vector coupling constant has been used (the phase-space factors in Tables 1, 3 and 6 are given for this value of g_A). This is the value which has been used in most of the earlier calculations of the two-neutrino and neutrinoless modes of double beta decay. For heavy nuclei g_A is expected to renormalize near to its nuclear-matter value $g_A = 1.0$. However, no definite proof of this renormalization and knowledge about the degree of it in the various finite nuclei exists [210]. To avoid such considerations about the degree of renormalization of g_A we stick to the use of the bare value for g_A in the tables of this chapter. If one would like to use some renormalized value of g_A in the analysis of the experimental half-lives it is easy to do because the phase-space factors of Tables 1, 3 and 6 are easily re-evaluated since they scale by g_A^4.

6.1. *The case of* $\beta^-\beta^-$ *decays*

The case of the two-neutrino double beta decay is particularly illustrative about the variety of concepts and approximations which have been used to compute the associated nuclear matrix elements. The need of a test case is then clearly demonstrated by the close agreement which most of the approximations claim to have achieved in spite of their sometimes very different methodological background (see Section 3 and the references therein).

6.1.1. *Decay of* ^{48}Ca

The decay of ^{48}Ca is perhaps one of the most interesting cases, since for it also unrestricted p–f-shell-model results are available (see the references given in Table 7). The calculations listed in Table 7 reproduce the data quite well, particularly for the full p–f-shell-model calculations of [58,282]. Thus, one can compare the results of these shell-model treatments for the neutrinoless decay. The results are shown in Table 8. The coefficients of the half-life expression of Eq. (5.2), which are functions of the various nuclear matrix elements (see Section 5.2.1), are comparable in the case of the mass term, but very different from each other in the case of the other coefficients involving right–left and right–right weak couplings. Unless these differences are attributed to the choice of neutrino potentials [85] they should be rather explained in terms of the acceptability imposed on the limits of the couplings of the weak hamiltonian (see Section 2).

The values of the half-lives corresponding to two different sets of couplings are shown in the last two lines of Table 8. The values of the couplings used are indicated in the caption of this table. This shows that even if we start from the well trusted shell-model wave functions, i.e. from wave functions which are able to reproduce the measured half-life of the two-neutrino double-beta-decay mode, one is still confronted with uncertainties coming from the initial and final ground states (if the closure approximation has been used) and/or the complete set of intermediate states (when the closure-approximation is abandoned). These uncertainties immediately reflect into the estimation of the structure of the weak hamiltonian. In fact, if only the mass term of the weak lagrangian is considered the obtained half-life (see Tables 6 and 8) would be three or four orders of magnitude above the observed limit 9.5×10^{21} yr [148]. Considering these uncertainties, the extracted limits for the shift of the neutrino mass would be of the order of 20–40 eV.

In Table 9 we show next the results of the QRPA treatment of the same neutrinoless transition. Typically the obtained quantities are one order of magnitude larger than the corresponding shell-model values. For the mass term, $C_{mm}^{(0)}$, the variation is now bigger than for the shell-model

Table 7
The DGT matrix elements for the $2\nu\beta^-\beta^-$ decay of ^{48}Ca to the ground state of ^{48}Ti calculated within the shell model. For more information on the various approaches see the text

$M_{GT}^{(2\nu)}$ (MeV^{-1})	$t_{1/2}^{(2\nu)}$ (yr)	References and explanations
0.073	2.0(19)	[264,282] (Muto–Horie in restricted p–f shell)
0.070	2.0(19)	[282] (MSOBEP in restricted p–f shell)
0.055	3.2(19)	[282] (Muto–Horie in restricted p–f shell)
0.053	3.4(19)	[193,282] (Muto–Horie in full p–f shell)
0.040	6.0(19)	[58] (Modified Kuo–Brown in full p–f shell)
0.070	2.0(19)	[285] (Modified Kuo–Brown in full p–f shell)
0.086	1.3(19)	[285] (FPY interaction in full p–f shell)
0.046	4.3(19)	[18] (experimental)

Table 8
Coefficients $C_\kappa^{(0)}$ of Eq. (5.2) in units of yr^{-1} (and for $g_A = 1.254$) and the majoron matrix element of Eq. (5.24) for the case of the $0\nu\beta^-\beta^-$ decay of ^{48}Ca to the ground state of ^{48}Ti calculated in the shell model. The values are shown in powers of 10, with the exponents indicated in parenthesis. The values shown in columns are deduced from the works quoted at the top of each column by using Eqs. (5.3), (5.4), (5.5), (5.6), (5.7) and (5.8). The two half-lives, $T_{1/2}^a$ and $T_{1/2}^b$, correspond to the parameter sets $|\langle m_\nu\rangle| = 0.65$ eV, $|\langle\lambda\rangle| = 0$, $|\langle\eta\rangle| = 0$ [17] and $|\langle m_\nu\rangle| = 0.74$ eV, $|\langle\lambda\rangle| = 1.1\times10^{-6}$, $|\langle\eta\rangle| = 7.3\times10^{-9}$, respectively. The latter set of effective quantities has been deduced from [17] by using the matrix elements of [186]

$C_\kappa^{(0)}$ (SM)	[186]	[194]	[209] (KB3)	[209] (RVJB)
mm	1.55(− 14)	4.91(− 14)	3.34(− 14)	4.09(− 14)
mλ	− 3.46(− 15)	1.00(− 14)	− 5.02(− 15)	− 7.81(− 15)
mη	1.45(− 12)	8.05(− 14)	4.43(− 12)	5.12(− 12)
$\lambda\lambda$	4.61(− 14)	8.39(− 14)	8.10(− 14)	1.01(− 13)
$\eta\eta$	3.33(− 10)	1.76(− 12)	1.44(− 9)	1.57(− 9)
$\lambda\eta$	− 7.38(− 14)	− 1.17(− 13)	− 1.21(− 13)	− 1.44(− 13)
$\lvert M_{M^0}\rvert$	0.488	0.876	0.719	0.798
$T_{1/2}^a$(yr)	3.99(25)	1.26(25)	1.85(25)	1.51(25)
$T_{1/2}^b$(yr)	8.33(24)	4.34(24)	3.44(24)	2.92(24)

results. In particular, the result of the QRPA with the proton–neutron pairing included (the column [195](pn) in Table 9) deviates from the other QRPA results. Due to this variation of the matrix elements of the mass mode the extracted limits for the neutrino-mass shift would be of the order of 10–40 eV. It is also worth noting that in the calculation of [238] the particle-number projected results (the column [238] (pr.) in Table 9) deviate clearly from the unprojected ones. For the heavier nuclei the projected and unprojected QRPA results are practically the same for the $0\nu\beta^-\beta^-$ mode [241]. The dominant QRPA-matrix elements for the neutrinoless double beta decay with the emission of a singlet-majoron, are three times larger than the corresponding shell model ones, as seen from the listed magnitudes of the matrix element M_{M^0} defined in Eq. (5.24).

Table 9
The same as Table 8 for the $0\nu\beta^-\beta^-$ decay of ^{48}Ca to the ground state of ^{48}Ti calculated in various QRPA frameworks. For more information see the text

$C_\kappa^{(0)}$ (QRPA)	[186]	[194]	[238]	[238](pr.)	[195]	[195](pn)
mm	1.69(− 13)	3.63(− 13)	7.60(− 14)	2.29(− 13)	1.07(− 13)	9.35(− 15)
mλ	− 4.84(− 14)	− 1.66(− 13)	− 4.98(− 14)	− 1.48(− 13)	− 4.75(− 14)	− 3.17(− 15)
mη	1.75(− 11)	2.12(− 12)	1.08(− 11)	2.94(− 11)	− 5.20(− 12)	− 2.97(− 13)
$\lambda\lambda$	3.45(− 13)	1.40(− 12)	3.61(− 13)	1.05(− 12)	3.68(− 13)	3.59(− 14)
$\eta\eta$	4.50(− 9)	4.08(− 10)	3.82(− 9)	9.33(− 9)	6.63(− 10)	2.32(− 11)
$\lambda\eta$	− 1.89(− 13)	− 1.97(− 12)	− 1.22(− 13)	− 4.86(− 13)	− 3.43(− 13)	− 8.80(− 14)
$\lvert M_{M^0}\rvert$	1.62	2.38	1.70	1.59	1.15	0.340
$T_{1/2}^a$ (yr)	3.66(24)	1.70(24)	8.13(24)	2.70(24)	5.78(24)	6.61(25)
$T_{1/2}^b$ (yr)	8.68(23)	4.23(23)	1.15(24)	4.13(23)	1.64(24)	1.69(25)

Thus, the situation for the decay of ^{48}Ca seems to be rather clear from the nuclear-structure point of view, and the discrepancies between the RPA and the shell-model results are not that dramatic, considering the relatively small configuration space of the RPA as compared with the shell-model one. However, the inclusion of the particle–particle correlations in the RPA and the renormalization of these correlations via the factor g_{pp} [68,275], is crucial for achieving the agreement between the shell-model and the RPA results.

6.1.2. Decay of ^{76}Ge

Concerning the QRPA the case of ^{76}Ge (and ^{82}Se) is perhaps the best example to study the power of the method to predict observables. In the past the decay of ^{76}Ge was made unique by the direct observation of its two-neutrino decay mode [173]. The early experiments [54], in fact, yielded to the discovery that the inclusion of renormalized particle–particle correlations is indeed needed to bring the theory closer to the data [68,275]. The results of the QRPA approximation, in different basis sets and with some modifications in the single-particle energies, are shown in Table 10 (upper part). In this table also the matrix elements corresponding to the two-neutrino double beta decay to few first excited states of the final nucleus ^{76}Se are given. The QRPA value for the ground-state transition, calculated with a value of g_{pp} which reproduces single-beta-decay lateral feedings (the QRPA results of [13]), is quite close to the extracted matrix element. In this case the adjusted Woods–Saxon (abbreviated as AWS in Table 10 (upper part)) single-particle energies were used. The AWS basis is essentially a Woods–Saxon (WS in Table 10 (upper part)) one with slight modifications near the proton and neutron Fermi surfaces. The modifications have been done in order to improve the quasiparticle spectrum of the BCS calculation to better correspond to the low-energy spectra of the neighboring odd-neutron and odd-proton nuclei.

In Table 10 (lower part) we present the corresponding results for the projected Hartree–Fock–Bogoliubov (HFB in Table 10 (lower part)) mean-field description of [83], the second-QRPA (a boson-expansion extension of the QRPA [203,204]) results of [234] and the renormalized QRPA (RQRPA) results of [257]. The approach of [83] uses an axially symmetric

Table 10
Upper part: QRPA-calculated DGT matrix elements and the corresponding transition half-lives for the 2νββ decay of ^{76}Ge to the ground state (g.s.) and 2_1^+, 0_1^+ and 2_2^+ excited states of ^{76}Se. Also the experimental half-lives and extracted matrix elements are given. The calculations have been done in the Woods–Saxon (WS) or adjusted WS (AWS) or HFB basis. The results of [45] correspond to $g_{pp} = 1.0$. For more information see the text. Lower part: The same calculated within the higher-RPA schemes (second QRPA [234], RQRPA [257]) and the model of [83]

Quantity	Exp. [16,23]	[75] (WS)	[45] (WS)	[13] (AWS)
$\lvert M^{(2\nu)}(\text{g.s.})\rvert$	0.074	0.092	—	0.100
$\lvert M^{(2\nu)}(2_1^+)\rvert$	< 0.87	0.001	~ 0.002	0.003
$\lvert M^{(2\nu)}(0_1^+)\rvert$	< 1.8	0.363	—	0.838
$\lvert M^{(2\nu)}(2_2^+)\rvert$	< 27	0.003	—	0.003
$t_{1/2}^{(2\nu)}$(g.s.)	1.4(21)	9(20)	—	7.7(20)
$t_{1/2}^{(2\nu)}(2_1^+)$	$> 1.1(21)$	5(26)	$\sim 2(26)$	7.8(25)
$t_{1/2}^{(2\nu)}(0_1^+)$	$> 1.7(21)$	4(22)	—	7.5(21)
$t_{1/2}^{(2\nu)}(2_2^+)$	$> 1.4(21)$	1(29)	—	1.3(29)

Quantity	[83] (HFB)	[234] (WS)	[257] (WS)	[257] (AWS)
$\lvert M^{(2\nu)}(\text{g.s.})\rvert$	0.077	0.083	0.074	0.074
$\lvert M^{(2\nu)}(2_1^+)\rvert$	0.038	0.013	0.003	0.003
$\lvert M^{(2\nu)}(0_1^+)\rvert$	—	0.056	0.229	0.130
$\lvert M^{(2\nu)}(2_2^+)\rvert$	—	—	0.007	0.012
$t_{1/2}^{(2\nu)}$(g.s.)	1.3(21)	1.1(21)	1.4(21)	1.4(21)
$t_{1/2}^{(2\nu)}(2_1^+)$	5.8(23)	5.0(24)	1.0(26)	1.0(26)
$t_{1/2}^{(2\nu)}(0_1^+)$	—	1.7(24)	1.0(23)	3.1(23)
$t_{1/2}^{(2\nu)}(2_2^+)$	—	—	2.2(28)	7.2(27)

Hartree–Fock–Bogoliubov (HFB) state and obtains the physical observables via a variation-after-projection procedure applied on the HFB state.

From Table 10 one can extract some common features shared by most of the results in these tables:

- The nuclear matrix elements associated with transitions to 0^+ final states are much larger than the ones associated with transitions to 2^+ final states.
- The 0_1^+ matrix element, when interpreted as a two-phonon excitation, can be larger in magnitude than the g.s. matrix element.

The above-listed properties are not only characteristic of ^{76}Ge, but seem to be more universal [13,240,257]. This means that the best candidates for measurements of excited-state transitions are the decays to the 0_1^+ final state (the phase-space factors corresponding to the 2_1^+ final states are not essentially larger than the ones corresponding to 0_1^+ final states). This was also pointed out by Barabash [21] and confirmed by the positive result of the ^{100}Mo decay in [22]. A third rather general property of the excited-state transitions, first noticed in [75,243], and later confirmed in the works of [13,45,257], is the following:

- The nuclear matrix elements associated with transitions to excited final states are, on the average, less sensitive to the proton–neutron particle–particle strength g_{pp} than the one associated with the ground-state transition.

In many cases the above property of the excited-state transitions makes the prediction of the decay rates to excited states easier than the prediction of the decay rate to the ground state.

The results for the neutrinoless decay are shown in Tables 11 and 12. Table 11 summarizes the results of various QRPA calculations using the proton–neutron QRPA formalism of Section 3.3. In this case also the particle-number-projected results ([241](pr.) in Table 11) and results with proton–neutron pairing ([195](pn) in Table 11) have been included. Both of these methods yield to modifications in the RPA equations of motion. In Table 12 also results of some other approaches than the QRPA have been shown. These results include the shell-model calculations of [125] and [59] which were made in the $p_{1/2}$–$p_{3/2}$–$f_{5/2}$–$g_{9/2}$ valence space both for protons and neutrons. In [125] the weak-coupling limit of the shell model was used whereas a full shell-model calculation was carried out in [59]. The column [261](V) summarizes the results of a projected mean-field approach (VAMPIR) of the Tübingen-Jülich group [222].

Table 11
The same as Table 8 for the $0\nu\beta^-\beta^-$ decay of ^{76}Ge to the ground state of ^{76}Se calculated within the QRPA framework. For more information see the text

C_κ^0 (QRPA)	[185]	[194]	[241]	[241](pr.)	[195]	[195](pn)
mm	1.12(− 13)	5.59(− 14)	6.97(− 14)	7.51(− 14)	7.33(− 14)	1.42(− 14)
mλ	− 4.11(− 14)	− 2.96(− 14)	− 4.24(− 14)	− 4.51(− 14)	− 4.49(− 14)	− 5.13(− 15)
mη	2.19(− 11)	4.82(− 12)	8.15(− 12)	8.47(− 12)	− 1.54(− 11)	− 2.50(− 12)
$\lambda\lambda$	1.36(− 13)	8.07(− 14)	1.33(− 13)	1.39(− 13)	1.12(− 13)	2.43(− 14)
$\eta\eta$	4.44(− 9)	5.02(− 10)	9.32(− 10)	9.29(− 10)	3.22(− 9)	4.37(− 10)
$\lambda\eta$	− 4.99(− 14)	− 1.63(− 13)	− 8.45(− 14)	− 8.44(− 14)	− 2.11(− 13)	− 6.83(− 14)
$\lvert M_{M^0}\rvert$	4.19	2.96	5.18	5.38	3.04	1.34
$T^a_{1/2}$(yr)	5.52(24)	1.11(25)	8.87(24)	8.23(24)	8.43(24)	4.35(25)
$T^b_{1/2}$(yr)	1.23(24)	3.99(24)	2.59(24)	2.48(24)	4.28(24)	2.02(25)

Table 12
The same as Table 8 for the $0\nu\beta^-\beta^-$ decay of ^{76}Ge to the ground state of ^{76}Se calculated within the QRPA, the shell model (SM) and the VAMPIR (V) approach. For more information see the text

$C_\kappa^{(0)}$	[125] (SM)	[261] (V)	[259] (QRPA)	[59] (SM)
mm	1.58(− 13)	2.88(− 13)	1.18(− 13)	1.90(− 14)
mλ	− 6.10(− 14)	− 1.02(− 13)	− 1.73(− 14)	− 5.89(− 15)
mη	− 1.07(− 12)	2.34(− 11)	2.05(− 11)	3.00(− 12)
$\lambda\lambda$	1.71(− 13)	2.97(− 13)	7.41(− 14)	1.70(− 14)
$\eta\eta$	7.59(− 12)	1.98(− 9)	3.47(− 9)	4.62(− 10)
$\lambda\eta$	− 2.40(− 13)	− 2.34(− 13)	− 8.56(− 14)	− 2.77(− 14)
$\lvert M_{M^0}\rvert$	5.00	6.96	4.32	1.73
$T^a_{1/2}$(yr)	3.91(24)	2.15(24)	5.24(24)	3.25(25)
$T^b_{1/2}$(yr)	2.26(24)	8.50(23)	1.40(24)	9.23(24)

From Tables 11 and 12 it is seen that the QRPA and shell-model results are not very different, particularly, at the level of the calculated coefficient for the mass term of the lagrangian. The calculated value of this coefficient is rather similar for practically all the decay systems which we have analyzed in this report, as shown in the other tables presented in this section. If one assumes a value of the order of $10^{-13}\,\mathrm{yr}^{-1}$ for this coefficient and takes the lower limit of the half-life for the neutrinoless mode, as extracted from the measurements [17], to be 5.6×10^{24} yr, then the upper limit for the neutrino mass shift would be of the order of 0.7 eV. Note, that in Table 8 the value 0.65 eV was obtained by using the $C^{(0)}_{mm}$ coefficient of [185] given in Table 11 on the second column.

It is worth noting that the particle-number projection does not affect the $C^{(0)}$ coefficients (columns [241] and [241](pr.) in Table 11) whereas the inclusion of the proton–neutron pairing (columns [195] and [195](pn) in Table 11) into the RPA framework seems to affect the results considerably. On general physical grounds this could be expected in the case of ^{48}Ca where protons and neutrons occupy the same orbitals whereas for a medium-heavy nucleus near the β-stability line, like for ^{76}Ge, this large effect is a surprising one. The same feature of the proton–neutron pairing results of [195] persists also for the heavy nuclei as seen in the corresponding tables later in this section. For an interested reader some discussion of the proton–neutron pairing formalism, including further references, is carried out in Section 3.4.8.

6.1.3. *Decay of ^{82}Se*

In Table 13 we present the results concerning the two-neutrino double beta decay to the ground state and to few lowest excited states of ^{82}Se. The QRPA results of [13] are obtained in the adjusted Woods–Saxon basis (AWS) and base on the study of the lateral single-beta-decay feeding of the nuclei participant in the double-beta-decay transitions. We also show results of some higher-RPA approaches (SRPA, RQRPA) and results concerning the projected Hartree–Fock–Bogoliubov

Table 13
Calculated DGT matrix elements and the corresponding transition half-lives for the 2νββ decay of ^{82}Se to the ground state (g.s.) and $2^+_1, 0^+_1$ and 2^+_2 excited states of ^{82}Kr. Also the experimental half-lives [97,254] and extracted matrix elements are given for comparison. The calculations have been done in the Woods–Saxon (WS), adjusted WS (AWS) or HFB basis. For more information see the text

Quantity	Exp.	[204] SRPA WS	[83] Proj. HFB	[231] SRPA WS	[13] QRPA AWS	[257] RQRPA WS	[257] RQRPA AWS
$\lvert M^{(2\nu)}(\text{g.s.})\rvert$	0.046	0.133	0.040	0.052	0.072	0.046	0.046
$\lvert M^{(2\nu)}(2^+_1)\rvert$	<0.058	0.0035	0.029	0.0024	1.2(−4)	0.0041	0.0018
$\lvert M^{(2\nu)}(0^+_1)\rvert$	<0.17	—	—	—	0.244	0.159	0.228
$\lvert M^{(2\nu)}(2^+_2)\rvert$	<0.59	—	—	—	0.0094	0.043	0.061
$t^{(2\nu)}_{1/2}$(g.s.)	1.1(20)	1.3(19)	1.5(20)	8.6(19)	4.5(19)	1.1(20)	1.1(20)
$t^{(2\nu)}_{1/2}(2^+_1)$	$>1.4(21)$	4.0(23)	5.5(21)	8.3(23)	3.3(26)	2.8(23)	1.5(24)
$t^{(2\nu)}_{1/2}(0^+_1)$	$>3.0(21)$	—	—	—	1.4(21)	3.3(21)	1.6(21)
$t^{(2\nu)}_{1/2}(2^+_2)$	$>1.6(21)$	—	—	—	6.3(24)	3.0(23)	1.5(23)

approach [83]. These methods were briefly discussed in the context of the ^{76}Ge decay and further information on these models can be found in Section 3.4. As in the ^{76}Ge case also here the theoretical decay rates to the 2^+ states are much slower than to the 0^+ states. Exceptions are the ^{76}Ge and ^{82}Se results in the HFB description where the nuclear matrix element for the decay to the 2_1^+ state is comparable to the one of the ground-state transition.

The results for the neutrinoless mode of decay are presented in Table 14 and they are based on the QRPA model (including the proton–neutron pairing in [195]) and on the full shell-model calculation of [59] in the $p_{1/2}$–$p_{3/2}$–$f_{5/2}$–$g_{9/2}$ basis. The agreement between the QRPA and the shell-model results is quite good for the half-life coefficients $C^{(0)}$ as well as for the values of the calculated matrix element for the singlet-majoron emission, the variations being rather small from one calculation to the other.

6.1.4. Decay of ^{96}Zr

The two-neutrino and neutrinoless double beta decay of ^{96}Zr are discussed in Tables 15 and 16, respectively. The same type of approaches have been used as in the cases of ^{76}Ge and ^{82}Se.

In the case of the two-neutrino decay it has to be pointed out that the decay rates both to the ground state and the excited states depend rather strongly from the excitation energy of the first 1^+ state in the intermediate nucleus ^{96}Nb. This was noticed in [24] (the 4th column of Table 15) where the excitation energy was varied within 1 MeV and the resulting changes in the double Gamow–Teller (DGT) matrix element (see Eqs. (4.2) and (4.6)) were registered. These changes are indicated on column 4 of Table 15. To remove this type of uncertainties in the DGT matrix element one should use the experimental excitation energy of the first 1^+ state of the intermediate nucleus in evaluating the energy denominators of Eqs. (4.2) and (4.6). This amounts to rescaling of the absolute energies of the theoretical 1^+ spectrum of the intermediate nucleus and is easy to do. In ^{96}Nb, however, the experimental location of the first 1^+ state is not known and only rough guesses about the location of it can be made on basis of 1^+ systematics in some neighboring odd–odd nuclei.

Table 14
The same as Table 8 for the $0\nu\beta^-\beta^-$ decay of ^{82}Se to the ground state of ^{82}Kr calculated within the QRPA model and the shell model (SM). For more information see the text

$C_\kappa^{(0)}$	[185] QRPA	[259] QRPA	[252] QRPA	[195] QRPA	[195] QRPA(pn)	[59] SM
mm	4.33(− 13)	4.20(− 13)	1.82(− 13)	1.75(− 13)	9.38(− 14)	1.30(− 13)
mλ	− 1.60(− 13)	− 1.00(− 13)	− 1.52(− 13)	− 8.77(− 14)	− 7.11(− 14)	− 5.68(− 14)
mη	6.37(− 11)	5.87(− 11)	1.04(− 11)	− 1.31(− 11)	− 1.08(− 11)	1.56(− 11)
$\lambda\lambda$	1.01(− 12)	5.55(− 13)	8.80(− 13)	4.78(− 13)	2.27(− 13)	2.51(− 13)
$\eta\eta$	1.54(− 8)	1.24(− 8)	8.98(− 10)	1.53(− 9)	1.93(− 9)	2.83(− 9)
$\lambda\eta$	− 3.84(− 13)	− 6.54(− 13)	− 6.12(− 13)	− 9.32(− 13)	− 2.53(− 13)	− 4.14(− 13)
$\lvert M_{M^0}\rvert$	3.92	3.94	4.07	2.23	1.63	2.18
$T^a_{1/2}$(yr)	1.43(24)	1.47(24)	3.40(24)	3.53(24)	6.59(24)	4.75(24)
$T^b_{1/2}$(yr)	2.89(23)	3.68(23)	6.92(23)	1.27(24)	2.74(24)	1.22(24)

Table 15
Calculated DGT matrix elements and the corresponding transition half-lives for the $2\nu\beta\beta$ decay of ^{96}Zr to the ground state (g.s.) and $2_1^+, 0_1^+$ and 2_2^+ excited states of ^{96}Mo. Also the experimental half-lives [24,147] and extracted matrix elements are given for comparison. The calculations have been done in the Woods–Saxon (WS) and adjusted WS (AWS) basis. For more information see the text

Quantity	Exp.	[232] SRPA WS	[24] QRPA AWS	[257] RQRPA WS	[257] RQRPA AWS
$\lvert M^{(2\nu)}(\text{g.s.})\rvert$	$(38 \pm 4)(-3)$	0.022	0.12–0.31	0.036	0.036
$\lvert M^{(2\nu)}(2_1^+)\rvert$	< 0.078	$8.1(-5)$	0.005–0.038	0.011	0.010
$\lvert M^{(2\nu)}(0_1^+)\rvert$	< 0.18	0.012	0.04–0.10	0.030	0.028
$\lvert M^{(2\nu)}(2_2^+)\rvert$	< 0.49	—	0.0006–0.0091	0.0015	0.0016
$t_{1/2}^{(2\nu)}$(g.s.)	$(3.9 \pm 0.9)(19)$	1.1(20)	(5.8–39)(17)	4.2(19)	4.4(19)
$t_{1/2}^{(2\nu)}(2_1^+)$	$> 7.9(19)$	7.2(25)	(3.3–220)(20)	3.8(21)	4.8(21)
$t_{1/2}^{(2\nu)}(0_1^+)$	$> 6.8(19)$	1.5(22)	(2.1–13)(20)	2.4(21)	2.7(21)
$t_{1/2}^{(2\nu)}(2_2^+)$	$> 6.1(19)$	—	(1.8–410)(23)	6.3(24)	6.0(24)

Table 16
The same as Table 8 for the $0\nu\beta^-\beta^-$ decay of ^{96}Zr to the ground state of ^{96}Mo calculated within the QRPA. For more information see the text

$C_\kappa^{(0)}$ (QRPA)	[195]	[195] (pn-pairing)
mm	$4.28(-13)$	$9.48(-15)$
$m\lambda$	$-2.43(-13)$	$-1.74(-14)$
$m\eta$	$-3.99(-11)$	$2.58(-12)$
$\lambda\lambda$	$1.07(-12)$	$3.60(-14)$
$\eta\eta$	$6.74(-9)$	$1.26(-9)$
$\lambda\eta$	$-1.72(-12)$	$1.02(-13)$
$\lvert M_{M^0}\rvert$	2.40	0.357
$T_{1/2}^a$(yr)	1.44(24)	6.52(25)
$T_{1/2}^b$(yr)	5.46(23)	7.50(24)

6.1.5. *Decay of* ^{100}Mo

Two cases should be mentioned as good (and demanding) testing grounds for nuclear models, namely the decays of ^{100}Mo and ^{150}Nd. The effect of deformations, which is not accounted for in the QRPA calculations, can certainly be one of the missing physical effects which can explain for the failure of this approach in dealing with transitions in the $A = 100$ system, particularly when electromagnetic and double-beta-decay transitions to the ground state and to excited states of the final nucleus are considered [119,245]. On the other hand, for the case of the $A = 150$ system deformations and dominant quadrupole interactions are included in the definition of the group-theoretical pseudo SU(3) scheme [56,127–130]. There, effective single-particle transitions (without

including pairing effects) are, in spite of the radically simplifying assumptions of the model, good enough to yield realistic values for the half-lives (see also Table 28).

The above means that a complete realistic description should be able to deal both with deformations of the mean field and with the collectivity of the two-quasiparticle excitations in a deformed single-particle potential. Such an approach is still missing from the variety of models which we have compiled in Section 3 and in the tables of this section. So far, the physics of these two cases remains largely unexplained, partly because of difficulties inherent within the treatment of the QRPA-type models in situations where the renormalization of the particle–particle interactions brings in too large ground state correlations.

As seen from Table 17, the discrepancies of the QRPA description of the double-beta-decay observables [119,245] has been removed in the second-QRPA description (SRPA) of the ^{100}Mo decay [232]. At the same time also the description of the lateral beta-decay feeding of the ^{100}Mo and ^{100}Ru nuclei is improved [232]. However, as stated in [232], the discrepancies in the elecromagnetic observables still remain and thus one concludes that deformation most likely plays a role at least in the final nucleus ^{100}Ru, either for all final states or only part of them (shape coexistence). This conclusion is supported also by the studies of [263,150].

In the pseudo-SU(3) scheme the double-beta-decay rates are strongly dependent on the occupation numbers for protons and neutrons in the normal- and abnormal-parity Nilsson single-particle states [56]. In [128] the calculations have been performed with two different sets of nucleon-occupation numbers of the normal- and abnormal-parity orbitals, namely a set corresponding to the axially-symmetric deformation $\beta \simeq 0.23$ (DEF in column 7 of Table 17) and a set corresponding to the spherical limit ($\beta \leq 0.09$) (SPH in column 6 of Table 17). It is interesting to note that both pseudo-SU(3) results for the decay to the 2_1^+ final state approach the value given by the SRPA calculation of [232].

An interesting hypothesis raised in [1] is the so-called single-state dominance of the (ground-state-to-ground-state, g.s.–g.s.) two-neutrino double beta decay. According to it the lowest 1^+ state

Table 17
Calculated DGT matrix elements and the corresponding half-lives for the $2\nu\beta\beta$ decay of ^{100}Mo to the ground state (g.s.) and $2_1^+, 0_1^+$ and 2_2^+ excited states of ^{100}Ru. Experimental half-lives [22,82] and extracted matrix elements are given for comparison. The calculations have been done using Woods–Saxon (WS), empirical (EMP) [66] and the pseudo-SU(3) basis with spherical (SPH) or deformed (DEF) nucleon-occupation numbers, as described in the text

Quantity	Exp.	[119] QRPA EMP	[245] QRPA EMP	[232] SRPA WS	[128] SU(3) SPH	[128] SU(3) DEF
$\lvert M^{(2\nu)}(\text{g.s.})\rvert$	0.109	0.256	0.197	0.059	0.152	0.108
$\lvert M^{(2\nu)}(2_1^+)\rvert$	< 0.019	—	0.033	$3.9(-4)$	$7.3(-5)$	$1.5(-4)$
$\lvert M^{(2\nu)}(0_1^+)\rvert$	$(81^{+8}_{-10})(-3)$	0.256	0.271	0.027	—	0.098
$\lvert M^{(2\nu)}(2_2^+)\rvert$	< 0.25	—	0.0082	—	—	—
$t^{(2\nu)}_{1/2}$(g.s.)	0.95(19)	1.7(18)	2.9(18)	3.2(19)	4.9(18)	9.6(18)
$t^{(2\nu)}_{1/2}(2_1^+)$	$> 1.6(21)$	—	5.3(20)	3.9(24)	1.1(26)	2.5(25)
$t^{(2\nu)}_{1/2}(0_1^+)$	$(6.1^{+1.8}_{-1.1})(20)$	6.1(19)	5.4(19)	5.5(21)	—	4.2(20)
$t^{(2\nu)}_{1/2}(2_2^+)$	$> 1.3(21)$	—	1.2(24)	—	—	—

of the intermediate nucleus, 1_1^+, dominates in the sum over the intermediate states in the double Gamow–Teller (DGT) matrix element of Eq. (4.2) whenever the ground state of the intermediate nucleus has the multipolarity 1^+. In these cases the DGT matrix element can be extracted, in principle, from the measured decay characteristics of the 1_1^+ state, i.e. its β^- and β^+/EC decay logft values and the corresponding decay energies (Q values). This assumption was shown to be compatible with the measured g.s.–g.s. double-beta-decay rate in ^{100}Mo [113]. For ^{100}Mo the verification of this result by a microscopic nuclear model might be hard due to the above-described coexistence, etc. problems. Better decay candidates for such a study would be $^{110}_{46}$Pd, $^{114}_{48}$Cd, $^{116}_{48}$Cd and $^{128}_{52}$Te on the $\beta^-\beta^-$ side, and ^{136}Ce$_{78}$ and $^{106}_{48}$Cd on the β^+/EC side. In these cases the participant nuclei are nearly proton or neutron semi-magic (indicated above by writing explicitly either Z or N) and thus most likely spherical.

The results concerning the neutrinoless decay of ^{100}Mo are presented in Table 18. From the results of the neutrinoless transition (Table 18) one can observe the same kind of incoherence as seen in the description of the two-neutrino mode. This means that the description of the ^{100}Mo decay within a model based on a spherical mean field is not at least a very stable one. Thus, one has to be careful when making conclusions about the structure of the effective weak lagrangian on basis of this decay.

6.1.6. Decay of ^{116}Cd and ^{124}Sn

The two-neutrino mode of the ^{116}Cd and ^{124}Sn decays has been studied in Tables 19–21. Only few theoretical results are available for the excited-state transitions and the corresponding experimental half-life limits are not yet very stringent, especially for the ^{124}Sn decay. The only exception is the decay of ^{116}Cd to the final 0_1^+ state in ^{116}Sn where the experimental half-life limit is approaching the calculated half-life of the QRPA approach [13]. In Table 20 we review the available theoretical results for the neutrinoless decay of ^{116}Cd. All these calculations have been performed within the QRPA approach (including also the proton–neutron pairing in the column [195](pn)). In this case the results of [7,229] are remarkably close to each other despite the differences in details of the calculations (see the discussion in [7]).

Table 18
The same as Table 8 for the $0\nu\beta^-\beta^-$ decay of ^{100}Mo to the ground state of ^{100}Ru calculated within the QRPA model. For more information see the text

$C_\kappa^{(0)}$ (QRPA)	[185]	[259]	[194]	[245]	[195]	[195](pn)
mm	2.05(− 13)	2.49(− 12)	3.07(− 13)	1.00(− 12)	6.77(− 14)	7.22(− 17)
mλ	− 1.61(− 13)	5.11(− 14)	− 1.55(− 13)	− 5.85(− 13)	− 5.64(− 15)	− 1.21(− 15)
mη	6.48(− 11)	4.01(− 10)	2.10(− 11)	1.48(− 10)	− 1.11(− 11)	6.38(− 14)
$\lambda\lambda$	1.05(− 12)	2.47(− 12)	8.59(− 13)	2.30(− 12)	3.28(− 14)	9.65(− 14)
$\eta\eta$	3.50(− 8)	9.91(− 8)	1.23(− 9)	3.28(− 8)	2.91(− 9)	9.73(− 11)
$\lambda\eta$	7.03(− 13)	− 2.47(− 12)	− 2.08(− 12)	− 1.35(− 12)	2.45(− 14)	− 3.71(− 13)
$\lvert M_{M^0}\rvert$	2.12	2.35	2.59	4.67	1.09	0.036
$T_{1/2}^a$(yr)	3.01(24)	2.48(23)	2.01(24)	6.18(23)	9.13(24)	8.56(27)
$T_{1/2}^b$(yr)	2.44(23)	5.55(22)	5.58(23)	1.34(23)	4.69(24)	7.78(24)

Table 19
Calculated DGT matrix elements and the corresponding transition half-lives for the $2\nu\beta\beta$ decay of ^{116}Cd to the ground state (g.s.) and $2_1^+, 0_1^+$ and 2_2^+ excited states of ^{116}Sn. Also the experimental half-lives [7,197] and extracted matrix elements are given for comparison. The calculations have been done in the Woods–Saxon (WS) and adjusted WS (AWS) basis. For more information see the text

Quantity	Exp.	[13] (QRPA, AWS)	[234] (SRPA, WS)
$\lvert M^{(2\nu)}(\text{g.s.})\rvert$	0.060	0.051	0.036
$\lvert M^{(2\nu)}(2_1^+)\rvert$	< 0.27	0.013	0.0016
$\lvert M^{(2\nu)}(0_1^+)\rvert$	< 0.50	0.21	0.023
$\lvert M^{(2\nu)}(2_2^+)\rvert$	—	0.020	—
$t_{1/2}^{(2\nu)}$(g.s.)	3.75(19)	5.1(19)	1.0(20)
$t_{1/2}^{(2\nu)}(2_1^+)$	$> 2.3(21)$	1.1(24)	7.8(25)
$t_{1/2}^{(2\nu)}(0_1^+)$	$> 2.0(21)$	1.1(22)	9.5(23)
$t_{1/2}^{(2\nu)}(2_2^+)$	—	4.6(27)	—

Table 20
The same as Table 8 for the $0\nu\beta^-\beta^-$ decay of ^{116}Cd to the ground state of ^{116}Sn calculated within the QRPA framework. For more information see the text

$C_\kappa^{(0)}$ (QRPA)	[229]	[7]	[195]	[195](pn)
mm	5.36(− 13)	6.61(− 13)	5.57(− 14)	5.35(− 14)
mλ	− 3.00(− 13)	− 4.05(− 13)	− 2.27(− 15)	− 5.17(− 15)
mη	6.79(− 11)	1.05(− 10)	− 4.47(− 12)	− 2.08(− 12)
$\lambda\lambda$	1.31(− 12)	1.55(− 12)	2.56(− 14)	9.18(− 15)
$\eta\eta$	1.18(− 8)	2.28(− 8)	5.20(− 10)	1.20(− 10)
$\lambda\eta$	− 8.71(− 13)	− 9.35(− 13)	2.96(− 14)	6.25(− 14)
$\lvert M_{M^0}\rvert$	—	5.91	0.942	0.924
$T_{1/2}^a$(yr)	1.15(24)	9.35(23)	1.11(25)	1.16(25)
$T_{1/2}^b$(yr)	2.71(23)	1.97(23)	7.84(24)	9.93(24)

6.1.7. Decay of ^{128}Te and ^{130}Te

Tables 22–25 discuss the double beta decay of ^{128}Te and ^{130}Te. In Tables 22 and 24 the ground-state data come from a host of geochemical measurements (see the experimental reviews of Moe [176], Moe and Vogel [177] and Tretyak and Zdesenko [262], and references therein, for further details) and thus include all final states and both the two-neutrino and the neutrinoless modes. As a matter of fact, the ratio of the decay half-lives of ^{128}Te and ^{130}Te is rather well known [38,172], of the order of $t_{1/2}(^{130}\text{Te})/t_{1/2}(^{128}\text{Te}) = 3.5 \times 10^{-4}$ [38], but the individual half-lives are still under dispute. It is interesting to note that for ^{130}Te the (lowest) experimental half-life limit exceeds the calculated [13,257] half-life for the transition to the first excited 0^+ state. This means that the calculated decay rate to the 0^+ state is too fast and the theoretical description of the first

Table 21
Calculated DGT matrix elements and the corresponding transition half-lives for the 2νββ decay of ^{124}Sn to the ground state (g.s.) and 2_1^+, 0_1^+ and 2_2^+ excited states of ^{124}Te. Also the experimental half-lives [262] and extracted matrix elements are given for comparison. The calculation has been done in the adjusted Woods–Saxon (AWS) basis

Quantity	Exp.	[13] (QRPA,AWS)
$\lvert M^{(2\nu)}(\text{g.s.})\rvert$	< 2.6	0.092
$\lvert M^{(2\nu)}(2_1^+)\rvert$	< 0.99	2.5(− 4)
$\lvert M^{(2\nu)}(0_1^+)\rvert$	< 9.9	0.284
$\lvert M^{(2\nu)}(2_2^+)\rvert$	< 140	0.0046
$t_{1/2}^{(2\nu)}$(g.s.)	$> 1.0(17)$	7.8(19)
$t_{1/2}^{(2\nu)}(2_1^+)$	$> 4.1(19)$	6.5(26)
$t_{1/2}^{(2\nu)}(0_1^+)$	$> 2.2(18)$	2.7(21)
$t_{1/2}^{(2\nu)}(2_2^+)$	$> 2.0(18)$	1.7(27)

Table 22
Calculated DGT matrix elements and the corresponding transition half-lives for the 2νββ decay of ^{128}Te to the ground state (g.s.) and the 2_1^+ excited state of ^{128}Xe (only these final states are allowed by the Q-value). The lowest experimental half-life for the g.s. transition, suggested by a number of recent experiments, is given for comparison. The experimental limit for the 2_1^+ transition is taken from [35]. The calculations have been done in the Woods–Saxon (WS) and adjusted WS (AWS) basis. For more information see the text

Quantity	Exp.	[13] (QRPA,AWS)	[231] (SRPA,WS)
$\lvert M^{(2\nu)}(\text{g.s.})\rvert$	< 0.024	0.046	0.0056
$\lvert M^{(2\nu)}(2_1^+)\rvert$	< 260	0.014	0.0003
$t_{1/2}^{(2\nu)}$(g.s.)	$> 2.0(24)$	5.6(23)	3.7(25)
$t_{1/2}^{(2\nu)}(2_1^+)$	$> 4.7(21)$	1.6(30)	4.4(33)

Table 23
The same as Table 8 for the $0\nu\beta^-\beta^-$ decay of ^{128}Te to the ground state of ^{128}Xe calculated within the QRPA model. For more information see the text

$C_\kappa^{(0)}$ (QRPA)	[185]	[259]	[252]	[194]	[195]	[195](pn)
mm	3.36(− 14)	2.48(− 14)	1.45(− 14)	1.01(− 14)	1.36(− 14)	1.71(− 15)
mλ	− 4.86(− 15)	− 4.43(− 16)	− 4.96(− 15)	2.39(− 15)	− 5.24(− 15)	− 4.63(− 16)
mη	9.46(− 12)	7.35(− 12)	1.66(− 12)	− 1.07(− 12)	− 4.73(− 12)	− 1.35(− 12)
$\lambda\lambda$	7.39(− 15)	2.36(− 15)	6.76(− 15)	7.54(− 16)	4.32(− 15)	6.05(− 16)
$\eta\eta$	1.50(− 9)	1.07(− 9)	9.31(− 11)	4.55(− 11)	8.17(− 10)	5.23(− 10)
$\lambda\eta$	− 1.87(− 15)	− 2.77(− 15)	− 2.89(− 15)	− 2.03(− 15)	− 8.51(− 15)	− 1.99(− 15)
$\lvert M_{M^0}\rvert$	4.29	3.87	4.64	2.35	2.48	0.877
$T_{1/2}^a$(yr)	1.84(25)	2.49(25)	4.26(25)	6.12(25)	4.54(25)	3.61(26)
$T_{1/2}^b$(yr)	3.98(24)	5.30(24)	1.87(25)	5.79(25)	5.30(25)	5.85(25)

Table 24
Calculated DGT matrix elements and the corresponding transition half-lives for the 2νββ decay of ^{130}Te to the ground state (g.s.) and $2_1^+, 0_1^+$ and 2_2^+ excited states of ^{130}Xe. Also the experimental half-lives [35,172] and extracted matrix elements are given for comparison. The calculations have been done in the Woods–Saxon (WS) and adjusted WS (AWS) basis. For more information see the text

Quantity	Exp.	[231] SRPA WS	[13] QRPA AWS	[257] RQRPA WS	[257] RQRPA AWS
$\|M^{(2\nu)}(\text{g.s.})\|$	< 0.016	0.016	0.028	0.009	0.009
$\|M^{(2\nu)}(2_1^+)\|$	< 0.028	0.001	0.004	0.005	0.011
$\|M^{(2\nu)}(0_1^+)\|$	—	—	0.257	0.289	0.175
$\|M^{(2\nu)}(2_2^+)\|$	—	—	2(− 4)	0.001	0.005
$t_{1/2}^{(2\nu)}$(g.s.)	> 8.0(20)	8.1(20)	2.6(20)	2.7(21)	2.7(21)
$t_{1/2}^{(2\nu)}(2_1^+)$	> 4.5(21)	2.8(24)	2.7(23)	1.4(23)	3.0(22)
$t_{1/2}^{(2\nu)}(0_1^+)$	—	—	3.3(20)	2.6(20)	7.1(20)
$t_{1/2}^{(2\nu)}(2_2^+)$	—	—	1.0(28)	3.2(26)	2.0(25)

Table 25
The same as Table 8 for the $0\nu\beta^-\beta^-$ decay of ^{130}Te to the ground state of ^{130}Xe calculated within the QRPA model. For more information see the text

$C_\kappa^{(0)}$ (QRPA)	[185]	[259]	[252]	[194]	[195]	[195](pn)
mm	5.34(− 13)	4.65(− 13)	3.13(− 13)	1.83(− 13)	3.02(− 13)	1.24(− 13)
mλ	− 2.17(− 13)	− 9.91(− 14)	− 2.49(− 13)	2.25(− 14)	− 2.28(− 13)	− 1.15(− 13)
mη	9.10(− 11)	8.10(− 11)	2.09(− 11)	− 7.30(− 12)	− 6.24(− 11)	− 3.07(− 11)
λλ	1.05(− 12)	4.64(− 13)	1.12(− 12)	1.23(− 13)	7.44(− 13)	4.48(− 13)
ηη	2.25(− 8)	1.73(− 8)	1.69(− 9)	4.01(− 10)	1.61(− 8)	9.50(− 9)
λη	− 4.13(− 13)	− 5.34(− 13)	− 6.89(− 13)	− 3.47(− 13)	− 1.49(− 12)	− 1.10(− 12)
$\|M_{M^0}\|$	3.47	3.35	4.32	2.02	2.33	1.50
$T_{1/2}^a$(yr)	1.16(24)	1.33(24)	1.97(24)	3.38(24)	2.05(24)	4.98(24)
$T_{1/2}^b$(yr)	2.33(23)	3.13(23)	4.93(23)	1.90(24)	7.04(23)	1.20(24)

0^+ state as a member of a two-phonon triplet, assumed in [13,257], is most likely not an adequate one (see [257] for further discussion).

The neutrinoless mode of the Te decays has been discussed in Tables 23 and 25. The theoretical approaches are based on the QRPA model and are the ones discussed in the context of the ^{76}Ge and ^{82}Se decays. As seen already for the lighter double-beta-decaying nuclei the mass term of the half-life is rather uniformly described in all the models yielding a rough value of $2 \times 10^{-14}\text{yr}^{-1}$ for ^{128}Te and $3 \times 10^{-13}\text{yr}^{-1}$ for ^{130}Te. The experimental lower limits of the half-lives, 1.3×10^{19}yr for ^{128}Te [174] and 1.8×10^{22}yr for ^{130}Te [5] yield for the effective neutrino mass the upper limits 1 keV and 7 eV, respectively (when only the mass mechanism is active).

6.1.8. Decay of ^{136}Xe

In Tables 26 and 27 we discuss the double beta decay of ^{136}Xe. Not much is known experimentally about the decay rates of the two-neutrino mode as seen in Table 26. The theoretical numbers have been calculated either with the QRPA or the second-QRPA (SRPA) model. The calculation of [13] is based on data on single beta decays and is thus parameter-free in the description of the double-beta-decay observables. It has to be noted that the ^{136}Xe decay should be ideal to study with nuclear models since the participant nuclei are very close to the doubly-magic shell closure $Z = 50$, $N = 82$ and no traces of deformation should be there. This is the reason why this nucleus is also accessible to the nuclear shell model, as seen in the last column of Table 27. This table summarizes the calculations concerning the neutrinoless mode of the ^{136}Xe decay, and in addition to the various QRPA calculations a full shell-model calculation in the $s_{1/2}$–$d_{3/2}$–$d_{5/2}$–$g_{7/2}$–$h_{11/2}$ valence space has been performed in [59]. In this case the QRPA calculations (including the proton-neutron-pairing calculation in the column QRPA(pn)) give a very uniform value, somewhat different from the shell-model result, for the mass parameter $C^{(0)}_{mm}$. Still, overall, the QRPA and the shell-model values for the $C^{(0)}$ coefficients agree rather nicely.

6.1.9. Decay of ^{150}Nd

Finally, the decay of the heaviest nucleus of our review, ^{150}Nd, is presented in Tables 28 and 29. The case of ^{150}Nd was already mentioned in connection with the ^{100}Mo decay since both ^{100}Mo and ^{150}Nd decays have characteristic properties of deformation effects setting in. Actually, the situation is more clean-cut for the ^{150}Nd decay since there it is more obvious that deformation plays a dominant role in the nuclear structure of both the initial and the final (^{150}Sm) nuclei.

The pseudo-SU(3) model has been applied to calculate both the two-neutrino ([129], Table 28) and the neutrinoless ([130], Table 29) decay modes. In view of the two-neutrino results of Table 28 the deformed approach seems to work well for the ground-state transition, the experimental limits

Table 26
Calculated DGT matrix elements and the corresponding transition half-lives for the $2\nu\beta\beta$ decay of ^{136}Xe to the ground state (g.s.) and 2_1^+, 0_1^+ and 2_2^+ excited states of ^{136}Ba. Also the available experimental data are given. The calculations have been done in the Woods–Saxon (WS) or adjusted WS (AWS) basis. The results of [45] correspond to $g_{pp} = 1.0$. For more information see the text

Quantity	[276] Exp.	[75] QRPA (WS)	[45] QRPA (WS)	[13] QRPA (AWS)	[231] SRPA (WS)
$\lvert M^{(2\nu)}(\text{g.s.})\rvert$	< 0.031	< 0.143	—	0.040	0.038
$\lvert M^{(2\nu)}(2_1^+)\rvert$	—	0.008	~ 0.003	0.004	0.002
$\lvert M^{(2\nu)}(0_1^+)\rvert$	—	0.527	—	0.577	—
$\lvert M^{(2\nu)}(2_2^+)\rvert$	—	0.018	—	0.008	—
$t^{(2\nu)}_{1/2}(\text{g.s.})$	$> 2.1(20)$	$> 1(19)$	—	1.3(20)	1.4(20)
$t^{(2\nu)}_{1/2}(2_1^+)$	—	4(23)	$\sim 3(24)$	2.0(24)	5.4(24)
$t^{(2\nu)}_{1/2}(0_1^+)$	—	3(21)	—	2.5(21)	—
$t^{(2\nu)}_{1/2}(2_2^+)$	—	1(26)	—	5.1(26)	—

Table 27
The same as Table 8 for the $0\nu\beta^-\beta^-$ decay of ^{136}Xe to the ground state of ^{136}Ba calculated within the QRPA model and the shell model (SM). For more information see the text

$C_\kappa^{(0)}$	[185] QRPA	[259] QRPA	[252] QRPA	[195] QRPA	[195] QRPA(pn)	[59] SM
mm	1.18(− 13)	1.57(− 13)	1.13(− 13)	1.43(− 13)	9.33(− 14)	2.48(− 14)
$m\lambda$	− 2.80(− 14)	− 3.98(− 14)	− 1.02(− 13)	− 1.18(− 13)	− 7.06(− 14)	− 9.00(− 15)
$m\eta$	2.61(− 11)	3.13(− 11)	9.12(− 12)	− 3.08(− 11)	− 2.82(− 11)	3.29(− 12)
$\lambda\lambda$	2.04(− 13)	1.65(− 13)	5.17(− 13)	3.67(− 13)	2.26(− 13)	3.24(− 14)
$\eta\eta$	8.27(− 9)	7.43(− 9)	8.72(− 10)	8.11(− 9)	1.04(− 8)	5.13(− 10)
$\lambda\eta$	− 6.22(− 14)	− 1.86(− 13)	− 3.02(− 13)	− 7.79(− 13)	− 4.85(− 13)	− 4.86(− 14)
$\lvert M_{M^0}\rvert$	1.58	1.90	2.52	1.55	1.26	0.753
$T^a_{1/2}$(yr)	5.24(24)	3.94(24)	5.47(24)	4.32(24)	6.62(24)	2.49(25)
$T^b_{1/2}$(yr)	8.45(23)	8.31(23)	1.12(24)	1.45(24)	1.60(24)	7.08(24)

Table 28
Calculated DGT matrix elements and the corresponding transition half-lives for the $2\nu\beta\beta$ decay of ^{150}Nd to the ground state (g.s.) and $2_1^+, 0_1^+$ and 0_2^+ excited states of ^{150}Sm. Also the experimental half-lives [8,9,36] and extracted matrix elements are given for comparison. The calculations have been done in the pseudo-SU(3) framework assuming two different axial deformations β indicated in the table. For more information see the text

Quantity	Exp.	[129] $\beta = 0.28$	[129] $\beta = 0.19$
$\lvert M^{(2\nu)}$(g.s.)$\rvert$	$(35 \pm 8)(-3)$	0.055	0.055
$\lvert M^{(2\nu)}(2_1^+)\rvert$	< 0.37	5.4(− 5)	4.1(− 5)
$\lvert M^{(2\nu)}(0_1^+)\rvert$	< 0.14	0	0.0045
$\lvert M^{(2\nu)}(0_2^+)\rvert$	< 0.71	0.0050	0
$t^{(2\nu)}_{1/2}$(g.s.)	$(1.7^{+1.1}_{-0.6})(19)$	6.7(18)	6.7(18)
$t^{(2\nu)}_{1/2}(2_1^+)$	$> 8.0(18)$	7.2(24)	1.2(25)
$t^{(2\nu)}_{1/2}(0_1^+)$	$> 8.8(18)$	∞	8.6(21)
$t^{(2\nu)}_{1/2}(0_2^+)$	$> 2.1(18)$	4.3(22)	∞

for the excited-state transitions being still too insensitive to make definite conclusions about these transitions. In these calculations both the initial and final nucleus are assumed to have the same axial deformation. In [129] the calculation has been performed for two values of deformation, namely $\beta = 0.19$ and $\beta = 0.28$. The former deformation corresponds to the deformation of the daughter nucleus ^{150}Sm and the latter to the deformation of the mother nucleus ^{150}Nd. The effect of the different adopted deformations is (roughly) just to exchange the matrix elements of the two excited 0^+ final states, as seen in Table 28. It has to be noted, that in the case of the neutrinoless decay mode also spherical QRPA calculations [185,259] are available and at least for the mass mode the results differ by an order of magnitude from the pseudo-SU(3) results.

Table 29
The same as Table 8 for the $0\nu\beta^-\beta^-$ decay of ^{150}Nd to the ground state of ^{150}Sm calculated within the QRPA and the Pseudo-SU(3) approach. For more information see the text

$C_k^{(0)}$	[185] QRPA	[259] QRPA	[130] Pseudo-SU(3)
mm	7.74(− 12)	5.32(− 12)	4.78(− 13)
mλ	− 3.57(− 12)	− 7.85(− 13)	—
mη	1.02(− 9)	7.16(− 10)	—
$\lambda\lambda$	2.68(− 11)	7.64(− 12)	—
$\eta\eta$	2.95(− 7)	1.67(− 7)	—
$\lambda\eta$	− 8.39(− 12)	− 8.40(− 12)	—
$\lvert M_{M^0}\rvert$	6.07	5.24	1.57
$T^a_{1/2}$(yr)	7.98(22)	1.16(23)	1.29(24)
$T^b_{1/2}$(yr)	1.39(22)	2.76(22)	9.98(23)

Finally, in Figs. 1 and 2 we present a compilation of the magnitudes of the double β^--decay matrix elements for the transitions to the 0_1^+ and 2_1^+ final states, respectively. The numerical values depicted in these figures have been taken from the tables of this Chapter and the pictorial presentation is just for the purpose of better seeing the overall trends (if any) of the magnitudes of the nuclear matrix elements. In these figures we have indicated the experimental results by dashed vertical bars (note that for ^{100}Mo the bar is short) and have taken only those experimental values which have any relevance in comparison with the theoretical values of the matrix elements. The rest of the experimental results would correspond to bars extending outside the scales of the figures. If two or more theoretical calculations with the same model are available they have been connected by a solid vertical line. In the case of ^{96}Zr the span in the MCM (multiple commutator model, see Section 3.4.7) has to do with the uncertainty in the energy of the first intermediate 1^+ state as discussed earlier in this section. The other models in this compilation, namely the RQRPA, SQRPA, pseudo SU(3) (P-SU3 in the legend of the figure) and the projected mean-field model based on the HFB approach have been discussed earlier in this section and in Section 3.4.

From the figures it is not easy to recognize any general trends exhibited by the magnitudes of the nuclear matrix elements. Generally, the second QRPA method (SQRPA) predicts smaller values for the matrix elements than the MCM and the RQRPA (renormalized QRPA) methods. According to [232] this behaviour is associated with the improved description of the beta-decay amplitudes in the SQRPA formalism. In the SQRPA the beta-decay amplitudes contain, in addition to the ordinary QRPA contributions of Eqs. (3.29) and (3.30), higher-order terms which partly cancel the leading contribution coming from the QRPA order. At least in the beta-decay observables concerning the decay of ^{100}Tc, the improvement over the QRPA level of description is clearly visible [232]. No clear general trend of the matrix elements can be seen in the figures and thus the results are specific to each nucleus and no extrapolation or interpolation of the results seems possible. A possible reason for this is the dependence of the decay amplitudes on the small components of the involved wave functions which, in turn, strongly depend on the specific structure of each individual nucleus participating in the double-beta-decay process.

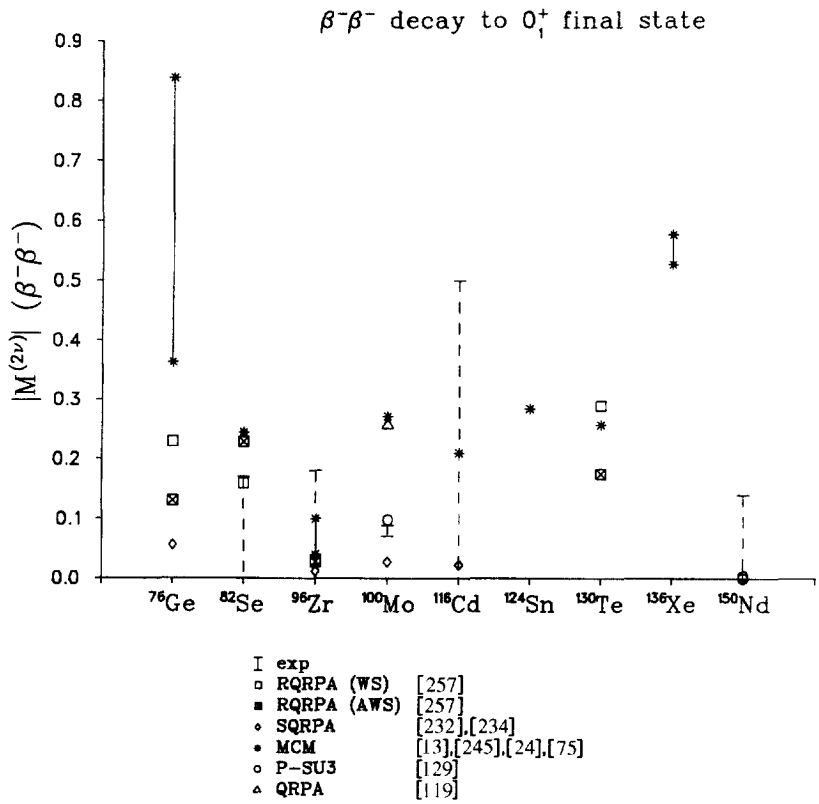

Fig. 1. Compilation of the magnitudes of the two-neutrino double-β^--decay matrix elements for transitions to the first excited 0^+ state. For each symbol we have indicated the corresponding theoretical method and references for the numerical results. For more information see the text.

6.2. *The case of β^+/EC decays*

The side of double β^+/EC decays ($\beta^+\beta^+$, β^+EC, ECEC) is far less explored, both experimentally and theoretically, than the side of double β^- decay ($\beta^-\beta^-$). One reason for the scarse experimental activity are the low decay energies (Q values) of the double β^+/EC transitions when compared with decay energies on the double β^- side. This makes the phase space of the double β^+/EC decays small and results in long decay half-lives. This is especially true for the $\beta^+\beta^+$ mode where two positrons are emitted. The two emitted positrons can easily be detected but at the same time the decay rate is heavily suppressed by the available decay energy. For the other modes, β^+EC and ECEC, the phase space is larger but the experimental detection more involved. However, for the excited states the ECEC decay can, in principle, be detected as argued by Barabash [21]. This issue is discussed in Section 4.2.2 of this report.

Next we go into discussion about specific examples of experimental and theoretical data concerning the double β^+/EC decay transitions. The data on the two-neutrino mode has been summarized in Tables 30–35.

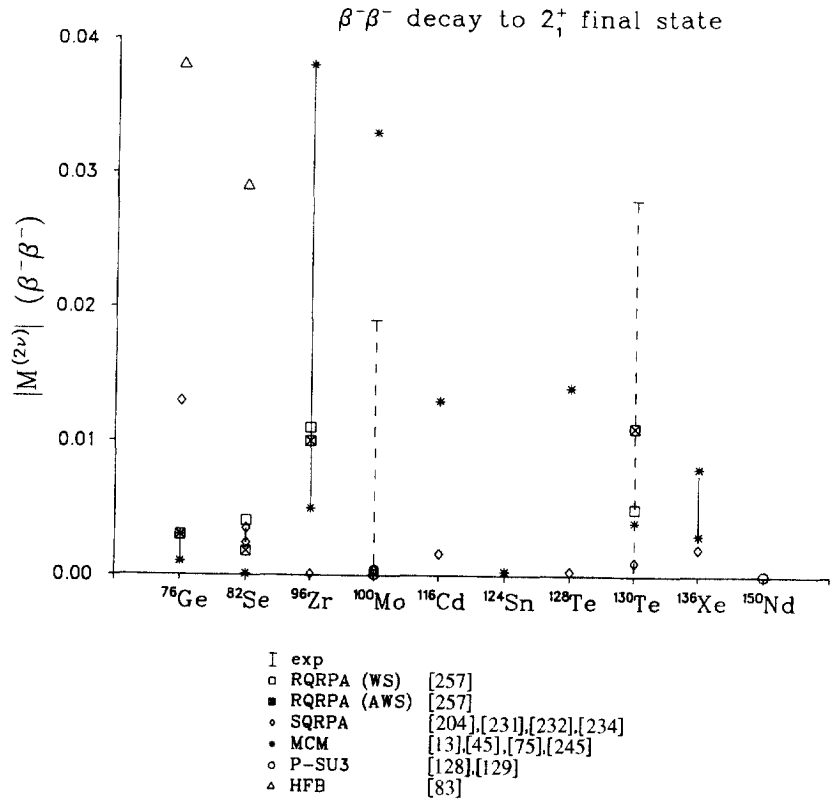

Fig. 2. Compilation of the magnitudes of the two-neutrino double-β^--decay matrix elements for transitions to the first excited 2^+ state. For each symbol we have indicated the corresponding theoretical method and references for the numerical results. For more information see the text.

Table 30
Calculated DGT matrix elements and the corresponding transition half-lives for the $2\nu\beta^+$EC and 2νECEC decay of ^{58}Ni, ^{96}Ru and ^{136}Ce to the ground states (g.s.) of ^{58}Fe, ^{96}Mo and ^{136}Ba. The calculations have been done using the QRPA in the Woods–Saxon basis. The available experimental half-lives are $t^{(2\nu)}_{1/2}$(g.s.; β^+EC)$_{exp.} > 6.2\times10^{19}$ [191] for ^{58}Ni and $t^{(2\nu)}_{1/2}$(g.s.; β^+EC)$_{exp.} > 6.7\times10^{16}$ [192] for ^{96}Ru. For more information see the text

Nucleus	$\lvert M^{(2\nu)}$(g.s.)$\rvert$		$t^{(2\nu)}_{1/2}$(g.s.; ECEC)		$t^{(2\nu)}_{1/2}$(g.s.; β^+EC)	
	[239]	[140]	[239]	[140]	[239]	[140]
^{58}Ni	0.243	0.077	3.9(23)	3.9(24)	5.8(24)	5.5(25)
^{96}Ru	0.226	0.263	2.8(21)	2.1(21)	1.8(22)	1.2(22)
^{136}Ce	0.626	0.038	6.4(19)	1.7(22)	4.0(21)	9.2(23)

In Table 30 we present the available theoretical results concerning the transitions to the ground-state in the two-neutrino β^+EC and ECEC decays of ^{58}Ni, ^{96}Ru and ^{136}Ce. The two sets of theoretical results, [140,239], have been calculated by using the QRPA model in Woods–Saxon basis. In [239] the Woods–Saxon parameters of [47] were used but in [140] the strength of the

Table 31
Calculated DGT matrix elements and the corresponding transition half-lives for the $2\nu\beta^+\beta^+$, $2\nu\beta^+$EC and 2νECEC decays of ^{78}Kr to the ground state (g.s.) and 2_1^+, 0_1^+ and 2_2^+ excited states of ^{78}Se. Also the experimental half-lives [217] and the corresponding extracted matrix element are given for comparison. The calculations have been done in the Woods–Saxon (WS) or adjusted WS (AWS) basis. For more information see the text

Quantity	Exp.	[140] QRPA WS	[13] QRPA AWS	[257] RQRPA WS	[257] RQRPA AWS
$\lvert M^{(2\nu)}(\text{g.s.})\rvert$	< 2.8	0.12	0.37	0.086	0.247
$\lvert M^{(2\nu)}(2_1^+)\rvert$	—	—	1.8(− 3)	1.0(− 4)	7.8(− 4)
$\lvert M^{(2\nu)}(0_1^+)\rvert$	—	—	0.076	0.003	0.067
$\lvert M^{(2\nu)}(2_2^+)\rvert$	—	—	1.7(− 3)	9(− 6)	8.1(− 4)
$t_{1/2}^{(2\nu)}$(g.s.; ECEC)	—	3.7(22)	3.7(21)	6.8(22)	8.2(21)
$t_{1/2}^{(2\nu)}$(g.s.; β^+EC)	$> 1.1(20)$	5.3(22)	6.2(21)	1.1(23)	1.4(22)
$t_{1/2}^{(2\nu)}$(g.s.; $\beta^+\beta^+$)	$> 2.0(21)$	—	2.2(25)	4.0(26)	4.8(25)
$t_{1/2}^{(2\nu)}(0_1^+$; ECEC)	—	—	3.7(24)	2.1(27)	4.7(24)
$t_{1/2}^{(2\nu)}(0_1^+$; β^+EC)	—	—	3.8(28)	2.5(31)	5.1(28)

Table 32
Calculated DGT matrix elements and the corresponding transition half-lives for the $2\nu\beta^+$EC and 2νECEC decays of ^{92}Mo to the ground state (g.s.) and 2_1^+, 0_1^+ and 2_2^+ excited states of ^{92}Zr. Also the experimental half-lives [27] and the corresponding extracted matrix elements are given for comparison. The calculations have been done in the adjusted Woods–Saxon (AWS) or in the shell-model (SM1,SM2) basis. For more information see the text

Quantity	Exp.	[13,27] QRPA (AWS)	[248] SM1 (1 + 2)	[248] SM2 (1 + 2)
$\lvert M^{(2\nu)}(\text{g.s.})\rvert$	< 210	0.29	0.23	0.11
$\lvert M^{(2\nu)}(2_1^+)\rvert$	—	0.0036	0.0019	0.0027
$\lvert M^{(2\nu)}(0_1^+)\rvert$	< 440	0.015	0.060	0.037
$\lvert M^{(2\nu)}(2_2^+)\rvert$	—	3.1(− 4)	—	—
$t_{1/2}^{(2\nu)}$(g.s.; ECEC)	—	2.7(22)	4.6(22)	2.1(23)
$t_{1/2}^{(2\nu)}$(g.s.; β^+EC)	$> 4.5(19)$	2.4(25)	3.9(25)	1.8(26)
$t_{1/2}^{(2\nu)}(0_1^+$; ECEC)	$> 2.7(20)$	2.4(29)	1.5(28)	3.9(28)

spin–orbit coupling was varied in order to obtain a smooth behaviour of the double Gamow–Teller (DGT) matrix element of the double β^+/EC decay. Also, the values of [239] correspond to the proton–neutron particle–particle interaction strength $g_{pp} = 1.0$ (unrenormalized G matrix) but the g_{pp} values of [140] are based on an averaging method [184] developed on the $\beta^-\beta^-$ side of double beta decay. These arguments explain the big differences in the predicted magnitudes of the DGT matrix elements and the associated half-lives in the cases of ^{58}Ni and ^{136}Ce. Anyway, results of both calculations are quite far above the available measured lower limits of half-lives for the β^+EC decay modes in ^{58}Ni and ^{96}Ru.

Table 33
Calculated DGT matrix elements and the corresponding transition half-lives for the $2\nu\beta^+$EC and 2νECEC decays of ^{106}Cd to the ground state (g.s.) and 2_1^+, 0_1^+ and 2_2^+ excited states of ^{106}Pd. Also the experimental half-lives [28,192] and the corresponding extracted matrix elements are given for comparison. The calculations have been done in the Woods–Saxon (WS) or adjusted WS (AWS) basis. For more information see the text

Quantity	Exp.	[140] QRPA WS	[28] QRPA WS	[28] QRPA AWS	[257] RQRPA WS	[257] RQRPA AWS
$\|M^{(2\nu)}(\text{g.s.})\|$	< 8.7	0.27	0.84	0.78	0.55	0.56
$\|M^{(2\nu)}(2_1^+)\|$	—	—	0.0029	0.0031	3.3(− 4)	0.0050
$\|M^{(2\nu)}(0_1^+)\|$	< 12	—	0.52	0.096	0.30	0.081
$\|M^{(2\nu)}(2_2^+)\|$	—	—	0.021	0.025	0.012	0.0023
$t_{1/2}^{(2\nu)}$(g.s.; ECEC)	$> 1.5(17)$	8.7(20)	9.0(19)	1.0(20)	2.1(20)	2.0(20)
$t_{1/2}^{(2\nu)}$(g.s.; β^+EC)	$> 6.6(18)$	4.1(21)	7.1(20)	8.2(20)	1.7(21)	1.6(21)
$t_{1/2}^{(2\nu)}(0_1^+$; ECEC)	$> 6.2(18)$	—	3.4(21)	1.0(23)	1.0(22)	1.4(23)
$t_{1/2}^{(2\nu)}(0_1^+$; β^+EC)	$> 8.1(18)$	—	5.9(24)	1.7(26)	1.7(25)	2.4(26)

Table 34
Calculated DGT matrix elements and the corresponding transition half-lives for the $2\nu\beta^+$EC and 2νECEC decays of ^{124}Xe to the ground state (g.s.) and 2_1^+, 0_1^+ and 2_2^+ excited states of ^{124}Te. Also the available experimental half-life [25] and the corresponding extracted matrix element are given for comparison. The calculations have been done in the Woods–Saxon (WS) or in the adjusted WS (AWS) basis. For more information see the text

Quantity	Exp.	[140] QRPA (WS)	[13] QRPA (AWS)
$\|M^{(2\nu)}(\text{g.s.})\|$	< 69	0.082	0.0071
$\|M^{(2\nu)}(2_1^+)\|$	—	—	5.2(− 4)
$\|M^{(2\nu)}(0_1^+)\|$	—	—	0.0073
$\|M^{(2\nu)}(2_2^+)\|$	—	—	3.5(− 4)
$t_{1/2}^{(2\nu)}$(g.s.; ECEC)	—	2.9(21)	3.9(23)
$t_{1/2}^{(2\nu)}$(g.s.; β^+EC)	$> 4.8(16)$	3.0(22)	4.5(24)
$t_{1/2}^{(2\nu)}(0_1^+$; ECEC)	—	—	5.3(24)
$t_{1/2}^{(2\nu)}(0_1^+$; β^+EC)	—	—	1.0(28)

In Tables 31–35 the available information (both experimental and theoretical) on ground-state and excited-state two-neutrino β^+/EC transitions is summarized for the decays of ^{78}Kr, ^{92}Mo, ^{106}Cd, ^{124}Xe and ^{130}Ba. The calculations are based on the QRPA model or its self-consistent extension RQRPA (renormalized QRPA). Only in the case of ^{92}Mo decay shell-model results are also available [248]. These shell-model calculations base on the work of [145,226,227]. As seen from the tables, the available experimental half-life limits are not very stringent and thus they cannot be used in judging the validity of the theoretical results.

Table 35
Calculated DGT matrix elements and the corresponding transition half-lives for the $2\nu\beta^+$EC and 2νECEC decays of ^{130}Ba to the ground state (g.s.) and $2_1^+, 0_1^+$ and 2_2^+ excited states of ^{130}Xe. The available experimental half-life [26] $t_{1/2}^{(2\nu+0\nu)} > 4\times10^{21}$ yr is a geochemical one and thus concerns all final states. The calculations have been done in the Woods–Saxon (WS) or in the adjusted WS (AWS) basis

Quantity	[140] QRPA (WS)	[13] QRPA (AWS)
$\lvert M^{(2\nu)}(\text{g.s.})\rvert$	0.076	0.21
$\lvert M^{(2\nu)}(2_1^+)\rvert$	...	1.4(−4)
$\lvert M^{(2\nu)}(0_1^+)\rvert$	...	0.024
$\lvert M^{(2\nu)}(2_2^+)\rvert$	...	5.6(−4)
$t_{1/2}^{(2\nu)}$(g.s.; ECEC)	4.2(21)	5.4(20)
$t_{1/2}^{(2\nu)}$(g.s.; β^+EC)	1.0(23)	1.6(22)
$t_{1/2}^{(2\nu)}(0_1^+$; ECEC)	...	6.9(23)
$t_{1/2}^{(2\nu)}(0_1^+$; β^+EC)	...	1.4(28)

As seen in Tables 31–35, the theoretically predicted half-lives for the ground-state transitions (ECEC and/or β^+EC mode) are not very long, especially for the ^{106}Cd decay where all the calculations, except [140], give rather uniform results for the half-life of the ground-state transition. Thus experimental verification of such a transition might be possible in the near future. According to Table 33 for ^{106}Cd also the transition to the first excited 0^+ state could be possible to measure by the use of the techniques proposed in [21]. For the other nuclei the excited-state transitions are most likely too slow to be measurable in the near future.

As a general observation from Tables 31–35 one can say that the nuclear matrix elements corresponding to decays to final states of multipolarity 2^+ are very small, as also was the case for the $\beta^-\beta^-$ transitions, and thus the experimental detection of the associated double-beta transitions is not as tempting to try as the detection of transitions to the first excited 0^+ (0_1^+) state. However, contrary to observations in the $\beta^-\beta^-$ transitions, in most cases the nuclear matrix element for the 0_1^+ transition is much smaller than for the ground-state transition, and the assumption of [21] about equal magnitudes of the ground-state and 0_1^+ matrix elements is not satisfied. In this context it has to be noted that this statement relies on the interpretation of the 0_1^+ state as a member of a two-quadrupole-phonon triplet. If the real character of the 0_1^+ state is different, say like a monopole one-phonon excitation in the QRPA, the assumption of equal magnitudes of the ground-state and 0_1^+ matrix elements may be justified.

For the decay of ^{92}Mo (see Table 32) a comparison between the QRPA and the shell model is rendered possible by the previous shell-model studies on nuclear-structure properties of $N = 50$–52 nuclei [145,226,227] in this mass region. In these studies two different valence spaces (SM1 and SM2 in Table 32) have been used either with completely fitted two-body interaction matrix elements (the smaller SM1 space) or with two-body matrix elements corresponding to effective interactions based on second-order corrections to the Sussex matrix elements [93] (the larger SM2 space). In the SM2 calculation the single-particle energies have been determined by fitting them to the observed levels in the $N = 50$ and $N = 51$ nuclei. These two shell-model valence spaces,

supplemented with the above-mentioned effective interactions, seem to yield good results for the level energies and electromagnetic observables of the $N = 51, 52$ isotones. Also both model spaces have been used previously to analyze the Gamow–Teller decay of the $N = 50$ nuclei [144,227].

The beta decay of $N = 50$ isotones has been studied by using a renormalized Gamow–Teller operator where the renormalization is stemming from the neglected single-particle orbitals outside the valence space through a perturbation-series approach. The effects of the renormalization upon the calculated double-beta-decay rates has been studied in [248]. In Table 32 the shell-model matrix elements for both basis sets correspond to a renormalized Gamow–Teller operator with one- and two-body corrections included into the renormalization (the (1 + 2) notation of columns 4 and 5). From the values of the various matrix elements listed in this table one can conclude that the shell-model values are quite close to the values calculated by using the QRPA model in a larger valence space (two major oscillator shells). When comparing the decay amplitudes in the shell-model and the QRPA one notices that in the QRPA one has some important virtual single-particle transitions which are coming from those components of the QRPA wave functions which have no overlap with the valence space of the shell model. Thus it is questionable if low-order perturbation corrections to the effective Gamow–Teller operator can account for such single-particle transitions in the shell-model calculation [248].

The results of the neutrinoless double β^+/EC decays have been summarized in Table 36 (upper part and lower part). The associated nuclear matrix elements have been taken from [140] and the phase-space factors from [88]. The description of the $0\nu\beta^+$/EC decay is analogous to the description of the $0\nu\beta^-\beta^-$ decay [88], the available phase space varying according to the type ($0\nu\beta^+\beta^+$, $0\nu\beta^+$EC, 0νECEC) of the decay mode.

In [88,268] it has been argued that the 0νECEC mode should be very slow in comparison with the $0\nu\beta^+$EC mode, at least 4 orders of magnitude slower than it. This makes the neutrinoless double electron-capture mode almost impossible to detect and thus we omit its discussion in this review and concentrate on results concerning the other two modes (Table 36 (upper part) for the $0\nu\beta^+\beta^+$ and Table 36 (lower part) for the $0\nu\beta^+$EC results).

The expression for the $0\nu\beta^+$/EC half-lives is given in Section 5 and by inserting the coefficients $C^{(0)}$ from Table 36 (upper and lower part) one obtains the half-lives for the $0\nu\beta^+\beta^+$ and $0\nu\beta^+$EC modes when the effective electron-neutrino mass $\langle m_\nu \rangle$ and the effective right-handed coupling parameters $\langle \lambda \rangle$ and $\langle \eta \rangle$ are known. In the above-mentioned tables the half-lives, listed in the last two lines of these tables, have been obtained by using the most stringent experimentally deduced upper limits (see the caption of Table 7) for the neutrino mass and right-handed parameters when only the mass mechanism is assumed ($T^a_{1/2}$) or when also the right-handed weak currents are included ($T^b_{1/2}$).

Already a simple phase-space consideration indicates that the $C^{(0)}$ coefficients for the mixed mode, $0\nu\beta^+$EC, should be larger than the coefficients of the double positron-emission mode. This is confirmed by a comparison of the numbers of the upper part of Table 36 with those of the lower part. As can be seen, the biggest effects of the phase-space are seen for coefficients associated to $\langle \lambda \rangle$ and the corresponding mechanism has been discussed in [140]. The big enhancement of these $C^{(0)}$ coefficients leads to the conclusion that the $0\nu\beta^+$EC mode is relatively more sensitive to the $\langle \lambda \rangle$-type of right-handed contribution than the $0\nu\beta^-\beta^-$ mode.

In general, however, the $0\nu\beta^+$/EC coefficients are much smaller in magnitude than the corresponding $0\nu\beta^-\beta^-$ coefficients as seen clearly by comparing the presently discussed tables with the

Table 36
Upper part: Coefficients $C_\kappa^{(0)}$ of Eq. (5.2) in units of yr^{-1} (and for $g_A = 1.254$) for several $0\nu\beta^+\beta^+$ decays to the ground state calculated in the proton–neutron QRPA model. The values are shown in powers of 10, with the exponents indicated in parenthesis. The values shown in columns are deduced from the nuclear matrix elements of Hirsch et al. [140]. The two half-lives, $T^a_{1/2}$ and $T^b_{1/2}$, correspond to the parameter sets given in the caption to Table 8. *Lower part*: The same for $0\nu\beta^+$EC decays to the ground state. Also the majoron matrix element of Eq. (5.24) has been included

$C_\kappa^{(0)}$ (QRPA)	^{78}Kr	^{96}Ru	^{106}Cd	^{124}Xe	^{130}Ba	^{136}Ce
mm	1.6(−16)	3.0(−17)	5.4(−17)	8.7(−17)	1.6(−17)	1.1(−18)
mλ	−9.3(−18)	−1.3(−18)	−2.6(−18)	−5.8(−19)	7.3(−19)	7.2(−20)
mη	−4.3(−14)	−9.2(−15)	−1.6(−14)	−2.1(−14)	−4.8(−15)	−4.0(−16)
$\lambda\lambda$	1.9(−17)	2.0(−18)	4.4(−18)	8.5(−18)	5.5(−19)	1.8(−20)
$\eta\eta$	6.0(−12)	1.4(−12)	2.4(−12)	2.8(−12)	6.5(−13)	5.9(−14)
$\lambda\eta$	−3.3(−18)	−6.5(−19)	−1.6(−18)	−4.9(−18)	−6.0(−19)	−4.2(−20)
$T^a_{1/2}$(yr)	3.9(27)	2.1(28)	1.1(28)	7.1(27)	3.9(28)	5.6(29)
$T^b_{1/2}$(yr)	4.8(27)	2.5(28)	1.4(28)	8.4(27)	5.2(28)	7.3(29)

$C_\kappa^{(0)}$ (QRPA)	^{58}Ni	^{78}Kr	^{96}Ru	^{106}Cd	^{124}Xe	^{130}Ba	^{136}Ce
mm	9.1(−18)	4.0(−16)	3.5(−16)	7.7(−16)	1.6(−15)	1.5(−15)	5.6(−16)
mλ	3.9(−17)	2.4(−15)	2.0(−15)	4.5(−15)	9.2(−15)	8.0(−15)	2.9(−15)
mη	1.2(−15)	7.4(−14)	7.1(−14)	1.5(−13)	2.9(−13)	2.8(−13)	1.1(−13)
$\lambda\lambda$	6.2(−17)	5.9(−15)	4.8(−15)	1.1(−14)	2.2(−14)	1.7(−14)	5.8(−15)
$\eta\eta$	1.2(−13)	8.9(−12)	9.4(−12)	2.0(−11)	3.3(−11)	3.5(−11)	1.6(−11)
$\lambda\eta$	−6.2(−17)	−2.5(−15)	−2.8(−15)	−6.6(−15)	−1.4(−14)	−9.8(−15)	−2.9(−15)
$\lvert M_{M^0}\rvert$	1.66	4.70	3.60	4.56	5.27	5.52	3.45
$T^a_{1/2}$(yr)	6.8(28)	1.5(27)	1.8(27)	8.0(26)	3.9(26)	4.1(26)	1.1(27)
$T^b_{1/2}$(yr)	5.4(27)	7.2(25)	8.6(25)	3.8(25)	1.9(25)	2.3(25)	6.4(25)

tables of Section 6.1. This yields to long estimated decay half-lives, much longer than on the double β^- side, as clearly seen in the last two rows of the upper and lower parts of Table 36. In this sense the $0\nu\beta^+$/EC decays are not as useful in estimating the values of the effective neutrino mass and the couplings of the right-handed weak currents as the $0\nu\beta^-\beta^-$ decays when combined with experimental data. In addition, the data on the $0\nu\beta^+$/EC side is of lower quality than the data on the $0\nu\beta^-\beta^-$ side.

As for the double β^- side at the end of Section 6.1, we have performed here a compilation of the magnitudes of the double β^+-decay matrix elements for the transitions to the 0^+_1 and 2^+_1 final states in Figs. 3 and 4, respectively. As before, the numerical values depicted in these figures have been taken from the tables of this section and we use the pictorial presentation for picking up possible overall trends in the magnitudes of the nuclear matrix elements.

In these figures no experimental results are indicated since the calculated results are still quite far beyond the reach of the sensitivity of experimental measurements. Otherwise the notation is the same as in Figs. 1 and 2, and the reader may consult the end of Section 6.1 for further information on the used symbols. As in the double β^- side, no general trends can be seen in the theoretical

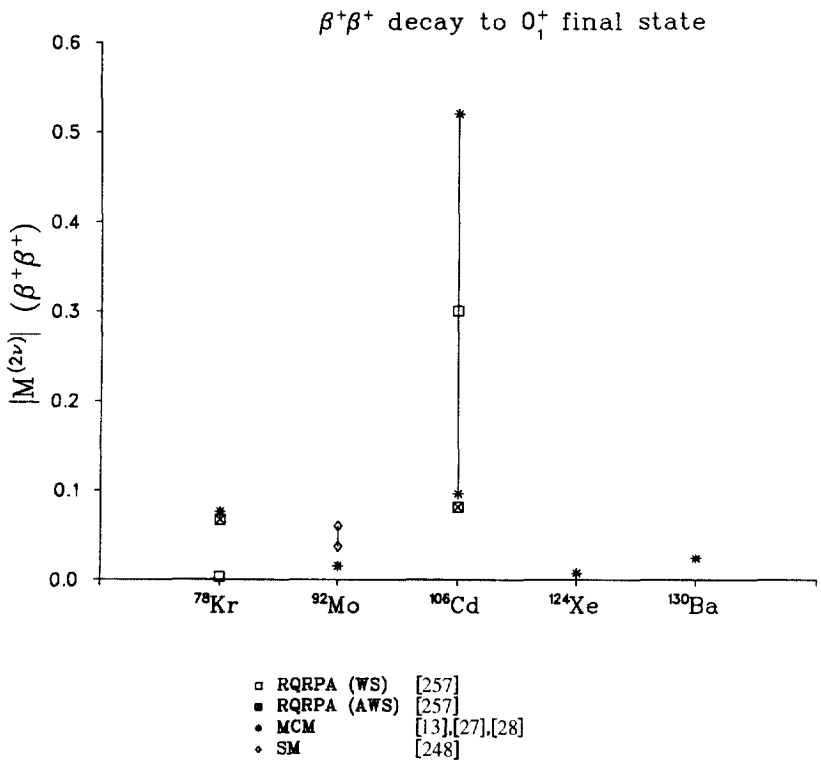

Fig. 3. Compilation of the magnitudes of the two-neutrino double-β^+-decay matrix elements for transitions to the first excited 0^+ state. For each symbol we have indicated the corresponding theoretical method and references for the numerical results. For more information see the text.

results. As already stated in connection with Figs. 1 and 2, a possible reason for this is the dependence of the decay amplitudes on the small components of the involved wave functions indicating a strong dependence on the specific structure of nuclei participating in the double beta decay.

6.3. Connection with single-beta-decay transitions

Most of the discussion presented until now has been dealing with the way in which double-beta-decay transitions are calculated. The possibility of reducing the number of free parameters entering in the double-beta calculations (mainly in the QRPA ones) by looking at the single-beta-decay transitions feeding some of the states of the initial and final nucleus, participant in the double-beta-decay transitions, has been explored in [13,240]. The results of such a systematics, where the *ft*-values for allowed and first-forbidden transitions are calculated, show that the matrix elements for double-beta-decay transitions can be calculated in a less "parameter-dependent" fashion. Experimental efforts to measure various lateral feeding paths of beta decay, leading to initial or final states of a double-beta-decay chain, have also been reported [42,113].

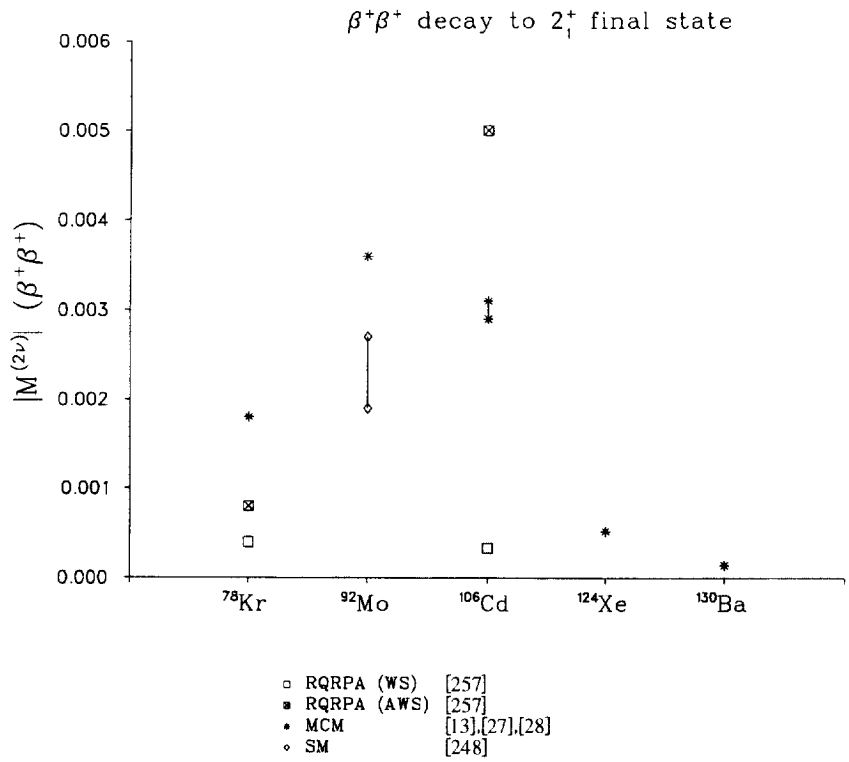

Fig. 4. Compilation of the magnitudes of the two-neutrino double-β^+-decay matrix elements for transitions to the first excited 2^+ state. For each symbol we have indicated the corresponding theoretical method and references for the numerical results. For more information see the text.

As an example, the results of the calculations and measurements [42,43], for the case of the decay of ^{116}Cd, are shown in Fig. 5 and Table 37. The calculations have been done using the multiple-commutator model (MCM) of Ref. [237], combining the proton–neutron QRPA with the charge-conserving QRPA (for further information see Section 3.4.7). In this case the single-particle energies of the initial and final nuclei of the double beta decay are based on the systematics developed in the study of a number of tin and cadmium isotopes in [247].

The decay of the intermediate nucleus, ^{116}In, is of interest in the double-beta-decay study. Both the logft values of the electron-capture transition to the ground state of ^{116}Cd and of the β^- transition to the ground state of ^{116}Sn from the 1^+ ground state of ^{116}In can be reproduced by the value $g_{pp} = 0.75$ for the proton–neutron particle–particle strength parameter in a proton–neutron QRPA calculation. In addition, one obtains the log ft values of Table 37 in the MCM calculation using this value of g_{pp}. This results in a calculated two-neutrino double-beta-decay half-life of 0.76×10^{19} yr to be compared with the experimental half-life of 3.75×10^{19} yr [7]. In this case the intermediate states other than the first one yield a non-negligible contribution to the double Gamow–Teller matrix element and thus the theoretical decay half-life is too short (taking only the first intermediate 1^+ state into account in the calculation would yield approximately to the experimental half-life value).

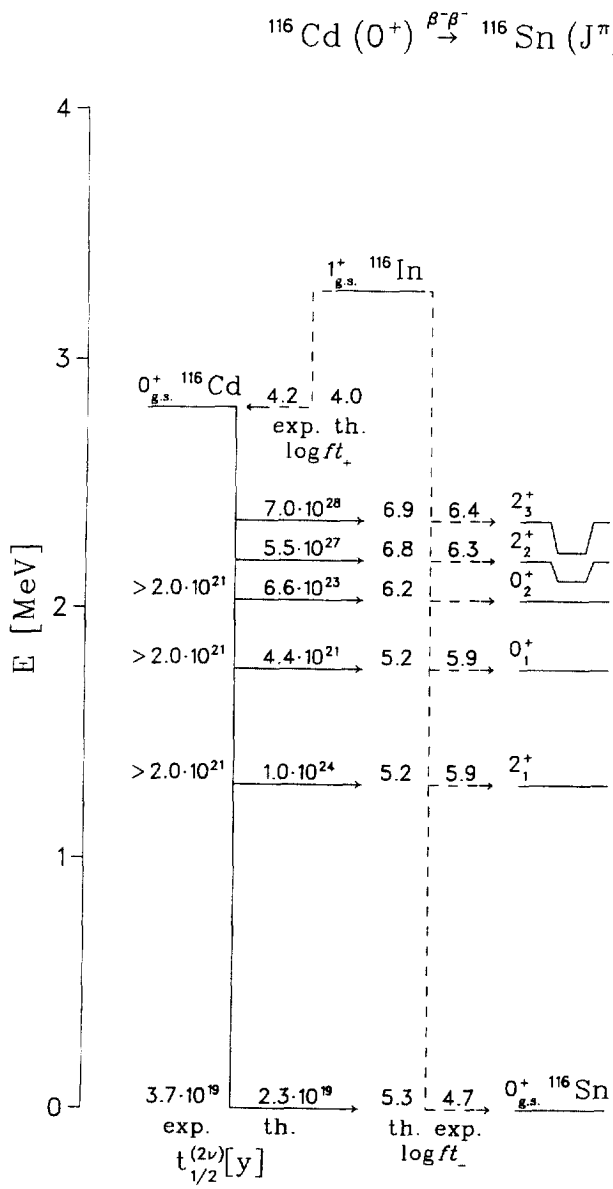

Fig. 5. Comparison of the experimental and theoretical results for the double beta decay of ^{116}Cd to the ground state ($0^+_{g.s.}$) and excited 0^+ and 2^+ states of the final nucleus ^{116}Sn. Also the logft values of the electron-capture and β^- decays of the intermediate odd–odd nucleus ^{116}In have been indicated.

On the other hand, the value $g_{pp} = 1.0$ would fit the experimental ground-state half-life much better (see Fig. 5) but would yield a slightly too fast electron-capture transition and a too slow β^- transition in ^{116}In as seen in Fig. 5 where we also give theoretical $\beta^-\beta^-$ half-lives for decays to several excited final states. In addition, in Table 27 we list calculated and experimental data on excitation energies of ^{116}Sn and the logft values corresponding to the Gamow–Teller β^- feeding of

Table 37
Comparison of experimental data and the results of a QRPA calculation (the MCM method of Section 3.4.7) for the β^- decay of ^{116}In to the final ground state and 0^+ and 2^+ excited states in ^{116}Sn. In this calculation the value $g_A = 1.0$ was used for the axial-vector coupling constant and the values $g_{pp} = 0.75$ (column 5) and $g_{pp} = 1.0$ (column 6) for the proton–neutron particle–particle strength parameter. In this table the excitation energy of the final state and the log ft value of its β^--decay feeding is given

	Excitation energy [MeV]		Log ft for $1^+_{g.s.} \to J^\pi_f$ transitions		
J^π_f	Exp.	Th.	Exp.	Th.($g_{pp} = 075$)	Th.($g_{pp} = 1.0$)
$0^+_{g.s.}$	0.00	0.00	4.66	4.66	5.32
2^+_1	1.29	1.29	5.85	5.20	5.18
0^+_1	1.76	1.71	5.88	5.21	5.23
0^+_2	2.03	2.58	---	6.24	6.25
2^+_2	2.11	2.58	6.31	6.81	6.84
2^+_3	2.23	2.35	6.40	6.91	6.94
0^+_3	2.55	2.57	5.99	4.15	4.14
2^+_4	2.65	2.49	5.79	5.92	5.89
$(0)^+$	2.79	2.70(2^+)	5.98	5.75	5.73

these states. In this calculation we have assumed the states 0^+_2 and 2^+_2 to have a two-phonon structure and the rest to be simple one-phonon QRPA states. In particular, the 0^+_1 state is supposed to have a monopole-phonon structure and not a two-phonon structure as is the usual assumption in the calculations [13,75,119]. This interpretation better fits the experimental log ft data and closely resembles the situation found in the case of the ^{96}Zr $\to$ ^{96}Mo decay in Ref. [232].

It is important to note that in this case one would have a perfect single-state dominance of the ^{116}Cd transition (see the discussion in the context of ^{100}Mo and Ref. [42]). This feature of the ^{116}Cd decay suggests that the QRPA is able to yield realistic rates for the single-beta-decay and double-beta-decay transitions but that some improvement of the theory is needed to exactly reproduce both the single- and double-beta-decay data. We want to point out that similar situation is encountered in the ^{100}Mo decay in [245], but the discrepancies between the data and the theory are much more severe. This is explained by the more complicated structure of the final nucleus ^{100}Ru with possible deformation and coexistence effects setting in. In this sense the ^{116}Cd decay is more clean-cut and better accessible to nuclear theories based on a spherical mean field.

A good candidate for the above-mentioned improvement in the QRPA approach could be some type of higher-QRPA framework yielding to a more consistent treatment of the proton–neutron and like-nucleon degrees of freedom on an equal footing. Work along these lines has been performed in [203,204,206] and concrete results concerning double beta decay have been produced in [232,234].

7. Summary and conclusions

From the results of the previous chapters we can extract some definite conclusions about the status of the agreement between data and theory as well as about the status of

the theory, more specifically, of the nuclear-structure component of the theory. They are the following:

- Conclusions about the double Gamow–Teller matrix element $M_{GT}^{(2\nu)}$: In the presence of strong cancellations among the main components of the wave functions the matrix elements $M_{GT}^{(2\nu)}$ are mostly driven by small components of the wave functions. Thus the sensitivity of the theoretical results upon the inclusion and/or removal of some of these small components, by restricting the number of valence orbitals, truncating the configuration space or by renormalizing some components of the wave functions, is very noticeable. However, the order of magnitude of the matrix elements remains about the same for the few cases where results of both approximate models (like the QRPA) and the full shell model are available. This is also true for other cases where restricted shell-model calculations have been performed and compared with results of the QRPA method. From this we can conclude that the agreement between the shell-model and the QRPA results can only be achieved if attractive two-particle correlations between neutrons and protons are included in the definition of the QRPA matrices. The strong dependence of the QRPA results upon the renormalization of these interactions is an essential feature of the model which is also present in the shell-model results. The dependence upon renormalization can be circumvented by resorting to an analysis of the single-beta-decay transitions feeding the states of nuclei involved in double-beta-decay transitions.
- Conclusions about the single-intermediate-state dominance: In some selected cases, like in the decays of ^{100}Mo and ^{116}Cd, it has been confirmed, by using effective matrix elements (for single beta decay and electron capture) extracted from the lateral (one-step) transitions and effective energy denominators, that the extracted matrix elements for the two-neutrino double-beta-decay mode can be approximated by a single virtual two-step process involving only the ground state of the participant doubly-odd nucleus. However, for some other cases where 1^+ is not the multipolarity of the ground-state, like the decay of Ge, the "single-state" dominance does not manifest itself in the final value of the two-neutrino double-beta-decay matrix elements. Rather, the participation of few low-lying 1^- states of the intermediate nucleus is needed to produce the observed suppression of the final matrix element. Still, confirmation of the hypothesis of the single-state dominance in the case of a 1^+ intermediate ground state clearly needs some further studies.
- Conclusions about quenching, symmetries and fragmentation of the single-beta-decay and double-beta-decay intensities: theoretical results show that the fragmentation of the β^+ strength is perhaps the most sensitive quantity in a double-beta-decay calculation and also the one with the largest theoretical uncertainties. Concerning the quenching of the beta-decay intensities on the proton-rich side of the nuclear chart, this mechanism does not influence significantly the final values of the involved nuclear matrix elements the magnitude of which, as said before, seems to be the result of a cancellation between attractive and repulsive proton–neutron interactions. This has been confirmed by the available shell-model results and so far the appearance of a highly symmetric situation involving a complete spin–isospin degeneracy of the single-particle basis, as in the case of the SU(4) symmetry, is supported neither by the data nor by the theoretical results.
- Conclusions about the power of the QRPA to predict values of relevant nuclear matrix elements: predicting power of the QRPA can certainly be improved and a good amount of work has been done already leading to this direction. However, most of the attempted fine tunings of the model

fail in one respect or the other. The need to bring the theory to a "cancellation-free" status seems to be out of context because of the features exhibited by the shell-model results. Apparently the most difficult task is to correct for the prediction of the β^+ strengths, which is the place where the theoretical description has failed thus far.

- Conclusions concerning the study of neutrinoless transitions: results of the calculations show a less drastic dependence on nuclear-model assumptions than in the case of the two-neutrino decay but still they are sensitive to the models used to describe the neutrino-physics sector of the calculations. The overall trend extracted from data (which are only upper or lower limits for the weak-interaction parameters and the half-lives, respectively) shows a sort of universality in the extracted (and predicted) mass term of the weak lagrangian, establishing an upper limit for the neutrino-mass shift of the order of 1 eV. This limit is compatible with the relative strength of the parity-violating effective left-right coupling, which for most models has a sort of universal upper limit of the order of 10^{-7}. The same can be said about the singlet-majoron–nucleon coupling constant, which for most cases has an upper limit of the order of 10^{-4}, implying a scale of about 100 keV for the spontaneous symmetry breaking of the U(1) B–L symmetry. The corresponding matrix element seems to be of the order of 2.8. Naturally, these limits will improve as the already going-on experiments increase their statistics and the future experiments start their operation. From these considerations and from the fact that the mixing with a right-handed second generation of gauge bosons is predicted in a similar fashion by nuclear-structure studies and studies of muon decay and supernova neutrinos, it is concluded that nuclear-structure studies of the neutrinoless double beta decay can be taken as good complementary tools for particle and astroparticle physics.
- Conclusions about the use of nuclear-structure-based information for experimental studies of nuclear double-beta-decay transitions: The compilation of the available theoretical results on the two-neutrino and neutrinoless double beta decays has been performed in Section 6 of this report. This data have been presented as tables and figures in this chapter and can be used in planning future experiments on double beta decay. The presented theoretical information on the two-neutrino and the neutrinoless mode of decay is presented in a form which is easily accessible for the experimentalists who want to decide which nucleus would be the optimum candidate to measure definite properties of the double-beta-decay transitions under some external constraints stemming from the limits of the measuring apparatus, measuring time, the size and form of the source etc.

Acknowledgements

This work has been partially supported by the Academy of Finland, the University of Jyväskylä, Finland, the CONICET and ANPCYT of Argentina and by the J.S. Guggenheim Memorial Foundation, USA.

The help of Matias Aunola and Jussi Toivanen with some of the tables and figures presented in this report is acknowledged with thanks.

The authors would like to thank Professors Pertti Lipas and Daniel Bes for many years of guidance and discussions about the fundamentals of nuclear structure.

One of the authors (O.C.) thanks gratefully the kind hospitality extended to him at the Department of Physics of the University of Jyväskylä.

The authors would also like to thank Dr. Alexander Barabash for his careful reading and suggestions concerning the experimental parts and data of the manuscript.

Appendix A. Calculation of the phase-space factors

In this appendix we give the integration formulae which were used in calculating the phase-space factors appearing in Section 4.

A.1. $2\nu\beta^-\beta^-$ phase-space integrals

The phase-space factors of the upper parts in Tables 1 and 5 have been calculated using the following numerical integrals over the electron energies ε_1 (electron 1) and ε_2 (electron 2):

$$G^{(2\nu)}(J) = g_J \int_1^{T+1} F_0(Z_f, \varepsilon_1) p_1 \varepsilon_1 I^{(J)}(T, \varepsilon_1)\, \mathrm{d}\varepsilon_1 , \tag{A.1}$$

where

$$I^{(J)}(T, \varepsilon_1) = \int_1^{T+2-\varepsilon_1} F_0(Z_f, \varepsilon_2) p_2 \varepsilon_2 f_J (T + 2 - \varepsilon_1 - \varepsilon_2)^{5+J} \mathrm{d}\varepsilon_2 , \tag{A.2}$$

and

$$f_J = \begin{cases} 1 & \text{if } J = 0 , \\ (\varepsilon_1 - \varepsilon_2)^2 & \text{if } J = 2 . \end{cases} \tag{A.3}$$

Here J is the angular momentum of the final nuclear state and T is the Q value of the $2\nu\beta^-\beta^-$ decay in units of the electron rest mass. In case of an excited final state this Q value takes into account the excitation energy of the final state. In the above integrals every quantity has been scaled by the electron rest mass. The electron momentum is $p = \sqrt{\varepsilon^2 - 1}$ and the coupling constants are given by (for the tables we take $g_A = 1.254$)

$$g_0 = 3.78 \times 10^{-24} g_A^4 \ \mathrm{yr}^{-1}; \qquad g_2 = \tfrac{1}{7} g_0 . \tag{A.4}$$

It has to be noted in this context that with the above-defined phase-space factors one has to use nuclear matrix elements with the energy denominator scaled by the electron rest mass.

The relativistic Fermi factor, $F_0(Z_f, \varepsilon)$, where Z_f is the atomic number of the $2\nu\beta^-\beta^-$ final nucleus, takes into account the Coulomb attraction between the electron and the daughter nucleus. It is defined as the square of the ratio of the values of the Dirac s-wave functions of the electron at the nuclear surface (i.e. at radius $R_A = 1.2A^{1/3}$ fm) with and without the Coulomb potential of a homogeneously charged sphere [44,170]. This Fermi function can be approximated as

$$F_0(Z_f, \varepsilon) = \frac{4}{[\Gamma(2\gamma_1 + 1)]^2} (2pR_A)^{2(\gamma_1 - 1)} |\Gamma(\gamma_1 + \mathrm{i}y)|^2 \mathrm{e}^{\pi y} , \tag{A.5}$$

with

$$|\Gamma(\gamma_1 + iy)|^2 \simeq \pi \sqrt{(\gamma - 1)^2 + y^2 \sin^2[\pi(\gamma_k - 1)] + \sinh^2(\pi y)} \times \frac{(2 - \gamma_k)^2 + y^2}{\gamma_k^2 + y^2}, \tag{A.6}$$

where $\alpha = \frac{1}{137}$ is the fine-structure constant, $y = \alpha Z_f \varepsilon / p$ and $\gamma_k = \sqrt{k^2 - (\alpha Z_f)^2}$.

If one replaces $F_0(Z_f, \varepsilon)$ by its Primakoff–Rosen (PR) approximation [198]

$$F_0(Z_f, \varepsilon) = \frac{\varepsilon}{p} F_0^{(\mathrm{PR})}(Z_f); \qquad F_0^{(\mathrm{PR})}(Z_f) = \frac{2\pi\alpha Z_f}{1 - e^{-2\pi\alpha Z f}}, \tag{A.7}$$

one can perform the integral (A.1) analytically to yield (see also [125])

$$G^{(2\nu)}(J) \simeq g_J h_J [F_0^{(\mathrm{PR})}(Z_f)]^2 T^{7+2J} [1 + a_J^{(1)} T + a_J^{(2)} T^2 + a_J^{(3)} T^3 + a_J^{(4)} T^4], \tag{A.8}$$

with

$$h_0 = \tfrac{1}{7},\ a_0^{(1)} = \tfrac{1}{2},\ a_0^{(2)} = \tfrac{1}{9},\ a_0^{(3)} = \tfrac{1}{90},\ a_0^{(4)} = \tfrac{1}{1980},$$
$$h_2 = \tfrac{1}{990},\ a_2^{(1)} = \tfrac{2}{3},\ a_2^{(2)} = \tfrac{2}{13},\ a_2^{(3)} = \tfrac{1}{91},\ a_2^{(4)} = \tfrac{1}{2730}. \tag{A.9}$$

These results can be compared against the corresponding result for the Gamow–Teller beta decay, namely

$$G^{(\mathrm{GT})} = g_{\mathrm{GT}} \int_1^{T+1} F_0(Z_f, \varepsilon) p\varepsilon (T + 1 - \varepsilon)^2 \, d\varepsilon \tag{A.10}$$

$$\simeq \frac{1}{3} g_{\mathrm{GT}} F_0^{(\mathrm{PR})}(Z_f) T^3 \left[1 + \frac{T}{2} + \frac{T^2}{10}\right], \tag{A.11}$$

where T is the β^--decay Q value in units of the electron rest mass, and

$$g_{\mathrm{GT}} = 1.63 \times 10^{-4}\ \mathrm{s}^{-1}. \tag{A.12}$$

A.2. $2\nu\beta^+\beta^+$, $2\nu\beta^+$EC and 2νECEC phase-space factors

The phase-space integrals are available only for the 0^+ final states and have been calculated according to Doi and Kotani [87]. In the present article we deviate from the notation of [87] to obtain a uniform presentation for Sections A.1 and A.2.

The phase space is different for the different double β^+/EC modes, namely for the $2\nu\beta^+\beta^+$, $2\nu\beta^+$EC and 2νECEC mode. As in the $2\nu\beta^-\beta^-$ case (following the same notation) the phase-space factors of the lower parts of Tables 1 and 5 can be computed from the following expressions:

$$G^{(2\nu)}(\beta^+\beta^+) = g_0 \int_1^{T(\beta^+\beta^+)+1} \int_1^{T(\beta^+\beta^+)+2-\varepsilon_1} h_{2\nu} R_{1,1}(\varepsilon_1) R_{1,1}(\varepsilon_2) F_0(-Z_f, \varepsilon_1)$$
$$\times F_0(-Z_f, \varepsilon_2) \varepsilon_1 p_1 \varepsilon_2 p_2 [T(\beta^+\beta^+) + 2 - \varepsilon_1 - \varepsilon_2]^5 \, d\varepsilon_1 \, d\varepsilon_2, \tag{A.13}$$

$$G^{(2\nu)}(\beta^+\mathrm{EC}) = g_0 B(\beta^+\mathrm{EC}) \int_1^{T(\beta^+\mathrm{EC})+1} h_{2\nu} R_{1,1}(\varepsilon_1) \times F_0(-Z_f, \varepsilon_1)\varepsilon_1 p_1 [T(\beta^+\mathrm{EC}) + 1 - \varepsilon_1]^5 \, \mathrm{d}\varepsilon_1, \tag{A.14}$$

$$G^{(2\nu)}(\mathrm{ECEC}) = g_0 B(\mathrm{ECEC}) T(\mathrm{ECEC})^5, \tag{A.15}$$

where $C_{F,0}B(\beta^+\mathrm{EC})$ can be read from [87], Eq. (3.10) and B(ECEC) from [87], Eq. (3.11). Here ε_1 and ε_2 are energies of the emitted positrons and $h_{2\nu}$ is an integral over both the phase space and the square of the energy denominators, but its value is, to a good approximation, unity and this is also the value adopted for $h_{2\nu}$ in the present work. The factor $R_{1,1}$ reflects the charge distribution inside the nucleus and it is to a good approximation unity except in the low-momentum region of the positron. The Fermi factor $F_0(-Z_f, \varepsilon)$ can be corrected for the electron screening of the nuclear charge as presented in Eqs. (A.39) and (A.40).

Due to insignificant likelihood of electron capture from higher shells than K or L these modes have been neglected. In the present work also the double L-electron capture has been omitted and the EC process is always handled as K-electron capture since the inclusion of the L-electron capture does not induce significant changes in the phase-space factors.

The scaled kinetic-energy release T is different for the $\beta^-\beta^-$ and $\beta^+\beta^+$ modes, i.e.

$$T(\beta^-\beta^-) = [m(A, Z-2) - m(A, Z)]/m_e, \tag{A.16}$$

$$T(\beta^+\beta^+) = [m(A, Z+2) - m(A, Z)]/m_e - 4, \tag{A.17}$$

where $m(A, Z)$ is the mass of the final neutral atom. For the mixed mode, β^+EC, and the double electron capture, ECEC, one has, instead

$$T(\beta^+EC) = [m(A, Z+2) - m(A, Z)]/m_e - 2 - \varepsilon_b, \tag{A.18}$$

$$T(\mathrm{ECEC}) = [m(A, Z+2) - m(A, Z)]/m_e - \varepsilon_{b1} - \varepsilon_{b2}, \tag{A.19}$$

where ε_b is the binding energy (in units of the electron rest mass) of the captured electron. Experimental values of this binding energy for a K-shell electron are given in Table 1 (lower part) in Section 4 and theoretical ones in Table IV of [87].

The Q values of the various decay modes can also be given in terms of the nuclear masses M. In this case

$$T(\beta^-\beta^-) = \Delta M - 2, \tag{A.20}$$

$$T(\beta^+\beta^+) = \Delta M - 2, \tag{A.21}$$

$$T(\beta^+\mathrm{EC}) = \Delta M - \varepsilon_b, \tag{A.22}$$

$$T(\mathrm{ECEC}) = \Delta M + 2 - \varepsilon_{b1} - \varepsilon_{b2}, \tag{A.23}$$

where we have defined the scaled nuclear mass difference as

$$\Delta M = (M_i - M_f)/m_e, \tag{A.24}$$

M_i and M_f being the initial and final nuclear masses, respectively.

From above one can easily see that the different kinetic-energy releases are related to each other in the following way

$$T(\beta^+\mathrm{EC}) = T(\beta^+\beta^+) + 2 - \varepsilon_b\,, \tag{A.25}$$

$$T(\mathrm{ECEC}) = T(\beta^+\beta^+) + 4 - \varepsilon_{b1} - \varepsilon_{b2}\,. \tag{A.26}$$

The above formulae, (A.25) and (A.26), are handy whenever one of the Q values is known and one has to find the values of the other ones.

A.3. Phase-space integrals for neutrinoless double beta decay

Here we give the explicit expressions of the phase-space integrals which have been used to compute the values of the phase-space factors of the neutrinoless $\beta^-\beta^-$ decays in Table 6. For completeness, we also list the corresponding factors for the $\beta^+\beta^+$ and β^+EC decay modes. Their numerical values have been given in [88].

The phase-space integral for the neutrinoless $\beta^-\beta^-$ mode can be given in the form [85][2]

$$G_k^{(0\nu)}(\beta\beta) = \frac{g^{(0\nu)}}{r_A^2}\int_1^{T+1} b_k^{(\beta\beta)} F_0(Z_f,\varepsilon_1)F_0(Z_f,\varepsilon_2)p_1p_2\varepsilon_1\varepsilon_2\,\mathrm{d}\varepsilon_1\,, \tag{A.27}$$

with

$$b_1^{(\beta\beta)} = 1\,, \tag{A.28}$$

$$b_2^{(\beta\beta)} = \frac{1}{2}\left(\frac{\varepsilon_1\varepsilon_2 - 1}{\varepsilon_1\varepsilon_2}\right)(\varepsilon_1 - \varepsilon_2)^2\,, \tag{A.29}$$

$$b_3^{(\beta\beta)} = (\varepsilon_1 - \varepsilon_2)^2/\varepsilon_1\varepsilon_2\,, \tag{A.30}$$

$$b_4^{(\beta\beta)} = \frac{2}{9}\left(\frac{\varepsilon_1\varepsilon_2 - 1}{\varepsilon_1\varepsilon_2}\right), \tag{A.31}$$

$$b_5^{(\beta\beta)} = \frac{4}{3}\left(\frac{(T+2)X_{\beta\beta}}{2r_A\varepsilon_1\varepsilon_2} - \frac{\varepsilon_1\varepsilon_2 + 1}{\varepsilon_1\varepsilon_2}\right), \tag{A.32}$$

$$b_6^{(\beta\beta)} = 4(T+2)/r_A\varepsilon_1\varepsilon_2\,, \tag{A.33}$$

$$b_7^{(\beta\beta)} = \frac{16}{3}\frac{1}{r_A\varepsilon_1\varepsilon_2}\left(\frac{\varepsilon_1\varepsilon_2 + 1}{2r_A}X_{\beta\beta} - T - 2\right), \tag{A.34}$$

[2] In [259] $G_k^{(0\nu)}(\beta^-\beta^-)$ is multiplied by a factor $(2R_A)^2$ to match the definitions of the nuclear matrix elements and the neutrino potentials in [259].

$$b_8^{(\beta\beta)} = \frac{2}{9}\frac{1}{r_A^2\varepsilon_1\varepsilon_2}\left[(\varepsilon_1\varepsilon_2+1)(X_{\beta\beta}^2+4r_A^2) - 4r_A X_{\beta\beta}(T+2)\right], \tag{A.35}$$

$$b_9^{(\beta\beta)} = \frac{8}{r_A^2}\left(\frac{\varepsilon_1\varepsilon_2+1}{\varepsilon_1\varepsilon_2}\right), \tag{A.36}$$

where $\varepsilon_2 = T+2-\varepsilon_1$, $p_i = \sqrt{\varepsilon_i^2-1}$, $i=1,2$, $r_A = m_e R_A$, $R_A = 1.2A^{1/3}$ fm, and

$$X_{\beta\beta} = 3\alpha Z_f + r_A(T+2), \tag{A.37}$$

$$g^{(0\nu)} = 2.80\times 10^{-22} g_A^4\ \mathrm{yr}^{-1}. \tag{A.38}$$

To get the corresponding phase-phase factors for the $\beta^+\beta^+$ decay one just has to replace Z_f by $-Z_f$ in the Fermi factor $F_0(Z_f,\varepsilon)$ and in $X_{\beta\beta}$, and possibly correct the Fermi factors F_0 for the electron-screening of the nuclear charge (important correction for positrons at low energies and high Z):

$$F_0(-Z_f,\varepsilon) \to F_0(-Z_f,\varepsilon+V_0)\left(\frac{\varepsilon+V_0}{\varepsilon}\right)\sqrt{\frac{(\varepsilon+V_0)^2-1}{\varepsilon^2-1}}, \tag{A.39}$$

where the shifting potential V_0 yields to

$$V_0 = 1.13\alpha^2 Z^{4/3} \tag{A.40}$$

in the Thomas–Fermi approximation. Here the Q values to be used are obtained from Eq. (A.16) or Eq. (A.20) for the $\beta^-\beta^-$ mode and from Eq. (A.17) or Eq. (A.21) for the $\beta^+\beta^+$ mode.

In the case of the mixed mode, β^+EC, the phase-space factors read to a good approximation (see [87,88])

$$\begin{aligned} G_k^{(0\nu)}(\beta^+\mathrm{EC}) &= \frac{g^{(0\nu)}}{r_A^2}4\pi^2 N_{0,-1}F_0(-Z_f,T+1)\sqrt{T(T+2)}\,b_k^{(\beta^-\mathrm{EC})} \\ &\simeq \frac{g^{(0\nu)}}{r_A^2}4\pi^2 N_{0,-1}F_0^{(\mathrm{PR})}(-Z_f)(T+1)b_k^{(\beta^+\mathrm{EC})}, \end{aligned} \tag{A.41}$$

where the latter form has been obtained by using the Primakoff–Rosen approximation for $F_0(-Z_f,T+1)$ with $F_0^{(\mathrm{PR})}(-Z_f)$ defined in Eq. (A.7). In this case $T \equiv T(\beta^+\mathrm{EC})$ defined in Eqs. (A.18) and (A.22). The quantity $N_{0,-1}$ is the normalization factor of the bound-state wave function of the captured electron and its definition can be found in [87]. Its non-relativistic approximation reads $N_{0,-1} \simeq [\alpha(Z_f+2)]^3/\pi$ which is enough for rough evaluation of the phase-space factors. Below we list the factors $b_k^{(\beta^+\mathrm{EC})}$

$$b_1^{(\beta^+\mathrm{EC})} = T+1, \tag{A.42}$$

$$b_2^{(\beta^+\mathrm{EC})} = \tfrac{1}{2}(T+2)(T+2-\varepsilon_b)^2, \tag{A.43}$$

$$b_3^{(\beta^+\mathrm{EC})} = (T+2)(T+2-\varepsilon_b), \tag{A.44}$$

$$b_4^{(\beta^+\mathrm{EC})} = \frac{2}{9}(T+2)\left(1-\frac{3\alpha}{2r_A}\right), \tag{A.45}$$

$$b_5^{(\beta^+\mathrm{EC})} = \frac{2}{3}T\left(\frac{X_{\beta\mathrm{EC}}}{r_A}-2\right), \tag{A.46}$$

$$b_6^{(\beta^+\mathrm{EC})} = \frac{4}{r_A}T, \tag{A.47}$$

$$b_7^{(\beta^+\mathrm{EC})} = \frac{8}{3}\frac{T}{r_A}\left(\frac{X_{\beta\mathrm{EC}}}{r_A}-2\right), \tag{A.48}$$

$$b_8^{(\beta^+\mathrm{EC})} = \frac{2}{9}T\left[\frac{X_{\beta\mathrm{EC}}^2}{r_A^2}-4\frac{X_{\beta\mathrm{EC}}}{r_A}+4\right], \tag{A.49}$$

$$b_9^{(\beta^+\mathrm{EC})} = \frac{8}{r_A^2}T. \tag{A.50}$$

Here

$$X_{\beta\mathrm{EC}} = 3\alpha(Z_f+1) - r_A(T+\varepsilon_b). \tag{A.51}$$

For the $\beta^-\beta^-$ decay to the final 2^+ state one obtains the following phase–phase factors [259]

$$G_{k\pm}^{(0\nu)}(\beta^-\beta^-;2^+) = \frac{g^{(0\nu)}}{12r_A^2}\int_1^{T+1} b_{k\pm}^{(\beta\beta 2)}F_0(Z_f,\varepsilon_1)F_0(Z_f,\varepsilon_2)p_1p_2\,\mathrm{d}\varepsilon_1\,, \tag{A.52}$$

where

$$b_{1\pm}^{(\beta\beta 2)} = P_{12}^{(+)}\left[(\varepsilon_1\varepsilon_2+1)\pm\varepsilon_{12}^{(+)}\right], \tag{A.53}$$

$$b_{2\pm}^{(\beta\beta 2)} = P_{12}^{(+)}(\varepsilon_1\varepsilon_2-1)\pm P_{12}^{(-)}\varepsilon_{12}^{(-)}, \tag{A.54}$$

with

$$\varepsilon_{12}^{(\pm)} = \varepsilon_1\pm\varepsilon_2\,, \tag{A.55}$$

$$P_{12}^{(\pm)} = p_1^2\pm p_2^2\,. \tag{A.56}$$

A.4. Phase-space integral for majoron emission

The phase-space factors $G^{(0\nu\mathrm{M})}$ for majoron emission in a neutrinoless $\beta^-\beta^-$ decay to the final ground state are shown in the last column of Table 6 and they have been calculated using the

following numerical integrals over the electron energies ε_1 (electron 1) and ε_2 (electron 2):

$$G^{(0\nu M)} = \frac{g^{(0\nu M)}}{r_A^2} \int_1^{T+1} F_0(Z_f, \varepsilon_1) p_1 \varepsilon_1 I^{(M)}(T, \varepsilon_1)\, d\varepsilon_1 , \tag{A.57}$$

where

$$I^{(M)}(T, \varepsilon_1) = \int_1^{T+2-\varepsilon_1} F_0(Z_f, \varepsilon_2) p_2 \varepsilon_2 k\, d\varepsilon_2 . \tag{A.58}$$

Here $r_A = m_e R_A$ is the nuclear radius scaled by the electron rest mass and T is the Q value of the neutrinoless $\beta^-\beta^-$ decay in units of the electron rest mass. The electron momentum is given by $p = \sqrt{\varepsilon^2 - 1}$ and k is the majoron momentum ($= T + 2 - \varepsilon_1 - \varepsilon_2$). The coupling constant reads (for the tables we take $g_A = 1.254$)

$$g^{(0\nu M)} = 3.55 \times 10^{-24} g_A^4 \text{ yr}^{-1} . \tag{A.59}$$

Appendix B. Partial-wave expansion of lepton vertices

In this appendix we give the formulae for the partial-wave expansion of the leptonic part of the weak-decay vertices of the beta and double beta decay. This form of the leptonic weak-interacti on vertices is particularly useful in dealing with the calculation of transition matrix elements in a separable lepton–hadron representation, like the one which we have used to compute the decay rates given in Section 2.

The leptonic currents can be expressed in terms of electron and electron–neutrino fields written in a separable partial-wave expansion

$$\psi_e(\boldsymbol{r}) = \sum_{\kappa_e, \mu_e} a_{\kappa_e \mu_e}(\hat{\boldsymbol{p}}_e, s_e) \psi^{\mu_e}_{\kappa_e}(\boldsymbol{r}) , \tag{B.1}$$

$$\psi_\nu(\boldsymbol{r}) = \sum_{\kappa_\nu, \mu_\nu} b_{\kappa_\nu \mu_\nu}(\hat{\boldsymbol{p}}_\nu, s_\nu) \psi^{\mu_\nu}_{\kappa_\nu}(\boldsymbol{r}) , \tag{B.2}$$

where the vectorial factors for the electron (e) and neutrino (ν) are defined as

$$a_{\kappa_e \mu_e}(\hat{\boldsymbol{p}}_e, s_e) = 4\pi i^{l_e} (l_e\, \mu_e - s_e \tfrac{1}{2} s_e | j_e \mu_e) Y^*_{l_e,\, \mu_e - s_e}(\hat{\boldsymbol{p}}_e) e^{-i\Delta_e} , \tag{B.3}$$

$$b_{\kappa_\nu \mu_\nu}(\hat{\boldsymbol{p}}_\nu, s_\nu) = 4\pi (l_\nu\, \mu_\nu - s_\nu \tfrac{1}{2} s_\nu | j_\nu \mu_\nu) Y^*_{l_\nu,\, \mu_\nu - s_\nu}(\hat{\boldsymbol{p}}_\nu) , \tag{B.4}$$

and they depend on the direction of the lepton momentum ($\hat{\boldsymbol{p}}$). The quantities $(\ldots|\ldots)$ are the usual Clebsh–Gordan coefficients [90] and κ is defined in the standard way of [34,221]. Electron Coulomb shifts are denoted by Δ_e. In terms of spinors the lepton fields read

$$\psi^{\mu}_{\kappa}(\boldsymbol{r}) = \begin{pmatrix} g_\kappa(r)\, \chi^{\mu}_{\kappa}(\hat{\boldsymbol{r}}) \\ i f_\kappa(r)\, \chi^{\mu}_{\kappa}(\hat{\boldsymbol{r}}) \end{pmatrix} . \tag{B.5}$$

The spinors χ are defined by

$$\chi_{\kappa}^{\mu}(\hat{\boldsymbol{r}}) = \sum_{\sigma=\pm 1/2} \left(l_{\kappa}\, \mu - \sigma \frac{1}{2}\, \sigma \,|\, j_{\kappa}\, \mu \right) Y_{l_{\kappa}, \mu-\sigma}(\hat{\boldsymbol{r}}) \chi_{\sigma}\,, \tag{B.6}$$

and the radial components of the electron field are

$$f_{\kappa_e}(r) = \alpha_{\kappa_e} \frac{(p_e r)^{k_e - 1}}{(2k_e - 1)!!} \sum_m a_{\kappa_e, m} \left(\frac{r}{R} \right)^m, \tag{B.7}$$

$$g_{\kappa_e}(r) = \alpha_{\kappa_e} \frac{(p_e r)^{k_e - 1}}{(2k_e - 1)!!} \sum_m b_{\kappa_e, m} \left(\frac{r}{R} \right)^m. \tag{B.8}$$

The radial dependence of the neutrino field is given by spherical Bessel functions

$$j_{\bar{l}_\nu}(p_\nu r) = \left(\frac{p_\nu r}{2} \right)^{\bar{l}_\nu} \sum_{j=0}^{\infty} \frac{(-1)^j}{j! \Gamma(j + \bar{l}_\nu + 1)} \left(\frac{p_\nu r}{2} \right)^{2j}, \tag{B.9}$$

where $\bar{l} \equiv l - \mathrm{sgn}(\kappa)$.

In terms of these expressions, the leptonic currents (see Section 2) can be written

$$\begin{aligned} &\bar{\psi}_e(\boldsymbol{r}) \gamma_\mu (1 - \gamma_5) \psi_\nu(\boldsymbol{r}) \\ &\quad = - \sum_{\kappa_e,\, \mu_e,\, \kappa_\nu,\, \mu_\nu} a^*_{\kappa_e \mu_e}(\hat{\boldsymbol{p}}_e, s_e) b_{\kappa_\nu \mu_\nu}(\hat{\boldsymbol{p}}_\nu, s_\nu) f_{\kappa_e}(r) j_l(p_\nu r)\, \chi^{\mu_e \dagger}_{-\kappa_e}(\hat{\boldsymbol{r}})\, \sigma_\mu\, \chi^{\mu_\nu}_{-\kappa_\nu}(\hat{\boldsymbol{r}})\,. \end{aligned} \tag{B.10}$$

With the above expressions, the leptonic sector of the weak-interaction vertex reads

$$\begin{aligned} h_W = {} & \frac{8\pi G}{\sqrt{2}} \sum_{jlm} (-1)^{I_f - M_f + 1} \sqrt{4\pi} \sqrt{2I_i + 1} \begin{pmatrix} I_f & j & I_i \\ -M_f & m & M_i \end{pmatrix} \\ & \times \int_0^\infty q^2\, \mathrm{d}q \int_0^\infty r^2\, \mathrm{d}r \int \mathrm{d}\hat{r} \sum_{l'=0}^{\infty} \sum_{m'} (-\mathrm{i})^{l'} \\ & \times \int \mathrm{d}\hat{q}\; Y^*_{lm}(\hat{\boldsymbol{q}}) \frac{(qR)^l}{(2l+1)!!} F_{jl}(q^2) j_{l'}(qr) Y_{l',m'}(\hat{\boldsymbol{r}}) Y^*_{l',m'}(\hat{\boldsymbol{q}}) \\ & \times \sum_{\kappa_e, \mu_e, \kappa_\nu, \mu_\nu} a^*_{\kappa_e \mu_e}(\hat{\boldsymbol{p}}_e, s_e) b_{\kappa_\nu \mu_\nu}(\hat{\boldsymbol{p}}_\nu, s_\nu) f_{\kappa_e}(r) j_l(p_\nu r) \chi^{\mu_e \dagger}_{-\kappa_e}(\hat{\boldsymbol{r}}) \sigma_\mu \chi^{\mu_\nu}_{-\kappa_\nu}(\hat{\boldsymbol{r}})\,. \end{aligned} \tag{B.11}$$

The above expression contains explicitly the leptonic components of the vertex and the q-dependence of the nuclear components given by the form factor $F_{jl}(q^2)$ [221]. This form of the leptonic weak-interaction vertices is the one which we were looking for and it is particularly useful in dealing with the calculation of transition matrix elements in a separable lepton–hadron representation.

References

[1] J. Abad, A. Morales, R. Nunez-Lagos, A.F. Pacheco, Ann. Fis. A 80 (1984) 9.
[2] I.J.R. Aitchison, A.J.G. Hey, Gauge Theories in Particle Physics, Adam Hilger, Bristol, 1982.

[3] H. Akimune, H. Ejiri, M. Fujiwara, I. Daito, T. Inomata, R. Hazama, A. Tamii, H. Toyokawa, M. Yosoi, Phys. Lett. B 394 (1997) 23.
[4] F. Alasia, O. Civitarese, Phys. Rev. C 42 (1990) 1335.
[5] A. Alessandrello, C. Brofferio, D.V. Camin, O. Cremonesi, F. Fiorini, E. Garcia, A. Giuliani, P. de Marcillac, A. Nucciotti, M. Pavan, G. Pessina, E. Previtali, L. Zanotti, Phys. Lett. B 335 (1994) 519.
[6] K. Allaart, E. Boeker, G. Bonsignori, M. Savoia, Y.K. Gambhir, Phys. Rep. 169 (1988) 209.
[7] R. Arnold, C. Augier, A.S. Barabash, D. Blum, V. Brudanin, J.E. Campagne, D. Dassié, V. Egorov, R. Eschbach, J.L. Guyonnet, F. Hubert, Ph. Hubert, S. Jullian, O. Kochetov, I. Kisel, V.N. Kornoukov, V. Kovalenko, D. Lalanne, F. Laplanche, F. Leccia, I. Linck, C. Longuemare, F. Mauger, P. Mennrath, H.W. Nicholson, A. Nozdrin, F. Piquemal, O. Purtov, J.-L. Reyss, F. Scheibling, J. Suhonen, C.S. Sutton, G. Szklarz, V.I. Tretyak, V. Umatov, I. Vanushin, A. Vareille, Yu. Vasilyev, Ts. Vylov, V. Zerkin, Z. Phys. C 72 (1996) 239.
[8] C. Arpesella, A.S. Barabash, E. Bellotti, C. Brofferio, E. Fiorini, P.P. Sverzellati, V.I. Umatov, Europhys. Lett. 27 (1994) 29.
[9] V.A. Artemiev, E.V. Brakchman, O.Ya. Zeldovich, A.K. Karelin, V.V. Kirichenko, O.M. Kozodaeva, V.A. Lubimov, A.I. Mitin, V.N. Paramokhin, T.N. Tsvetkova, S.I. Vesilyev, A.A. Klimenko, S.B. Osetrov, A.A. Pomansky, A.A. Smolnikov, JETP Lett. 58 (1993) 262.
[10] V. Artemiev, E. Brakchman, A. Karelin, V. Kirichenko, A. Klimenko, O. Kozodaeva, V. Lubimov, A. Mitin, S. Osetrov, V. Paramokhin, A. Pomansky, A. Smolnikov, T. Tsvetkova, S. Vesilyev, O. Zeldovich, Phys. Lett. B 345 (1995) 564.
[11] N. Auerbach, L. Zamick, D.C. Zheng, Ann. Phys. (N.Y.) 192 (1989) 77.
[12] C. Aulakh, R.N. Mohapatra, Phys. Lett. B 119 (1982) 136.
[13] M. Aunola, J. Suhonen, Nucl. Phys. A 602 (1996) 133.
[14] M. Aunola, O. Civitarese, J. Kauhanen, J. Suhonen, Nucl. Phys. A 596 (1996) 187.
[15] K.S. Babu, R.N. Mohapatra, Phys. Rev. Lett. 75 (1995) 2276.
[16] A. Balysh, M. Beck, S.T. Belyaev, F. Bensch, J. Bockholt, A. Demehin, A. Gurov, G. Heusser, H.V. Klapdor-Kleingrothaus, I. Kondratenko, D. Kotel'nikov, V.I. Lebedev, B. Maier, A. Müller, F. Petry, A. Piepke, A. Pronsky, H. Strecker, M. Völliger, K. Zuber, Phys. Lett. B 322 (1994) 176.
[17] A. Balysh, M. Beck, S.T. Belyaev, J. Bockholt, A. Demehin, A. Gurov, J. Hellmig, G. Heusser, M. Hirsch, Ch. Hoffmann, H.V. Klapdor-Kleingrothaus, I. Kondratenko, D. Kotel'nikov, V.I. Lebedev, B. Maier, A. Müller, H. Päs, F. Petry, A. Scheer, H. Strecker, M. Völliger, Phys. Lett. B 356 (1995) 450.
[18] A. Balysh, A. De Silva, V.I. Lebedev, K. Lou, M.K. Moe, M.A. Nelson, A. Piepke, A. Pronskiy, M.A. Vient, P. Vogel, Phys. Rev. Lett. 77 (1996) 5186.
[19] P. Bamert, C.P. Burgess, R.N. Mohapatra, Nucl. Phys. B 449 (1995) 25.
[20] A.S. Barabash, JETP Lett. 51 (1990) 207.
[21] A.S. Barabash, JETP Lett. 59 (1994) 644.
[22] A.S. Barabash, F.T. Avignone III, J.I. Collar, C.K. Guerard, R.J. Arthur, L.S. Brodzinski, H.S. Miley, J.H. Reeves, J.R. Meier, K. Ruddick, V.I. Umatov, Phys. Lett. B 345 (1995) 408.
[23] A.S. Barabash, A.V. Derbin, L.A. Popeko, V.I. Umatov, Z. Phys. A 352 (1995) 231.
[24] A.S. Barabash, R. Gurriarán, F. Hubert, Ph. Hubert, J.L. Reyss, J. Suhonen, V.I. Umatov, J. Phys. G 22 (1996) 487.
[25] A.S. Barabash, V.V. Kuzminov, V.M. Lobashev, V.M. Novikov, B.M. Ovchinnikov, A.A. Pomansky, Phys. Lett. B 223 (1989) 273.
[26] A.S. Barabash, R.R. Saakyan, Phys. Atom. Nucl. 59 (1996) 179.
[27] A.S. Barabash, V.I. Umatov, R. Gurriarán, F. Hubert, Ph. Hubert, M. Aunola, J. Suhonen, JETP Lett. 62 (1995) 706.
[28] A.S. Barabash, V.I. Umatov, R. Gurriarán, F. Hubert, Ph. Hubert, M. Aunola, J. Suhonen, Nucl. Phys. A 604 (1996) 115.
[29] M. Baranger, Phys. Rev. 120 (1960) 957.
[30] C. Barbero, F. Krmpotić, A. Mariano, Phys. Lett. B 345 (1995) 192.
[31] R.K. Bardin, P.J. Gollon, J.D. Ullman, C.S. Wu, Nucl. Phys. A 158 (1970) 337.
[32] M. Beck, J. Bockholt, J. Echternach, G. Heusser, M. Hirsch, H.V. Klapdor-Kleingrothaus, A. Piepke, H. Strecker, K. Zuber, A. Bakalyarov, A. Balysh, S.T. Belyaev, A. Demehin, A. Gurov, I. Kondratenko, V.I. Lebedev, A. Pronsky, A. Müller, Z. Phys. A 343 (1992) 397.

[33] M.A.B. Bég, R.V. Budny, R. Mohapatra, A. Sirlin, Phys. Rev. Lett. 38 (1977) 1252.
[34] H. Behrens, W. Bühring, Electron Radial Wave Functions and Nuclear Beta-Decay, Clarendon, Oxford, 1982.
[35] E. Bellotti, C. Cattadori, O. Cremonesi, E. Fiorini, C. Liguori, A. Pullia, P.P. Sverzellati, L. Zanotti, Europhys. Lett. 3 (1987) 889.
[36] E. Bellotti, E. Fiorini, C. Liguori, A. Pullia, A. Sarracino, L. Zanotti, Lett. Nuovo Cimento 33 (1982) 273.
[37] J. Bernabeu, B. Desplanques, J. Navarro, S. Noguera, Z. Phys. C 46 (1990) 323.
[38] T. Bernatowicz, J. Brannon, R. Brazzle, R. Cowsik, C. Hohenberg, F. Podosek, Phys. Rev. Lett. 69 (1992) 2341; ibid. Phys. Rev. C 47 (1993) 806.
[39] Z.G. Berezhiani, A.Yu. Smirnov, J.W.F. Valle, Phys. Lett. B 291 (1992) 99.
[40] D.R. Bes, R.A. Broglia, B.S. Nilsson, Phys. Rep. 16 (1975) 1.
[41] D.R. Bes, R.A. Broglia, G.G. Dussel, R.J. Liotta, H. Sofia, Nucl. Phys. A 260 (1976) 127.
[42] M. Bhattacharya et al., to be published.
[43] J. Blachot, G. Marguier, Nucl. Data Sheets 73 (1994) 81.
[44] J. Blatt, V. Weisskopf, Theoretical Nuclear Physics, Springer, Berlin, 1979.
[45] A. Bobyk, W.A. Kaminski, J. Phys. G 21 (1995) 229.
[46] F. Boehm, P. Vogel, Physics of Massive Neutrinos, Cambridge University Press, Cambridge, 1987; F. Boehm, P. Vogel, Physics of Neutrinos, 2nd ed., Cambridge University Press, Cambridge, 1992.
[47] A. Bohr, B.R. Mottelson, Nuclear Structure, vol. I, Benjamin, New York, 1969.
[48] A. Bohr, B.R. Mottelson, Nuclear Structure, vol. II, Benjamin, Reading, MA, 1975.
[49] G. Bonsignori, M. Savoia, K. Allaart, A. Van Egmond, G. te Velde, Nucl. Phys. A 432 (1985) 389.
[50] G.E. Brown, M. Bolsterli, Phys. Rev. Lett. 3 (1959) 472.
[51] D. Bryman, C. Picciotto, Rev. Mod. Phys. 50 (1978) 11.
[52] A. Buras, J. Ellis, M. Gailard, D. Nanopoulos, Nucl. Phys. B 135 (1978) 66.
[53] C.P. Burgess, J.M. Cline, Phys. Lett. B 298 (1993) 141; Phys. Rev. D 49 (1994) 5925.
[54] D.O. Caldwell, R.M. Eisberg, D.M. Grumm, D.L. Hale, M.S. Witherell, F.S. Goulding, D.A. Landis, N.W. Madden, D.F. Malone, R.H. Pehl, A.R. Smith, Phys. Rev. D 33 (1986) 2737.
[55] C.D. Carone, Phys. Lett. B 308 (1993) 85.
[56] O. Castaños, J.G. Hirsch, O. Civitarese, P.O. Hess, Nucl. Phys. A 571 (1994) 276.
[57] F. Catara, N. Dinh Dang, M. Sambataro, Nucl. Phys. A 579 (1994) 1.
[58] E. Caurier, A. Poves, A.P. Zuker, Phys. Lett. B 252 (1990) 13.
[59] E. Caurier, F. Nowacki, A. Poves, J. Retamosa, Phys. Rev. Lett. 77 (1996) 1954.
[60] D. Cha, Phys. Rev. C 27 (1983) 2269.
[61] M.K. Cheoun, A. Bobyk, A. Faessler, F. Šimkovic, G. Teneva, Nucl. Phys. A 561 (1993) 74.
[62] M.K. Cheoun, A. Bobyk, A. Faessler, F. Šimkovic, G. Teneva, Nucl. Phys. A 564 (1993) 329.
[63] M.K. Cheoun, A. Faessler, F. Šimkovic, G. Teneva, A. Bobyk, Nucl. Phys. A 587 (1995) 301.
[64] Y. Chikashige, R.N. Mohapatra, R.D. Peccei, Phys. Rev. Lett. 45 (1980) 265; Phys. Lett. B 98 (1981) 265.
[65] C.R. Ching, T.H. Ho, X.R. Wu, Phys. Rev. C 40 (1989) 304.
[66] D.S. Chuu, M.M. King Yen, Y. Shan, S.T. Hsieh, Nucl. Phys. A 321 (1979) 415.
[67] O. Civitarese, M. Reboiro, Phys. Rev. C, submitted.
[68] O. Civitarese, A. Faessler, T. Tomoda, Phys. Lett. B 194 (1987) 11.
[69] O. Civitarese, A. Faessler, J. Suhonen, X.R. Wu, Phys. Lett. B 251 (1990) 333.
[70] O. Civitarese, A. Faessler, J. Suhonen, X.R. Wu, J. Phys. G 17 (1991) 943.
[71] O. Civitarese, A. Faessler, J. Suhonen, X.R. Wu, Nucl. Phys. A 524 (1991) 404.
[72] O. Civitarese, M. Reboiro, Phys. Rev. C 56 (1997) 1179.
[73] O. Civitarese, M. Reboiro, P. Vogel, Phys. Rev. C 56 (1997) 1840.
[74] O. Civitarese, J. Suhonen, Phys. Rev. C 47 (1993) 2410.
[75] O. Civitarese, J. Suhonen, Nucl. Phys. A 575 (1994) 251.
[76] O. Civitarese, J. Suhonen, J. Phys. G 20 (1994) 1441.
[77] O. Civitarese, J. Suhonen, Nucl. Phys. A 578 (1994) 62.
[78] O. Civitarese, J. Suhonen, A. Faessler, Nucl. Phys. A 591 (1995) 195.
[79] O. Civitarese, J. Suhonen, Nucl. Phys. A 607 (1996) 152.

[80] F.A. Danevich, A.Sh. Georgadze, V.V. Kobychev, B.N. Kropivyansky, V.N. Kuts, A.S. Nikolaiko, V.I. Tretyak, Yu. Zdesenko, Phys. Lett. B 344 (1995) 72.
[81] F.A. Danevich, A.Sh. Georgadze, J. Hellmig, M. Hirsch, H.V. Klapdor-Kleingrothaus, V.V. Kobychev, B.N. Kropivyansky, V.N. Kuts, A. Müller, A.S. Nikolaiko, F. Petry, O.A. Ponkratenko, H. Strecker, V.I. Tretyak, M. Völlinger, Yu. Zdesenko, Z. Phys. A 355 (1996) 433.
[82] D. Dassié, R. Eschbach, F. Hubert, Ph. Hubert, M.C. Isaac, C. Izac, F. Leccia, P. Mennrath, A. Vareille, C. Longuemare, F. Mauger, F. Danevich, V. Kouts, V.I. Tretyak, Yu. Vassilyev, Yu. Zdesenko, A.S. Barabash, V.N. Kornoukov, Yu.B. Lepikhin, V.I. Umatov, I.A. Vanushin, C. Augier, D. Blum, J.E. Campagne, S. Jullian, D. Lalanne, F. Laplanche, F. Natchez, G. Pichenot, G. Szklarz, R. Arnold, J.L. Guyonnet, T. Lamhamdi, I. Linck, F. Piquemal, F. Scheibling, V. Brudanin, V. Egorov, O. Kochetov, A. Nozdrin, Ts. Vylov, Sh. Zaparov, H.W. Nicholson, C.S. Sutton, Phys. Rev. D 51 (1995) 2090.
[83] S.K. Dhiman, P.K. Raina, Phys. Rev. C 50 (1994) R2660.
[84] M. Doi, T. Kotani, H. Nishiura, E. Takasugi, Prog. Theor. Phys. 69 (1983) 602.
[85] M. Doi, T. Kotani, E. Takasugi, Prog. Theor. Phys. Suppl. 83 (1985) 1.
[86] M. Doi, T. Kotani, E. Takasugi, Phys. Rev. D 37 (1988) 2575.
[87] M. Doi, T. Kotani, Prog. Theor. Phys. 87 (1992) 1207.
[88] M. Doi, T. Kotani, Prog. Theor. Phys. 89 (1993) 139.
[89] J. Dukelsky, P. Schuck, Phys. Lett. B 387 (1996) 233.
[90] A.R. Edmonds, Angular Momentum in Quantum Mechanics, Princeton University Press, Princeton, NJ, 1960.
[91] H. Ejiri, K. Fushimi, T. Kamada, H. Kinoshita, H. Kobiki, H. Ohsumi, K. Okada, H. Sano, T. Shibata, T. Shima, N. Tanabe, J. Tanaka, T. Taniguchi, T. Watanabe, N. Yamamoto, Phys. Lett. B 258 (1991) 17.
[92] H. Ejiri, K. Fushimi, K. Hayashi, R. Hazama, T. Kishimoto, N. Kudomi, T. Kume, K. Nagata, H. Ohsumi, K. Okada, T. Shima, J. Tanaka, Nucl. Phys. A 611 (1996) 85.
[93] J.P. Elliott, A.D. Jackson, H.A. Mavromatis, E.A. Sanderson, B. Singh, Nucl. Phys. A 121 (1968) 241.
[94] S.R. Elliott, A.A. Hahn, M.K. Moe, Phys. Rev. Lett. 59 (1987) 2020; Phys. Rev. C 36 (1987) 2129.
[95] S.R. Elliott, A.A. Hahn, M.K. Moe, J. Phys. G 17 (1991) 943.
[96] S.R. Elliott, M.K. Moe, M.A. Nelson, M.A. Vient, J. Phys. G 17 (1991) S145.
[97] S.R. Elliott, A.A. Hahn, M.K. Moe, M.A. Nelson, M.A. Vient, Phys. Rev. C 46 (1992) 1535.
[98] S.R. Elliott, M.K. Moe, M.A. Nelson, M.A. Vient, Nucl. Phys. B (Proc. Suppl.) 31 (1993) 68.
[99] J. Engel, P. Vogel, M.R. Zirnbauer, Phys. Rev. C 37 (1988) 731.
[100] J. Engel, P. Vogel, O. Civitarese, M.R. Zirnbauer, Phys. Lett. B 208 (1988) 187.
[101] J. Engel, P. Vogel, X.-D. Ji, S. Pittel, Phys. Lett. B 225 (1989) 5.
[102] J. Engel, W.C. Haxton, P. Vogel, Phys. Rev. C 46 (1992) R2153.
[103] J. Engel, K. Langanke, P. Vogel, Phys. Lett. B 389 (1996) 211.
[104] J. Engel, S. Pittel, M. Stoitsov, P. Vogel, J. Dukelsky, Phys. Rev. C 55 (1997) 1781.
[105] M. Ericson, T. Ericson, P. Vogel, Phys. Lett. B 328 (1994) 259.
[106] A. Faessler, Prog. Part. Nucl. Phys. 21 (1988) 183.
[107] A. Faessler, W.A. Kaminski, G. Pantis, J.D. Vergados, Phys. Rev. C 43 (1991) R21.
[108] S. Ferrara, J. Ellis, P. van Nieuwenhuizen (Eds.), Unification of the fundamental particle interactions, Plenum, New York, 1980.
[109] R.P. Feynmann, M. Gell-Mann, Phys. Rev. 109 (1958) 193.
[110] J.L. Friar, Nucl. Phys. 87 (1966) 407.
[111] H. Fritzsch, P. Minkowski, Ann. Phys. (NY) 93 (1975) 193.
[112] S. Furui, A. Faessler, S.B. Khadkikar, Nucl. Phys. A 424 (1984) 495.
[113] A. García, Y.-D. Chan, M.T.F. da Cruz, R.M. Larimer, K.T. Lesko, E.B. Norman, R.G. Stokstad, F.E. Wietfeldt, I. Žlimen, D.M. Moltz, J. Batchelder, T.J. Ognibene, M.M. Hindi, Phys. Rev. C 47 (1993) 2910.
[114] G. Gelmini, M. Roncadelli, Phys. Lett. 99B (1981) 411.
[115] H. Georgi, S.L. Glashow, Phys. Rev. Lett. 32 (1974) 438.
[116] H.M. Georgi, S.L. Glashow, S. Nussinov, Nucl. Phys. B 193 (1981) 297.
[117] S.L. Glashow, J. Iliopoulos, L. Maiani, Phys. Rev. D 2 (1970) 1285.
[118] A. Goswami, Nucl. Phys. 60 (1964) 228.

[119] A. Griffiths, P. Vogel, Phys. Rev. C 46 (1992) 181.
[120] K. Grotz, H.V. Klapdor, J. Metzinger, J. Phys. G 9 (1983) L169.
[121] K. Grotz, H.V. Klapdor, Phys. Lett. B 157 (1985) 242; Nucl. Phys. A 460 (1986) 395.
[122] K. Grotz, H.V. Klapdor, The Weak Interaction in Nuclear, Particle and Astrophysics, Adam Hilger, Bristol, Philadelphia, 1990.
[123] H.E. Haber, G.L. Kane, Phys. Rep. 117 (1985) 75.
[124] J.A. Halbleib, R.A. Sorensen, Nucl. Phys. A 98 (1967) 542.
[125] W.C. Haxton, G.J. Stephenson Jr., Prog. Part. Nucl. Phys. 12 (1984) 409.
[126] J.G. Hirsch, E. Bauer, F. Krmpotić, Nucl. Phys. A 516 (1990) 304.
[127] J.G. Hirsch, O. Castaños, P.O. Hess, O. Civitarese, Nucl. Phys. B (Proc. Suppl.) 35 (1994) 381.
[128] J.G. Hirsch, O. Castaños, P.O. Hess, O. Civitarese, Phys. Rev. C 51 (1995) 2252.
[129] J.G. Hirsch, O. Castaños, P.O. Hess, O. Civitarese, Nucl. Phys. A 589 (1995) 445.
[130] J.G. Hirsch, O. Castaños, P.O. Hess, Nucl. Phys. A 582 (1995) 124.
[131] J.G. Hirsch, P.O. Hess, O. Civitarese, Phys. Rev. C 54 (1996) 1976.
[132] J.G. Hirsch, P.O. Hess, O. Civitarese, Phys. Lett. B 390 (1997) 36.
[133] J.G. Hirsch, P.O. Hess, O. Civitarese, Phys. Rev. C 56 (1997) 199.
[134] M. Hirsch, O. Kadowaki, H.V. Klapdor-Kleingrothaus, K. Muto, T. Oda, Z. Phys. A 352 (1995) 33.
[135] M. Hirsch, H.V. Klapdor-Kleingrothaus, S.G. Kovalenko, Phys. Rev. Lett. 75 (1995) 17.
[136] M. Hirsch, H.V. Klapdor-Kleingrothaus, S.G. Kovalenko, Phys. Lett. B 352 (1995) 1.
[137] M. Hirsch, H.V. Klapdor-Kleingrothaus, S.G. Kovalenko, Phys. Lett. B 372 (1996) 181.
[138] M. Hirsch, H.V. Klapdor-Kleingrothaus, S.G. Kovalenko, H. Päs, Phys. Lett. B 372 (1996) 8.
[139] J.G. Hirsch, F. Krmpotić, Phys. Lett. B 246 (1990) 5.
[140] M. Hirsch, K. Muto, T. Oda, H.V. Klapdor-Kleingrothaus, Z. Phys. A 347 (1994) 151.
[141] D.J. Horen, C.D. Goodman, C.C. Foster, C.A. Goulding, M.B. Greenfield, J. Rapaport, D.E. Bainum, E. Sugarbaker, T.G. Masterson, F. Petrovich, W.G. Love, Phys. Lett. B 95 (1980) 27.
[142] D.J. Horen, C.D. Goodman, D.E. Bainum, C.C. Foster, C. Gaarde, C.A. Goulding, M.B. Greenfield, J. Rapaport, T.N. Taddeucci, E. Sugarbaker, T. Masterson, S.M. Austin, A. Galonsky, W. Sterrenburg, Phys. Lett. B 99 (1981) 383.
[143] K. Ikeda, T. Udagawa, H. Yamaura, Prog. Theor. Phys. 33 (1965) 22.
[144] I.P. Johnstone, Phys. Rev. C 44 (1991) 1476.
[145] I.P. Johnstone, L.D. Skouras, Phys. Rev. C 51 (1995) 2817.
[146] D. Karadjov, V.V. Voronov, F. Catara, Phys. Lett. B 306 (1993) 197.
[147] A. Kawashima, K. Takahashi, A. Masuda, Phys. Rev. C 47 (1993) 2452.
[148] Ke You, Y. Zhu, J. Lu, H. Sun, W. Tian, W. Zhao, Z. Zheng, M. Ye, C. Ching, T. Ho, F. Cui, C. Yu, G. Jiang, Phys. Lett. B 95 (1991) 27.
[149] S.B. Khadkikar, S.K. Gupta, Phys. Lett. B 124 (1983) 523.
[150] E. Kirchuk, P. Federman, S. Pittel, Phys. Rev. C 47 (1993) 567.
[151] T. Kirsten, H. Richter, E. Jessberger, Phys. Rev. Lett. 50 (1983) 474.
[152] H.V. Klapdor (Ed.), Proc. Int. Symp. on Weak and Electromagnetic Interactions in Nuclei, Heidelberg, Germany, 1986, Springer, Berlin, 1986.
[153] H.V. Klapdor (Ed.), Neutrinos, Springer, Heidelberg, 1988.
[154] H.V. Klapdor, K. Grotz, Phys. Lett. B 142 (1984) 323.
[155] H.V. Klapdor-Kleingrothaus, S. Stoica (Eds.), Proc. Int. Workshop on Double Beta Decay and Related Topics, Trento, Italy, 1995, World Scientific, Singapore, 1996.
[156] S.E. Koonin, D.J. Dean, K. Langanke, Phys. Rep. 278 (1997) 1.
[157] F. Krmpotić, Phys. Rev. C 48 (1993) 1452.
[158] F. Krmpotić, T.T.S. Kuo, A. Mariano, E.J.V. de Passos, A.F.R. de Toledo Piza, Nucl. Phys. A 612 (1997) 223.
[159] F. Krmpotić, A. Mariano, T.T.S. Kuo, K. Nakayama, Phys. Lett. B 319 (1993) 393.
[160] F. Krmpotić, S.S. Sharma, Nucl. Phys. A 572 (1994) 329.
[161] N. Kudomi, H. Ejiri, K. Nagata, K. Okada, T. Shibata, T. Shima, J. Tanaka, Phys. Rev. C 46 (1992) R2132.

[162] K. Kume, H. Ejiri, K. Fushimi, R. Hazama, K. Kawasaki, V. Koutz, N. Kudomi, K. Nagata, V. Malishko, H. Ohsumi, K. Okada, H. Sano, T. Senoo, T. Shibata, T. Shima, J. Tanaka, Yu. Zdesenko, Nucl. Phys. A 577 (1994) 405c.
[163] J. Kumpulainen, R. Julin, J. Kantele, A. Passoja, W.H. Trzaska, E. Verho, J. Väärämäki, D. Cutoiu, M. Ivascu, Phys. Rev. C 45 (1992) 640.
[164] T.T.S. Kuo, G.E. Brown, Nucl. Phys. A 114 (1968) 241.
[165] P. Langacker, Phys. Rep. 72 (1981) 185.
[166] E. Leader, E. Predazzi, Gauge Theories and New Physics, Cambridge University Press, London, 1983.
[167] C.M. Lederer, V.S. Shirley (Eds.), Table of Isotopes, Wiley, New York, 1978.
[168] The LEP Collaboration, Phys. Lett. B 276 (1992) 247.
[169] G. Lhersonneau, B. Pfeiffer, J.R. Persson, J. Suhonen, J. Toivanen, P. Campbell, P. Dendooven, A. Honkanen, M. Huhta, P.M. Jones, R. Julin, S. Juutinen, M. Oinonen, H. Penttilä, K. Peräjärvi, A. Savelius, W. Jicheng, J.C. Wang, J. Äystö, Z. Phys. A 358 (1997) 317.
[170] C. Longmire, H. Brown, Phys. Rev. 75 (1949) 264.
[171] R. Madey, B.S. Flanders, B.D. Anderson, A.R. Baldwin, J.W. Watson, S.M. Austin, C.C. Foster, H.V. Klapdor, K. Grotz, Phys. Rev. C 40 (1989) 540.
[172] O.K. Manuel, J. Phys. G 17 (1991) 221.
[173] H.S. Miley, F.T. Avignone III, R.L. Brodzinski, J.I. Collar, J.H. Reeves, Phys. Rev. Lett. 65 (1990) 3092.
[174] L.W. Mitchell, P.H. Fisher, Phys. Rev. C 38 (1988) 895.
[175] M.K. Moe, D.D. Lowenthal, Phys. Rev. C 22 (1980) 2186.
[176] M.K. Moe, Int. J. Mod. Phys. E 2 (1993) 507.
[177] M.K. Moe, P. Vogel, Ann. Rev. Nucl. Part. Sci. 44 (1994) 247.
[178] R.N. Mohapatra, Phys. Rev. D 34 (1986) 3457.
[179] R.N. Mohapatra, Prog. Part. Nucl. Phys. 26 (1991) 1.
[180] R.N. Mohapatra, E. Takasugi, Phys. Lett. B 211 (1988) 192.
[181] S.A. Moszkovski, Phys. Rev. 110 (1958) 403.
[182] K. Muto, Phys. Lett. B 277 (1992) 13.
[183] K. Muto, Phys. Lett. B 391 (1997) 243.
[184] K. Muto, E. Bender, H.V. Klapdor, Z. Phys. A 334 (1989) 177.
[185] K. Muto, E. Bender, H.V. Klapdor, Z. Phys. A 334 (1989) 187.
[186] K. Muto, E. Bender, H.V. Klapdor-Kleingrothaus, Z. Phys. A 339 (1991) 435.
[187] K. Muto, H.V. Klapdor, Phys. Lett. B 201 (1988) 420.
[188] H. Nakada, T. Sebe, K. Muto, Nucl. Phys. A 535 (1996) 509.
[189] G.-H. Niephaus, M. Gari, B. Sommer, Phys. Rev. C 20 (1979) 1096.
[190] H.P. Nilles, Phys. Rep. 110 (1984) 1.
[191] E.B. Norman, Phys. Rev. C 31 (1985) 1937.
[192] E.B. Norman, M.A. DeFaccio, Phys. Lett. B 148 (1984) 31.
[193] K. Ogawa, H. Horie, in: M. Morita, H. Ejiri, H. Ohtsubo, T. Sato (Eds.), Nuclear Weak Process and Nuclear Structure, World Scientific, Singapore, 1989, p. 308.
[194] G. Pantis, A. Faessler, W.A. Kaminski, J.D. Vergados, J. Phys. G 18 (1992) 605.
[195] G. Pantis, F. Šimkovic, J.D. Vergados, A. Faessler, Phys. Rev. C 53 (1996) 695.
[196] G. Pantis, J.D. Vergados, Phys. Lett. B 242 (1990) 1.
[197] A. Piepke, M. Beck, J. Bockholt, D. Glatting, G. Heusser, B. Maier, F. Petry, H. Strecker, M. Völlinger, H.V. Klapdor-Kleingrothaus, A.S. Barabash, V.I. Umatov, A. Müller, J. Suhonen, Nucl. Phys. A 577 (1994) 493.
[198] H. Primakoff, S.P. Rosen, Rep. Prog. Phys. 22 (1959) 121.
[199] H. Primakoff, S.P. Rosen, Phys. Rev. 184 (1969) 1925.
[200] H. Primakoff, S.P. Rosen, Ann. Rev. Nucl. Part. Sci. 31 (1981) 145.
[201] A.A. Raduta, D.S. Delion, A. Faessler, Phys. Lett. B 312 (1993) 13.
[202] A.A. Raduta, D.S. Delion, A. Faessler, Phys. Rev. C 51 (1995) 3008.
[203] A.A. Raduta, A. Faessler, S. Stoica, W.A. Kaminski, Phys. Lett. B 254 (1991) 7.
[204] A.A. Raduta, A. Faessler, S. Stoica, Nucl. Phys. A 534 (1991) 149.

[205] A.A. Raduta, A. Faessler, D.S. Delion, Nucl. Phys. A 564 (1993) 185.
[206] A.A. Raduta, J. Suhonen, Phys. Rev. C 53 (1996) 176; J. Phys. G 22 (1996) 123.
[207] P.B. Radha, D.J. Dean, S.E. Koonin, T.T.S. Kuo, K. Langanke, A. Poves, J. Retamosa, P. Vogel, Phys. Rev. Lett. 76 (1996) 2642.
[208] S. Raman, T.A. Walkiewicz, S. Kahane, E.T. Jurney, J. Sa, Z. Gacsi, J.L. Weil, K. Allaart, G. Bonsignori, J.F. Shriner Jr., Phys. Rev. C 43 (1991) 521.
[209] J. Retamosa, E. Caurier, F. Nowacki, Phys. Rev. C 51 (1995) 371.
[210] M. Rho, preprint nucl-th 9708060 (1997).
[211] P. Ring, P. Schuck, The Nuclear Many-body Problem, Springer, Berlin, 1980.
[212] M.E. Rose, Elementary Theory of Angular Momentum, Wiley, New York, 1957.
[213] M.E. Rose, R.K. Osborn, Phys. Rev. 93 (1954) 1315.
[214] D.J. Rowe, Rev. Mod. Phys. 40 (1968) 153.
[215] D.J. Rowe, Nuclear Collective Motion, Methuen, London, 1970.
[216] O.A. Rumyantsev, M.G. Urin, JETP Lett. 61 (1995) 361.
[217] C. Sáenz, E. Cerezo, E. Garcia, A. Morales, J. Morales, R. Núñez-Lagos, A. Ortiz de Solórzano, J. Puimedón, A. Salinas, M.L. Sarsa, J.A. Villar, A. Klimenko, V. Kuzminov, N. Metlinsky, V. Novikov, A. Pomansky, B. Pritychenko, Phys. Rev. C 50 (1994) 1170.
[218] A. Salam, in: N. Svartholm (Ed.), Proc. 8th NOBEL Symp., Stockholm, 1968.
[219] M. Sambataro, J. Suhonen, Phys. Rev. C 56 (1997) 782.
[220] A. Santamaria, J.W.F. Valle, Phys. Lett. 195 B (1987) 423; Phys. Rev. Lett. 60 (1988) 397; Phys. Rev. D 39 (1989) 1780.
[221] H.F. Schopper, Weak Interactions and Nuclear Beta Decay, North-Holland, Amsterdam, 1966.
[222] K.W. Schmid, F. Grümmer, A. Faessler, Nucl. Phys. A 431 (1984) 205.
[223] P. Schuck, S. Ethofer, Nucl. Phys. A 212 (1973) 269.
[224] J. Schwieger, F. Šimkovic, A. Faessler, Nucl. Phys. A 600 (1996) 179.
[225] F. Šimkovic, J. Schwieger, M. Veselský, G. Pantis, A. Faessler, Phys. Lett. B 393 (1997) 267.
[226] J. Sinatkas, L.D. Skouras, D. Strottman, J.D. Vergados, J. Phys. G 18 (1992) 1377.
[227] L.D. Skouras, P. Manakos, J. Phys. G 19 (1993) 731.
[228] L.D. Skouras, J.D. Vergados, Phys. Rev. C 28 (1983) 2122.
[229] A. Staudt, K. Muto, H.V. Klapdor-Kleingrothaus, Europhys. Lett. 13 (1990) 31.
[230] D.B. Stout, T.T.S. Kuo, Phys. Rev. Lett. 69 (1992) 1900.
[231] S. Stoica, Phys. Rev. C 49 (1994) 2240.
[232] S. Stoica, Phys. Lett. B 350 (1995) 152.
[233] S. Stoica, W.A. Kaminski, Phys. Rev. C 47 (1993) 867.
[234] S. Stoica, I. Mihut, Nucl. Phys. A 602 (1996) 197.
[235] E.C.G. Sudarshan, R. Marshak, Phys. Rev. 109 (1958) 1860.
[236] J. Suhonen, Phys. Lett. B 255 (1991) 159.
[237] J. Suhonen, Nucl. Phys. A 563 (1993) 205.
[238] J. Suhonen, J. Phys. G 19 (1993) 139.
[239] J. Suhonen, Phys. Rev. C 48 (1993) 574.
[240] J. Suhonen, M. Aunola, in: A.A. Raduta, D.S. Delion, I.I. Ursu (Eds.), Proc. Predeal Int. Summer School Collective Motion and Nuclear Dynamics, Predeal, Romania 1995, World Scientific, Singapore, 1996, p. 479.
[241] J. Suhonen, O. Civitarese, A. Faessler, Nucl. Phys. A 543 (1992) 645.
[242] J. Suhonen, O. Civitarese, Phys. Lett. B 280 (1992) 191.
[243] J. Suhonen, O. Civitarese, Phys. Lett. B 308 (1993) 212.
[244] J. Suhonen, O. Civitarese, Phys. Lett. B 312 (1993) 367.
[245] J. Suhonen, O. Civitarese, Phys. Rev. C 49 (1994) 3055.
[246] J. Suhonen, O. Civitarese, J. Phys. G 20 (1994) 347.
[247] J. Suhonen, O. Civitarese, Nucl. Phys. A 584 (1995) 449.
[248] J. Suhonen, P.C. Divari, L.D. Skouras, I.P. Johnstone, Phys. Rev. C 55 (1997) 714.
[249] J. Suhonen, A. Faessler, T. Taigel, T. Tomoda, Phys. Lett. B 202 (1988) 174.

[250] J. Suhonen, S.B. Khadkikar, A. Faessler, Phys. Lett. B 237 (1990) 8; Nucl. Phys. A 529 (1991) 727.
[251] J. Suhonen, E. Hammarén, Phys. Rev. C 47 (1993) 757.
[252] J. Suhonen, S.B. Khadkikar, A. Faessler, Nucl. Phys. A 535 (1991) 509.
[253] J. Suhonen, T. Taigel, A. Faessler, Nucl. Phys. A 486 (1988) 91.
[254] J. Suhonen, J. Toivanen, A.S. Barabash, I.A. Vanushin, V.I. Umatov, R. Gurriarán, F. Hubert, Ph. Hubert, Z. Phys. A 358 (1997) 297.
[255] J. Suhonen, J. Toivanen, A. Holt, T. Engeland, E. Osnes, M. Hjorth-Jensen, Nucl. Phys. A 628 (1998) 41.
[256] J. Toivanen, J. Suhonen, Phys. Rev. Lett. 75 (1995) 410.
[257] J. Toivanen, J. Suhonen, Phys. Rev. C 55 (1997) 2314.
[258] T. Tomoda, Nucl. Phys. A 484 (1988) 635.
[259] T. Tomoda, Rep. Prog. Phys. 54 (1991) 53.
[260] T. Tomoda, A. Faessler, Phys. Lett. B 199 (1987) 475.
[261] T. Tomoda, A. Faessler, K.W. Schmid, F. Grümmer, Nucl. Phys. A 452 (1986) 591.
[262] V.I. Tretyak, Yu.G. Zdesenko, At. Nucl. Data Tables 61 (1995) 43.
[263] D. Troltenier, J.A. Maruhn, W. Greiner, V. Velazquez Aguilar, P.O. Hess, J.H. Hamilton, Z. Phys. A 338 (1991) 261.
[264] T. Tsuboi, K. Muto, H. Horie, Phys. Lett. B 143 (1984) 293.
[265] H. Umezawa, Advanced Field Theory, AIP, New York, 1993.
[266] A.A. Vasenko, I.V. Kirpichnikov, V.A. Kuznetsov, A.S. Starostin, A.G. Djanyan, V.S. Pogosov, S.P. Shachysisyan, A.G. Tamanyan, Mod. Phys. Lett. A 5 (1990) 1299.
[267] J.D. Vergados, Phys. Rev. D 25 (1982) 914.
[268] J.D. Vergados, Nucl. Phys. B 218 (1983) 109.
[269] J.D. Vergados, Phys. Rep. 133 (1986) 1.
[270] J.D. Vergados, Phys. Lett. B 184 (1987) 55.
[271] J.D. Vergados, A. Faessler, T. Tomoda, Nucl. Phys. A 490 (1988) 556.
[272] J.D. Vergados, Nucl. Phys. A 506 (1990) 482.
[273] J.D. Vergados, S.B. Khadkikar, A. Faessler, Nucl. Phys. A 492 (1989) 654.
[274] P. Vogel, M. Ericson, J.D. Vergados, Phys. Lett. B 212 (1988) 259.
[275] P. Vogel, M.R. Zirnbauer, Phys. Rev. Lett. 57 (1986) 3148.
[276] J.-C. Vuilleumier, J. Busto, J. Farine, V. Jörgens, L.W. Mitchell, M. Treichel, J.-L. Vuilleumier, H.T. Wong, F. Boehm, P. Fisher, H.E. Henrikson, D.A. Imel, M.Z. Iqbal, B.M. O'Callaghan-Hay, J. Thomas, K. Gabathuler, Phys. Rev. D 48 (1993) 1009.
[277] S. Weinberg, Phys. Rev. Lett. 19 (1967) 1264.
[278] C.S. Wu, E. Ambler, R.W. Hayward, D.D. Hoppes, R.P. Hudson, Phys. Rev. 105 (1957) 1413.
[279] C.S. Wu, S.A. Moszkowski, Beta Decay, Interscience, New York, 1966.
[280] X.R. Wu, A. Staudt, H.V. Klapdor-Kleingrothaus, C.R. Ching, T.H. Ho, Phys. Lett. B 272 (1991) 169.
[281] X.R. Wu, A. Staudt, T.T.S. Kuo, H.V. Klapdor-Kleingrothaus, Phys. Lett. B 276 (1992) 274.
[282] L. Zhao, B.A. Brown, W.A. Richter, Phys. Rev. C 42 (1990) 1120.
[283] L. Zhao, B.A. Brown, Phys. Rev. C 47 (1993) 2641.
[284] D. Zheng, L. Zamick, N. Auerbach, Phys. Rev. C 40 (1989) 936.
[285] D. Zheng, L. Zamick, N. Auerbach, Ann. Phys. 197 (1990) 343.